

جامعة الزرقاء

نموذج تفويض

أنا لينا محمد بسام محمد تيسير شغليل، أفوض جامعة الزرقاء بتزويد نسخ من رسالتي/
أطروحتي للمكتبات، أو المؤسسات، أو الهيئات، أو الأشخاص عند طلبهم حسب التعليمات النافذة
في الجامعة.

التوقيع: 

التاريخ: 22/08/2021

Zarqa University

Authorization Form

**I Lina Moh'd Bassam M. T. Shaghilil, authorize Zarqa University to
supply copies of my 'Thesis/ Dissertation to libraries or establishments
or individuals on request, according to Zarqa University regulations.**

Signature: 

Date: 22/08/2021



**FORMULATION AND EVALUATION OF NASAL PATCH
FOR NOSE-TO-BRAIN DRUG DELIVERY OF
RIVASTIGMINE**

BY

Lena “Mohammad Bassam” Shaghilil

Supervisor

Dr. Anas Adib AlShishani

This Thesis Was Submitted in Partial Fulfillment of the Requirements for
the Master’s Degree of Pharmaceutical Science

Faculty of Graduate Studies

Zarqa University

August, 2021



صياغة و تقييم لرقعة انف لايصال الدواء من الانف إلى الدماغ لمادة الريفاستيجمين

إعداد

لينا "محمد بسام" شغليل

إشراف

الدكتور انس أديب الشيشاني

قدمت هذه الرسالة استكمالاً لمتطلبات الحصول على درجة الماجستير في العلوم الصيدلانية

كلية الدراسات العليا

جامعة الزرقاء

آب, 2021

COMMITTEE DECISION

This Thesis (Formulation and Evaluation of Nasal Patch for Nose-To-Brain drug delivery of rivastigmine) was Successfully Defended and Approved on 11/08/2021

Examination Committee

Signature

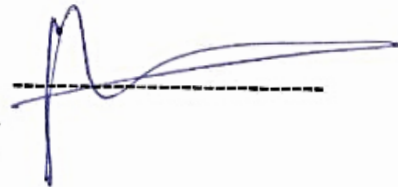
Dr. Anas Adib Alshishani (Supervisor)
Assistant Professor of Analytical Chemistry



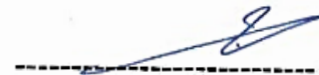
Dr. Ola Tarawneh (Member)
Assistant Professor of Industrial pharmacy



Dr. Ahlam Zaid Alkilani (Member)
Associate Professor of Pharmaceutical technology



Dr. Jameel Sulieman Alhesan (Member)
Assistant Professor of Analytical chemistry



Acknowledgement

In the first place, this work could never become reality without the guidance and blessing of Allah, the Beneficent, Bountiful, and Merciful.

Great thanks for my super family, for their amazing support and unique patience, their believe in me and in my dream was unlimited.

I acknowledge Al-Zarqa university for the financial support and the great opportunity to build up this project.

I am extremely grateful to my supervisor Dr. Anas Al-Shishani whose sincerity and encouragement that I will never forget. He has been an inspiration as I hurdled through the path of this Master's degree, he is the true definition of a leader and the ultimate role model, this thesis would not have been possible without his support.

I gratefully recognize the help of my colleagues, specially my road mat Asma'a Abu sealeek who encouraged me at those dark and Desperate times when it seemed impossible to continue and helped me throughout my thesis.

Special thanks go for Al-Zaytoonah University of Jordan, Dar al-dawa company, and Al Hikma company for giving me the opportunity and the required support for completing my thesis.

My thanks are also for the examination committee Dr. Ahlam Zaid Alkilani, Dr. Jameel Sulieman Alhesan and Dr. Ola Tarawneh For their valuable comments.

Table of Content

Subject	Page
Authorization Form	i
Title page	ii
Title page (Arabic)	iii
Committee Decision	iv
Acknowledgement	v
Table of Contents	vi
List of Tables	xi
List of Figures and Plates	xiii
List of Abbreviations	xv
Abstract	xvii
1. Introduction	1
1.1. Drug delivery to central nervous system CNS.....	1
1.2. Nasal drug delivery	3
1.3. Nasal anatomy	3
1.4. Nose-to-brain drug delivery	6
1.4.1. The systemic pathway	6
1.4.2. The neuronal pathway	6
1.5. Factors affecting drug transportation	8
1.6. Importance of the study	11
1.7. Objectives of the study	11
2. Literature Review	12
2.1. The history of nasal administration	12
2.2. Nasal dosage forms	12
2.3. Nose-to-brain drug delivery	16
2.4. Rivastigmine as a CNS disorders treatment drug	18
2.5. Nasal patches	20
3. Methods	22
3.1. Chemicals.....	22

3.2. Instruments and equipments	23
3.3. Simulated nasal fluid preparation	24
3.4. Chromatographic method	24
3.4.1. Standard solution preparation	24
3.4.2. First method	24
3.4.3. Second method	25
3.4.4. Third method	25
3.4.5. Fourth method	25
3.5. Validation of chromatographic method	26
3.5.1. Selectivity	26
3.5.1.1. Standard solution preparation	26
3.5.1.2. Tartaric acid solution preparation	26
3.5.1.3. Excipient in the simulated nasal fluid sample preparation	26
3.5.2. System suitability	27
3.5.3. Linearity	27
3.5.4. Precision	27
3.5.4.1. Sample solution preparation	28
3.5.4.2. Repeatability	28
3.5.4.3. Intermediate precision	29
3.5.5. Recovery	29
3.5.5.1. Sample solutions preparation	30
3.5.6. Limit of detection	31
3.5.7. Limit of quantitation	31
3.5.8. Robustness	32
3.6. Filtration compatibility	32
3.7. Stability in SNF	33
3.8. Nasal mucosa preparation	33
3.9. Nasal patch preparation	34
3.10. Nasal patch characterization	35
3.10.1. Physical appearance	35
3.10.2. Diameter and length	35

3.10.3.	pH determination of the patch Surface	35
3.10.4.	Mechanical properties assessment	35
3.10.4.1.	% Elongation at break	35
3.10.4.2.	Tensile strength	36
3.10.5.	Mucoadhesive properties assessment	36
3.10.5.1.	Detachment force	36
3.10.5.2.	Falling liquid test	37
3.11.	Content uniformity	38
3.12.	Release study	38
3.13.	Ex-vivo permeation study	39
3.14.	Release Kinetics	41
3.15.	Stability study	42
4.	Result	43
4.1.	Chromatographic method optimization	43
4.2.	Validation of analysis method	45
4.2.1.	Selectivity	45
4.2.2.	System suitability	46
4.2.3.	Linearity	46
4.2.4.	Precision	47
4.2.4.1.	Repeatability	47
4.2.4.2.	Intermediate precision	48
4.2.5.	Recovery	48
4.2.6.	Limit of detection and Limit of quantitation	49
4.2.7.	Robustness	49
4.2.7.1.	Column oven temperature robustness	49
4.2.7.2.	Wavelength	50
4.2.7.3.	Flow rate robustness	50
4.2.7.4.	Buffer pH robustness	51
4.2.7.5.	Mobile phase composition robustness	51
4.2.8.	Filtration compatibility	52
4.2.9.	Stability in SNF	52
4.3.	Nasal patch characterization	53

4.3.1. Physical appearance	53
4.3.2. Diameter and length	53
4.3.3. Mechanical properties assessment	54
4.3.3.1. %Elongation at break	54
4.3.3.2. Tensile strength	55
4.3.4. Mucoadhesive assessment	56
4.3.4.1. Detachment test	56
4.3.4.2. Falling liquid test	57
4.4. Content uniformity	57
4.5. Release study	58
4.6. Ex-vivo Permeation study	59
4.7. Release kinetics	60
4.8. Stability Study	62
5. Discussion	63
5.1. Method Optimization	63
5.2. Method Validation	64
5.2.1. Selectivity	65
5.2.2. System Suitability	65
5.2.3. Linearity	65
5.2.4. Precision	66
5.2.4.1. Repeatability	66
5.2.4.2. Intermediate Precision	67
5.2.5. Recovery	67
5.2.6. Limit of detection and limit of quantitation	68
5.2.7. Robustness	69
5.3. Filtration Compatibility	71
5.4. Stability in SNF	71
5.5. Nasal tissue preparation	72
5.6. Nasal Patch preparation	75
5.7. Nasal patch Characterization	79
5.7.1. Physical Appearance	79
5.7.2. Diameter and length	80

5.7.3. pH determination of the patch Surface	80
5.7.4. Mechanical properties assessment	81
5.7.4.1. % Elongation at break	81
5.7.4.2. Tensile strength	83
5.7.5. Mucoadhesive test	84
5.7.5.1. Detachment test	84
5.7.5.2. Falling liquid test	85
5.8. Content Uniformity	87
5.9. Release and Ex-vivo permeation study	88
5.10. Stability Study	91
5.11. Conclusion	92
5.12. Further work	94
6. References	95
Abstract in Arabic	121

List of Tables

Number	Table Caption	Page
3.1	Composition of the fabricated nasal patches	34
4.1	Characteristics the tested chromatographic methods.	45
4.2	Peak area and RT of 5 repeated injection of 20 $\mu\text{g ml}^{-1}$ standard solution of RvT.	46
4.3	The average peak area and the RSD% for the 3 replicates of the same concentration in the linearity curve, n=3.	46
4.4	The assay for repeatability result for 6 artificial sample solution preparation under the same condition	47
4.5	The assay results for intermediate precision: inter-day, inter-instrument, and inter-person precision.	48
4.6	The recovery study results, n=3.	48
4.7	Column oven temperature robustness results.	49
4.8	Wavelength robustness results.	50
4.9	Flow rate robustness results.	50
4.10	Buffer pH robustness results.	51
4.11	Mobile phase composition (ACN: MeOH: Buffer) robustness results.	51
4.12	Filtration compatibility result for 20 $\mu\text{g ml}^{-1}$ RvT sample solution; filter size, 0.45 μm , 32mm for each type, n=3.	52
4.13	The % stability in SNF result for RvT standard solution of 20 $\mu\text{g.ml}^{-1}$ for 24 and 48 hours in different condition, n=3.	52
4.14	The Diameter and the length for the nasal patches, for F1, F2, F3, and F4, n=6	53
4.15	The content uniformity result for each formula, n=10.	57

4.16	Permeation parameters for RvT in each formula.	59
4.17	Summery for model fitting values.	61
4.18	The result for stability study of RvT in the formulation under controlled normal condition (30 °C, 65 RH), n=5.	62

List of Figures and Plates

Number	Figure Caption	Page
1.1	Summary for the invasive and the non-invasive techniques that are used for CNS drug delivery (Yu et al., 2017; Barnabas, 2019; Xie et al., 2019).	2
1.2	Sagittal section of the nasal cavity, represents the main regions in the nasal cavity with the main part of the respiratory region (Gänger and Schindowski 2018).	4
1.3	The position and the spreading of the olfactory nerve (Davergaon and Nagar 2017)	5
1.4.	The pathways for drug molecule to transport through the olfactory or respiratory region to the CNS, 1) enter-axonal transport. 2) axonal transport. 3) transcellular. 4) paracellular. (Gänger and Schindowski 2018).	7
1.5	Rivastigmine tartrate structure, rivastigmine (above) and tartaric acid (below) (ChemicalBook 2021).	11
3.1	Scheme draw for the falling liquid apparatus.	38
3.2	Scheme draw to illustrate Franz cell parts and the mechanism of ex-vivo permeation study using Franz cell (Pund, Rasve and Borade, 2013).	40
4.1	Chromatogram of the first method. Sample concentration, $4\mu\text{g ml}^{-1}$; mobile phase, MeOH: ACN: ammonium buffer (15:15:70); column, C18 250 x 4.6 mm, 5 μm ; column oven temperature, 40 °C; flow rate, 1.5 ml.min ⁻¹ ; wavelength, 215 nm; injection volume, 20 μl .	43
4.2	Chromatogram of the second method. Sample concentration, $4\mu\text{g ml}^{-1}$; mobile phase, MeOH: ACN: ammonium buffer (20:20:60); column, C18 250 x 4.6 mm, 5 μm ; column oven temperature, 40 °C; flow rate, 1.5 ml.min ⁻¹ ; wavelength, 215 nm; injection volume, 20 μl .	43
4.3	Chromatogram of the third method. Sample concentration, $4\mu\text{g ml}^{-1}$; mobile phase, MeOH: ACN: ammonium buffer (25:25:50); column, C18 250 x 4.6 mm, 5 μm ; column oven temperature, 40 °C; flow rate, 1.5 ml.min ⁻¹ ; wavelength, 215 nm; injection volume, 20 μl .	44
4.4	Chromatogram of The Fourth Method for $4\mu\text{g ml}^{-1}$ RvT solution, Mobile phase: Methanol: Acetonitrile: Buffer (30:30:40), C18 column (250 x 4.6 mm; 5 μm) at 40° C, flow rate of 1.5 ml.min ⁻¹ , at 215 nm detector, and 20 μl injection volume.	44
4.5	The selectivity chromatograms of: Data 1, 20 $\mu\text{g.ml}^{-1}$ RvT standard; Data 2, 7.9 $\mu\text{g.ml}^{-1}$ tartaric acid; Data 3, SNF + excipients.	45
4.6	The linearity curve of RvT, n=3.	47
4.7	Nasal Patches appears to be transparent and colorless, and no remarkable visual difference between formulas.	53

4.8	Elongation percent result for each formula F1, F2, F3, and F4, calculated according to the equation (7) in section 3.10.4.1 . n=6.	54
4.9	Tensile Strength for each formula, A) Tensile profile, B) Tensile strength, n=6.	55
4.10	The detachment force (N) between the nasal patch and the nasal mucosa for each formula F1, F2, F3, and F4 using texture analyzer, n=6.	56
4.11	Falling liquid test; flow, 0.5 l.h ⁻¹ , n=3.	57
4.12	The release result carried out using sample tubes filled with 5 ml of SNF at 35 °C, result plotted in term of % released of RvT vs. time for F1, F2, F3, and F4, n=3.	58
4.13	The result for Ex-vivo permeation study of RvT through nasal mucosa tissue using Franz cell filled with 12 ml SNF at 35 °C with effective permeation area 1.767 cm ² , n=3.	59
4.14	The models fitting result for F1, F2, F3, and F4.	60
4.15	Plotting of residual data.	61
4.16	The % released of rivastigmine F1, F2, F3, and F4 for each formula in basket dissolution apparatus for 1 hour.	61
5.1	A) the olfactory and the respiratory region in the medial part of the sheep nasal cavity. B) the olfactory and the respiratory region of the lateral part of the sheep nasal cavity.	74
5.2	A schematic representation of the mechanism for the HPMC/gelation film and the plasticizing effect of HPMC (Liu et al. 2020).	82
5.3	Description for the adsorption theory and the regions of interaction between mucin protein and HPMC polymer at room temperature and under normal atmospheric pressure (Tangri and Madhav 2016).	85
5.4	The physical state of the gelatin solution according to the change of temperature, as the viscosity of the solutions a> b> c (Zhou et al. 2018)	87
5.5	Scheme draw illustrates the diffusion and the adsorption theory for the interaction between the mucin protein and HPMC polymer (Tekade et al. 2019).	87
5.6	The nasal patch shape after exposure to 35 °C	89

List of Abbreviations

Abbreviation/ Symbol	Definition
Ach	Acetylcholine
AChI	Acetylcholinesterase inhibitor
Avg	Average
ACN	Acetonitrile
AD	Alzheimer disease
AUC	Area under the curve
BBB	Blood-brain barrier
BChI	Butyrylcholinesterase inhibitor
CDER	Center for Drug Evaluation and Research
CNS	Central nervous system
FDA	Food and Drug Administration
FIDI	Facial intradermal injection
GIT	Gastrointestinal tract
HPLC	High Performance Liquid Chromatography
ICH	International Conference on Harmonization
IV	Intravenous
LOD	Limit of Detection

LOQ	Limit of Quantitation
MCC	Mucociliary clearance
MeOH	Methanol
N	Number of theoretical plates
NLT	Not Less Than
NMT	Not More Than
OM	Olfactory mucosa
PG	Propylene Glycol
RSD	Relative Standard Deviation
RvT	Rivastigmine Tartrate
RT	Retention Time
CU	Content Uniformity
SNF	Simulated Nasal Fluid
TF	Tailing Factor
USP	United States Pharmacopeia
UV	Ultraviolet
CSF	Cerebrospinal fluid

**FORMULATION AND EVALUATION OF NASAL PATCH
FOR NOSE-TO-BRAIN DRUG DELIVERY OF
RIVASTIGMINE**

BY

Lena “Mohammad Bassam” Shaghlil

Supervisor

Dr. Anas Adeeb Al-Shishani

ABSTRACT

Nose-to-Brain drug delivery can bypass blood-brain-barrier through the olfactory region using different devices and dosage forms. In this work we aim to fabricate and characterize a novel dosage form (Nasal patch) containing Rivastigmine tartrate. Analysis method for rivastigmine tartrate was optimized and validated. Four nasal patches were fabricated using gelatin/HPMC matrix in a different ratios and grades. The fabricated nasal patches were characterized in terms of physical appearance, surface pH, diameter and length, mechanical properties, and mucoadhesive behavior. The content uniformity, release profile, permeation of rivastigmine tartrate were also investigated. The release profiles for all nasal patches were fitted to kinetics model. Finally, the physical stability of the dosage form and the rivastigmine tartrate were also investigated. Formula F2 appeared to be a

promising formula, since it possesses the best sustained release profile with the best adhesive behavior and an acceptable elasticity and appearance.

Keywords: Nasal drug delivery, Nose-To-Brain, Rivastigmine, Nasal patch, Gelatin, HPMC, HPLC, method validation.

Chapter (1) Introduction

1.1. Drug delivery to the central nervous system (CNS)

Delivery of drugs to the brain remains a challenge in the development of valuable agents, mainly due to the nature of the blood brain barrier (BBB) which is a highly selective barrier in the human body (Wang and Wu, 2017). This may justify why CNS diseases -as Alzheimer's disease- are hardly intervened by a non-invasive method that requires passing through BBB (Chen, Li and Gao, 2019; Saeedi *et al.*, 2019).

The main route of brain drug delivery is the invasive routes that offers direct delivery system. Invasive methods, such as intrathecal, intracerebral, intracranial and direct injection to the brain, based on the transient modulation of blood-brain barrier, have many unfavorable side effects such as pain with a high incidence of neurotoxicity, hemorrhage, CNS infection, increasing in intracranial pressure, leaving an injury with glial scars (Emborg and Kordower, 2000). Moreover these methods show a slow rate of drug distribution within the cerebrospinal fluid (CSF) and require specialized trained persons with professional techniques, leads to be very limited for administration and unsuitable for chronic administration (Emborg and Kordower 2000; Pathan et al. 2009; Yu et al. 2017; Meng et al. 2019; Fang et al. 2017). However, looking for various alternative non-invasive

techniques with systemic drug administration is highly indispensable. These methods are summarized in **Figure 1.1**.

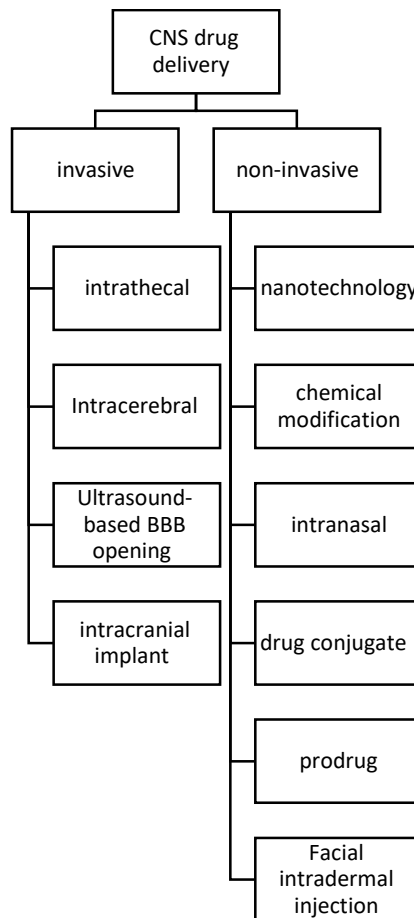


Fig. 1.1. Summary for the invasive and the non-invasive techniques that are used for CNS drug delivery (Barnabas 2019; Xie et al. 2019; Yu et al. 2017)

Interestingly, the intranasal delivery was found to be one of the noninvasive routes that drugs travel directly along neural pathways to the brain. It offers a pathway that bypasses the BBB quickly and efficiently (Gonçalves et al. 2019; Fine et al. 2020).

1.2. Nasal drug delivery

Previously, nasal drug delivery was mainly used for local and systemic therapies due to its high vascularization, high permeation and low enzymatic activity. In addition, the direct connection between the brain and nasal cavity through olfactory and trigeminal neurons was recognized for better brain targeting of drugs (Salazar et al. 2019; Alexander et al. 2020). Distinctively, nasal drug delivery is also used for vaccination since lymphoid tissue accommodate in the nose which offers a suitable needle-free protection (Hussein et al. 2020).

Traditionally, nasal drug delivery expressed safe, reliable, self-administrated and accomplish higher and faster levels of drug absorption, rapid onset of action, lower enzyme levels - compared to gastrointestinal tract and the liver- that enhances bioavailability (Akel, Ismail, and Csóka 2020).

1.3. Nasal Anatomy

Generally, the nasal cavity consists of three main regions as demonstrated in **Figure 1.2**. Posteriorly, the main two regions which comprise firstly the "respiratory" region where turbinates are located as inferior, middle and superior regions. The second region is the "olfactory" region located in the superior part of the nose as shown in Figure 1.2. The nose is separated into two sections by the "nasal septum". The nasal cavity is characterized by a surface is about 180 cm² , length about 12–14 cm and a pH range of about

5.5–6.5, In the nasal cavity, the temperature is slightly below the human body temperature and ranges between 32 and 35 °C (Salade et al. 2019). The nasal passage is about 12–14 cm deep from the nasal vestibule to the nasopharynx and has a volume of about 16–19 cm³ for both cavities (V. Pandey et al. 2019; Crowe et al. 2018). The olfactory region mucosa, which is the mucus-secreting membrane in the upper part of the nose that contains cells and neuron that are responsible for initiating olfactory sensation (Salazar et al. 2019).

The respiratory area has the largest surface area about 130 cm² which represents ~72% of the total surface area of the nose. It is covered with a

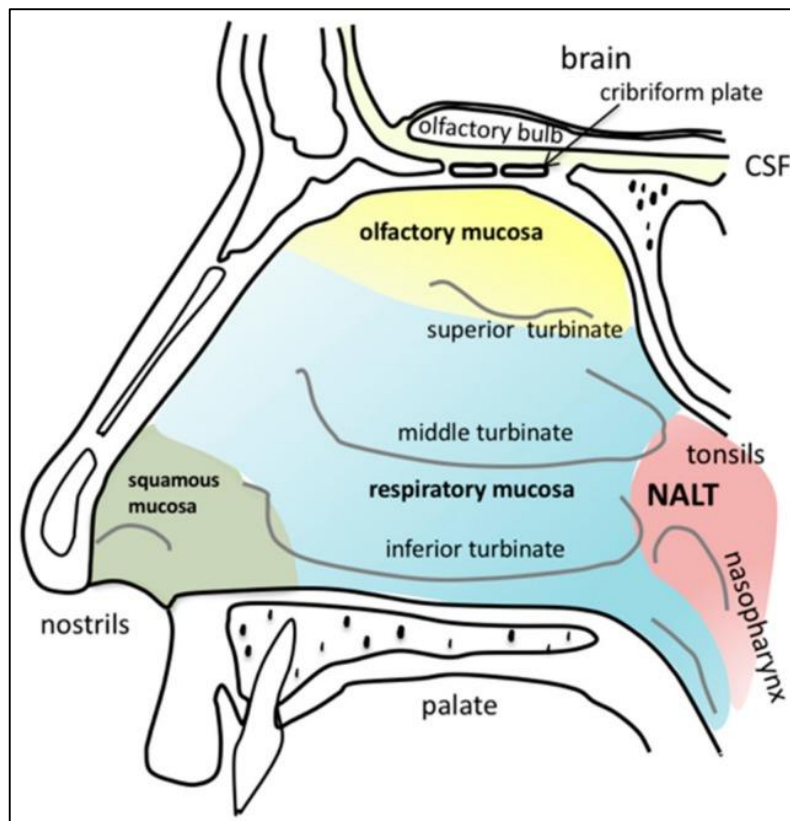


Fig. 1.2. Sagittal section of the nasal cavity, represents the main regions in the nasal cavity with the main parts of the respiratory region (Gänger and Schindowski 2018).

dense layer of mucus which facilitates the drug absorption for a drug. The ciliary mucus layer contains ~ 95% water, ~2% mucin, which is a protein, and the rest of ~3% are salt, albumin, lysozymes, lactoferrin, immunoglobulins and lipids (Hussein et al. 2020).

The olfactory region, which is below the cribriform plate of the ethmoid bone, is the most interesting and important region for transporting the drug to the brain and CSF it has a surface area of about 15 cm² which occupies around 20% of the nasal cavity as shown in **Figure 1.3**.

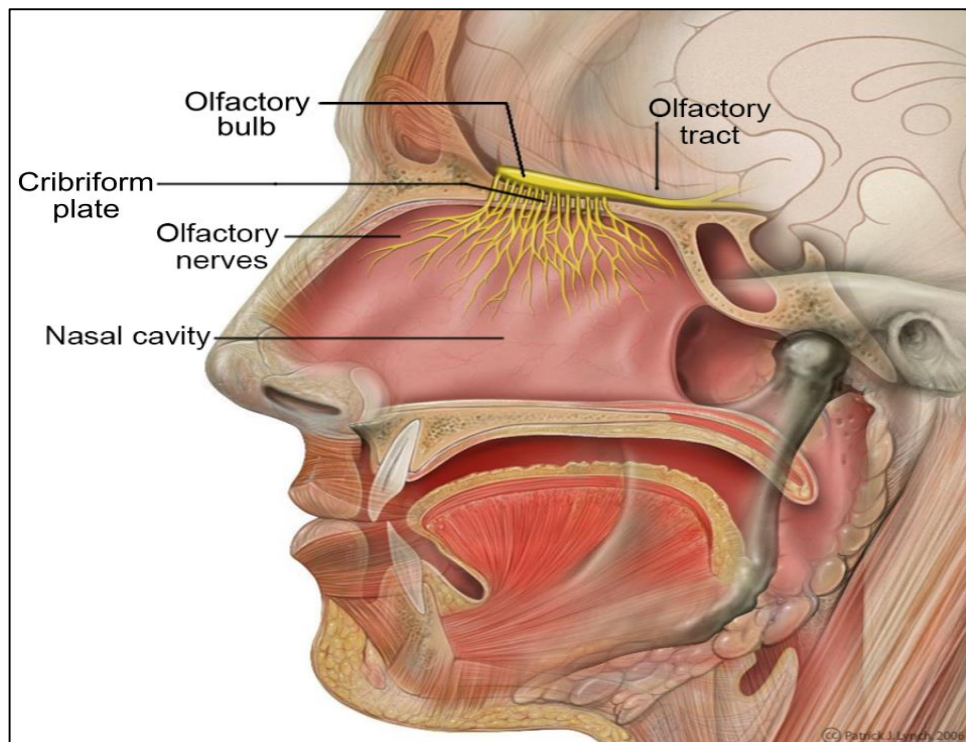


Fig. 1.3. The position and the spreading of the olfactory nerve (Davergaon and Nagar 2017).

1.4. Nose-to-brain drug delivery

There are two main pathways for any drug to reach the brain through the nasal route: Systemic pathway, which passes through respiratory region, and neuronal pathway, which pass the olfactory region (Agrawal et al. 2018).

1.4.1. The systemic pathway

The drug molecules follow the systemic pathway mainly when it reaches the respiratory region, which is an extremely vascular region. Consequently, if the drug molecule reaches this region, which will be transported by nasal epithelium through paracellular or transcellular route, where the paracellular route transports mainly the hydrophilic small molecules through the tight junction. In contrast, the transcellular route transports the lipophilic drug through either passive diffusion, receptor mediated transport, or endocytosis, which then passes through the vascular lamina propria. Molecules will finally reach the systemic circulation. This process requires passing the drug to the entire body organs and nerves which causes many side effects. Because of BBB, only the lipophilic drug molecule have more chances to reach the brain (Dinç, Bayar Muluk, and Vonakis 2020; Sekerdag 2017; Agrawal et al. 2018; Salazar et al. 2019).

1.4.2. The neuronal pathway

The drug molecules follow the neuronal pathway mainly through the olfactory region. The drug interacts majorly with the receptors in olfactory

neurons endings and as minor contact with trigeminal neurons. The drug moves through neuronal route transportation mechanism by axonal or enter-axonal pathway. Furthermore, the drug will be able to follow the nerve channel that is created by the olfactory ensheathing cells, passing through the cribriform plate and reaching the CSF. The axonal pathway delivers the drug directly to the brain but it requires very long onset of action and very with high lipophilic characteristic, The enter-axonal pathway through the ensheathing cells allows a rapid onset of action and wider range of molecules to be delivered (Djupesland, Messina, and Mahmoud 2014; Agrawal et al. 2018; Salazar et al. 2019; Sekerdag 2017; Dinç, Bayar Muluk, and Vonakis 2020). All pathways are described in **Figure 1.4**.

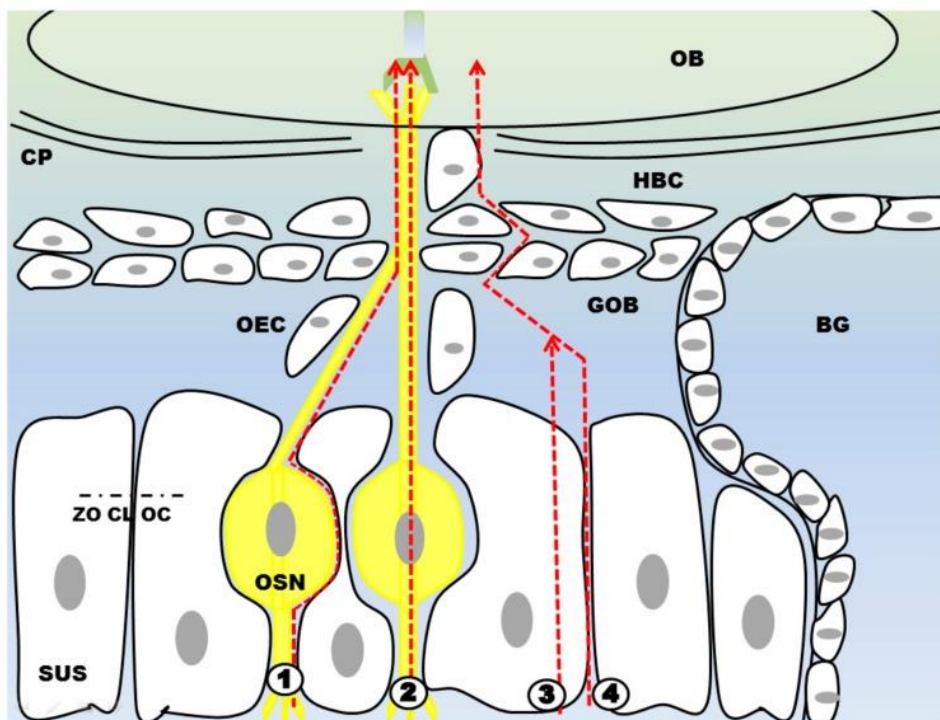


Fig. 1.4. The pathways for drug molecule that are transported through the olfactory or respiratory region to the CNS, 1) enter-axonal transport. 2) axonal transport. 3) transcellular. 4) paracellular. (Gänger and Schindowski 2018).

One of the main challenging limitations for drug absorption through nasal cavity is the mucociliary clearance (Erdő et al. 2018). It has been found that drugs was washed off within about 15 min, this making it challenging for hydrophilic drugs -such as Rivastigmine- to be efficiently absorbed and transported across the nasal membrane. To solve this issue, mucoadhesive system was proven to be the most promising approach that effectively increases residence time (Leal, Smyth, and Ghosh 2017).

1.5. Factors affecting drug transportation

The mechanism of drug transportation from nose-to brain depends on four factors type: 1) The physio-chemical properties of the drug such as the molecular weight, solubility, dissolution rate, logP, pka, charge, polarity, particle size, and polymorphism. 2) The formulation factor such as the excipient, pH, buffer capacity, dosage form and the drug concentration. 3) The physiological condition of the patient such as nasal blood flow, mucociliary clearance, enzymatic degradation, nasal mucus and the deposition of the formulation. 4) The administration factors such as the administration process or procedure and the device parameter which determine the rejoin where of the drug deposit (Hussein et al. 2020; Sekerdag 2017).

Some drugs, which are used intranasally showed high efficacy in treatment of CNS disorders compared to other routes of administration. For instance, Risperidone which acts as antipsychotic dopamine antagonist, Venlafaxine and Duloxetine used in the treatment of patients with major depressive disorder who exhibit emotional and painful physical symptoms, all showed improved status conditions. Erythropoietin is used in treatment of hypoxic/ischemic cerebral damages, influence a neuroprotective effect. Clonazepam which displays muscle relaxant when it was used as anticonvulsant, sedative and hypnotic drug. The effectiveness of Buspirone hydrochloride drug used to treat anxiety caused by smoking cessation or alcohol craving was demonstrated obviously after intranasal administration of the drug (Mittal et al. 2014).

Rivastigmine tartrate (RvT) is a semisynthetic drug from physostigmine extracted from (*Physostigma venenosum*) seed. RvT proved its efficacy for treating dementia associated with AD patient as well as Parkinson's disease (PD) for being selectively AChE and BuChE pseudo-irreversible inhibitor. It is an alkaloid with a half-life about 1.5 hour but its activity lasts for about 10 hours (Dehpour 2021; Eldufani and Blaise 2019). RvT is rapidly absorbed orally with 35.5% bioavailability and 40% protein bound, while it reaches its maximum concentration in the CSF after 1.4-3.8 hour, (Dehpour 2021; Eldufani and Blaise 2019).

RvT is available in the market as an oral dosage of capsules in 4 strengths (1.5mg, 3mg, 4.5mg, and 6mg) and as transdermal patch (4.6mg/24hr, 9.5mg/24hr and 13.3mg/24hr). Oral administration of RvT showed many incidences of side effects such as diarrhea, nausea, vomiting, and anorexia, dizziness, drowsiness, headache, agitation, cough, myalgia, malaise, fatigue, sweating, bradycardia, dyspepsia, (Dehpour 2021). On the other hand, transdermal patches increase tolerance of RvT and reduces the gastrointestinal side effects. However, other side effects were provoked such as complete heart block, atrioventricular block, fainting, slow heart rate and skin irritation (J.K. ARONSON MA, DPhil, MBChB, FRCP, FBPharmacolS 2010).

RvT is one of the widely used, most-known acetylcholinesterase inhibitor (AChI) for AD and Parkinson patient (Eskander et al. 2005). It was proved to affect the behavioral and psychological symptoms of dementia including apathy, anxiety, depression, delusions, cognition and hallucinations, due to its dual inhibition effect of acetyl- and butyryl-cholinesterase (T. H. Chen et al. 2017; Değirmenci and Keçeci 2016).

RvT is a weak base with pKa value about 8.8, reported solubility about 15 mg.ml⁻¹ at 25 °C, molecular weight: 400.4 and logP about 2, the chemical structure shown in **Figure 1.5** (ChemicalBook 2021).

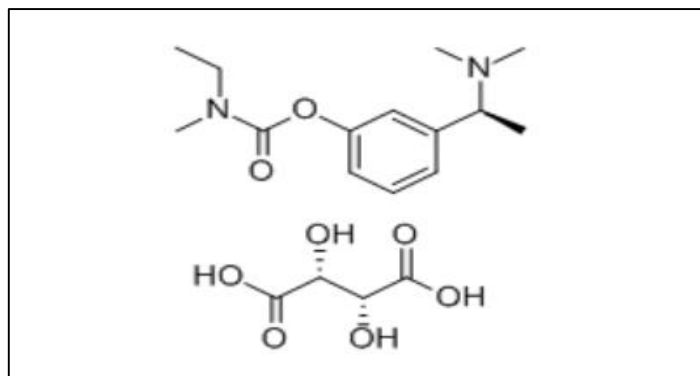


Fig. 1.5: Rivastigmine tartrate structure, rivastigmine (above) and tartaric acid (below) (ChemicalBook 2021).

1.6. Importance of the study

The aim of our study is to formulate new dosage form as nasal patch for a promising noninvasive route of administration (Nose-to-Brain) loaded with RvT to reduce side effects by bypassing systemic circulation and enhance patient compliance and tolerance. Designing novel mucoadhesive nasal patches will help in overcoming limitations of oral or systemic route and serve a wider range of patients suffering from brain disorder diseases.

1.7. Objectives of the study:

- Formulation of several nasal patches using different grades and concentration of hypromellose polymer.
- Characterization of the prepared patches by in-vitro strategies.
- Evaluation of release, permeation properties and content uniformity of each formula prepared.
- Validating an analytical method for nasal patch-loaded with RvT
- Determination of the stability of the formula and the RvT content in each of the prepared patches

Chapter (2) Literature Review

The intra-nasal pathway shows a promising novel pathway, where molecules can reach the CNS by passing the BBB (Onur 2004). Preferably, the nasal pathway can be used commonly for local, systemic or CNS drug delivery (Erdő et al. 2018).

2.1. The history of nasal administration

Before time, Red Indians in North America used the milled leaves of *Ranunculus acris* to relieve headaches and as tobacco for nasal snuffing. Indian tribes in Brazil use V-shaped tools known as “Tipi” to blow powdered tobacco for enjoyment, relaxation, and to refresh their memories. The Chinese used the extract of aloe wood and sandal through the nasal route inhalation for treating emesis. Nowadays, the non-invasive nasal route is still a favorable route for drug abuse (Hussein et al. 2020). Chitosan-coated nanoemulsion nasal administration elicits a neuroprotective effect against LPS-induced memory deficits, neuroinflammation, and oxidative stress in Wistar rats (Fachel et al. 2020)

2.2. Nasal dosage forms

Several drugs dosage forms are formulated as non-invasive administration routes. Non-invasive oral route administration of drugs used to treat brain dysfunction was accompanied by disadvantages of bioavailability. For

example, Rivastigmine showed only 36% bioavailability and is markedly affected by food. It was also affected by serum protein in circulation (Patel, Surti, and Mahajan 2019).

Different nasal dosage forms have been introduced to achieve the best delivery to the systemic circulation or for local nasal delivery of drugs. These forms are nasal drops, nasal spray, nasal powder, nanoparticle, nasal in-situ gelling cationic nanostructured lipid carriers, nasal in situ gelling polymer, nasal microemulsion, nasal nanoemulsion, and thermosensitive hydrogels (Menzel *et al.*, 2017; Wavikar, Pai and Vavia, 2017; Tiozzo Fasiolo *et al.*, 2018; Chatterjee *et al.*, 2019; Pandey *et al.*, 2019; Wang *et al.*, 2019).

Nasal preparation of testosterone as NATESTO® was used as an emulsion for treating testosterone deficiency, which shows effectiveness compared to oral and transdermal therapy (Ko, Needham and Zia, 1998). Non-invasive insulin delivery Miacalcin ® or Minirin ® been introduced in the market as a nasal spray and showed positive effects and improving insulin signaling in the brain of patients with mild cognitive impairment /AD in all patients (Wingrove *et al.* 2019; Yan-hua Li *et al.* 2015; Christian 2014)

Midazolam is commonly used as first-line treatment in patients with acute seizures. Intranasal administration leads to rapid T_{max} , consistent, and improved absorption with fast distribution to the CNS, compared with oral

dosing. However, co-administration of moderate or strong CYP3A4 inhibitors should be avoided (Ren et al. 2021)

Prepared nasal spray of Diazepam for treatment of seizure clusters provided patients and caregivers with more control of their treatment and daily routine with transient and mild discomfort (Penovich et al. 2021).

Nasal spray of Esketamine when used in a combination with oral antidepressant shows better tolerability than oral antidepressant alone with potentially efficacious intervention for treatment-resistant depression both acute and in longer-term maintenance use (Citrome, DiBernardo, and Singh 2020; Fantasia 2020).

Antimigraine Rizatriptan intranasal spray formulation containing 20% w/w ethanol exhibited highest exposure, faster onset of action, and maintained higher concentration than oral tablets or capsules. (Chokshi et al. 2019).

The effect of Fentanyl pectin nasal spray compared to oral morphine in providing rapid analgesia was found to be superior, highly well-tolerated and adverse effects were minimal. (Mercadante et al. 2016).

The effect of nasal dosage form varies according to the solvent ,i:e, the deep eutectic solvents were prepared from malic acid and choline chloride which demonstrated lower melting point ($-59.1\text{ }^{\circ}\text{C}$) and higher viscosity (120,000 cP) compared to hydrogels based on sodium carboxyl methyl cellulose (Yang Li et al. 2019). Biocompatible deep eutectic solvents developed as

carriers for improving the nasal delivery of insulin were found to maintain unchanged conformational structure of insulin characterized by circular dichroism. On the other hand, *in vitro* results showed that insulin in deep eutectic solvent dissociated gradually but did not disintegrate immediately upon contact with water. This was able to significantly improve the hypoglycemic effect of insulin at different doses, compared with hydrogels or other solutions of insulin. In addition, no observation for evident toxicity to nasal epithelia after nasal administration to rats for seven consecutive days. (Yang Li et al. 2019).

Development of spray-dried pectin/hypromellose microspheres as efficient melatonin carrier for olfactory targeted nasal delivery was investigated (Nižić et al. 2020). Result showed that combining pectin with hypromellose at 1:3% (w/w) ratio resulted in the formation of microspheres with highest potential, highest swelling ability and most prominent mucoadhesive properties. In addition, adequate deposition profile at turbinate and olfactory was revealed using mono-dose nasal insufflator as nasal powder delivery device (Nižić et al. 2020).

To investigate how the addition of a mucoadhesive agent can influence the absorption of drugs into the brain, it was shown that Buspirone concentrations in the brain administrated intranasally was about 2.5-times higher than intravenous method (Erdó et al. 2018).

Loaded domperidone as a mucoadhesive microemulsion increases the systemic absorption / bioavailability through nasal delivery around 2 folds. In addition, fasten the onset of action and lower the hepatic metabolism comparing to the conventional nasal spray (Rathod et al. 2019).

The combination of nanosuspension and simple addition of sodium hyaluronate as a mucoadhesive agent presented a promising platform for the nasal delivery of Loratadine (Alshweiat et al. 2020). It was concluded that using a mucoadhesive agent is crucial to increase the contact time between the formula and nasal mucosa and reducing particle size. This enhanced mucoadhesive properties. The evidence from the in vivo studies, showed that administration of nasal nanosuspension-based mucoadhesive formulation of loratadine have bioavailability 5.54 fold higher than the oral dose (Alshweiat et al. 2020).

2.3. Nose-to-Brain drug delivery

Nose to brain delivery detour the BBB with variety of carrier systems. Neuro-therapeutic agents such as micro-molecules (micro emulsion of donepezil, and polymeric nanoparticles) and macromolecules (proteins, hormones, and stem cells) can be delivered via this route to prevent and manage different neurological disorders (Patel, Surti, and Mahajan 2019).

Intranasal drug delivery, a non-invasive technique, has superior advantage over other routes since drugs may enter into the blood circulation or directly

permeate to the brain, due to its highly vascularization and highly permeable tissues in this area (Graff and Pollack 2005). It also supports the unique connections between the brain and external environment provided by the anatomical structure of olfactory and trigeminal nerves (Salade et al. 2019; Menzel et al. 2017). One of previous studies showed that intranasal insulin improves attention, memory, and cognitive function in both AD-type dementia and non-AD-type dementia models (Crowe et al. 2018). Another study indicated that administration of drug deep into the nasal cavity, led to direct transmission of drug such as oxytocin into brain via olfactory pathway (Kozlovskaya, Abou-Kaoud and Stepensky, 2014). It was clearly reported that olfactory epithelium pathway is faster way of drug transportation, via paracellular mechanism into perineural space and transferred directly to the brain (Khan et al. 2017). In addition, improvement of pharmacokinetic/pharmacodynamics (PK/PD) profile for CNS acting drugs was found (J. Chen et al. 2008).

Facial intradermal injection (FIDI) might be a novel strategy for bypassing the BBB via the trigeminal nerve. Intradermal injection into the rat mystacial pad, elevated the brain sub-areas and trigeminal Evans Blue concentrations (Yu et al. 2017). It was demonstrated that FIDI increased the brain drug targeting efficiency, brain direct transport percentage and brain. Moreover, trigeminal perineurium, epineurium, perivascular spaces, neurons and

Schwann cells were also involved by this brain targeted delivery (Yu et al. 2017).

Beside the formulation aspect, it has been depicted that application of aerosol nasal drug requires a special device to allow its deposition to be absorbed in the nasal cavity which depends on the nasal mucociliary clearance (Inoue et al. 2018; Salade et al. 2019).

2.4. Rivastigmine as a CNS disorders treatment drug

Oral Rivastigmine was first approved in the US in 2000, while the Rivastigmine transdermal system was approved in 2007 and since then, it has been used for patients with mild, moderate, and severe AD. Rivastigmine is used as transdermal patch form, showed a unique effect as a cholinesterase inhibitor.

Rivastigmine is studied in several forms, such as dry powder inhalation formulation, capsule, transdermal patches, nasal spray, nasal adhesive nanoparticle, nasal solid nanoparticles (Morgan and Soh 2017; Abouhussein et al. 2018; Simon et al. 2016; Malaiya et al. 2018; Shah et al. 2015; Articus, Hechenbichler, and Bornholdt 2011).

The efficacy of these forms varies among patients. It was found that transdermal patch of Rivastigmine was well tolerated than capsule form (Fuh et al. 2017), and have dose-dependent effect.

The Rivastigmine was used as nasal spray administration and investigated as single dose. The nasal spray of rivastigmine had outstanding absolute bioavailability compared to historical values for oral capsule and transdermal patch. It had rapid onset of action and a favorable safety and tolerability profile (Morgan and Soh 2017).

Investigation of another intranasal Rivastigmine as liposomes and cell-penetrating peptide modified liposomes revealed an improvement of Rivastigmine distribution in brain with enhanced pharmacodynamics and minimize side effects. (Yang et al. 2013).

Rivastigmine was also studied in a manner of brain targeting through the olfactory region. Investigation showed that the potential of nanostructured lipid carriers for nose to brain delivery of Rivastigmine was enhanced by incorporating into an in-situ gelling system, increasing retention in nasal cavity. Pharmacokinetics showed sustained release of intranasal and intravenous-nanostructured lipid carriers compared to rivastigmine solution by the same route. It showed significantly higher area under the curve (AUC) and T-half (Wavikar, Pai, and Vavia 2017). Moreover, nasal toxicity studies of nanostructured lipid carriers showed no signs of inflammation, maintaining the integrity of ciliary epithelial cell, thus confirming safety of the formulation for its

2.5. Nasal patches

Literature survey revealed that the known nasal patches studied till now are two nasal adhesive patches: for management of nasal impairments and for the dry nasal syndrome.

By the study of Laffleur *et al.* “The nasal patches containing naphazoline for management of nasal impairments”, the study aimed to formulate a solid dosage form as decongestant for local intranasal application. Nine formulations following the solvent evaporation method and based on gelatin and other polymers were manufactured. All patches were characterized according to uniformity of weight, thickness, transparency and surface pH, tensile strength and elongation at break. Adhesiveness was assessed by tack test, and bioadhesive assay on the nasal porcine mucosa. Naphazoline was incorporated in the different formulations and investigated for drug release, were the most prominent formulas were chosen according to the mucoadhesion and controlled drug release for the management of mucosal disorders (Laffleur et al. 2018).

The second nasal patch studied by Laffleur, 2018 as shown in her work “Nasal adhesive patches - Approach for topical application for dry nasal syndrome”, the study provides nasal adhesive formulations for treatment of dry nasal syndrome as a topical application. According to solvent evaporation method, mucoadhesive films were prepared consisting of

polymers such as gellan and carboxymethyl cellulose, 5 mucoadhesive films were evaluated in respect to their physicochemical properties, stability, disintegration behavior and tensile strength. Moreover, uptake capacity of adhesive films was investigated according to three assays vapor uptake, permeability and water uptake. Mucoadhesive assessment was carried out on porcine nasal mucosa in terms of adhesion time, wash off resistance and spreadability. A variety of humectants such as urea, Aloe vera, allantoin, and hyaluronic acid was incorporated in the formulations. All nasal adhesive films were convinced with their proficiency of mucoadhesiveness, and stability to be suitable in the management of dry nasal syndrome (Laffleur 2018).

Chapter (3) Methods

3.1. Chemicals

Rivastigmine Tartrate (API) was obtained from Anhui Puya Biological Technology co.,LTD (Shandong, china), tartaric acid obtained from local market, HPMC K4M and HPMC K100M was kindly received as a gift sample from Ashland Specialties (Belgium, BVBA), methanol HPLC grade and acetonitrile HPLC grade was obtained from Fisher Chemical (Belgium), Phosphoric Acid 85%, glycerol and propylene glycol (PG) was obtained from local market, silica gel high-purity grade and gelatin from porcine skin was obtained from Sigma-Aldrich (Munich, Germany) mucin from porcine stomach type 2 Sigma-Aldrich (Shanghai, China), ammonium phosphate dibasic obtained from Sigma-Aldrich (Ontario, Canada) di-Sodium hydrogen phosphate obtained from AZ Chem for chemicals (Selangor, Malaysia), sodium chloride (NaCl) salt and potassium chloride (KCl) obtained from Central Drug House (New Delhi, India), calcium chloride anhydrous obtained from Sigma-Aldrich (Tokyo, Japan), nylon syringe filter and PTFE syringe filter was obtained from local market, glass membrane (GF) syringe filter obtained from FilterBio® (Jiangsu, China), nylon filter obtained from Petratech (Jordan, Amman), pH test strips, pH-Fix 0–14, fixed indicator obtained from Macherey-Nagel GmbH & Co. KG® (Darmstadt, Germany), disposable insulin syringe obtained from Home care

(Berlin, Germany) and sheep nasal mucosa obtained from local slaughterhouse.

3.2. Instruments and equipments

Automated High Performance Liquid Chromatography (HPLC) system manufactured by Shimadzu (Tokyo, Japan) consisted of: LC20AT pump, SPD-20A photodiode array detector, SIL-20A Auto-sampler, CTO-20A temperature regulator oven. A (250 x 4.6 mm; 5 μ m) C18 reverse phase column manufactured by Fortis Technologies (Cheshire, United Kingdom), Manual HPLC system was manufactured by Shimadzu (Kyoto, Japan) consisted of: LC-20AT Pump, SPD-20A UV-Vis Detector, CTO-20A Column Oven and VI manual sample injector was obtained from FLOM (Tokyo, Japan), TA. XT plus Texture analyzer manufactured by Stable Micro Systems (Surrey, UK), Glass Franz diffusion cells, volume of receiver 12 mL, surface area of the receiver opening is 1.767 cm² manufactured by Perme gear (Road Hellertown, PA, USA), Dual syringe pump (Anhui, China), Water bath manufactured by Schutzart (Schwabach, Germany), Digital caliper micrometer obtained from local market, European 2-pin plug (Wertheim, Germany), aquarium pump obtained from local market, light microscope B-293 manufactured by OPTIKA (Ponteranica, Italy), MZ 2C NT vacuum pump was obtained from Vacuubrand (Wertheim, Germany), Inolab pH 720 pH-meter was manufactured by WTW (Oberbayern,

Germany), Bi-hydro still 4.1 water distillation apparatus was manufactured by POBEL (Madrid, Spain), plane tube 5 ml obtained from AFKO-DISPO (Amman, Jordan) and KMF 720 Constant climate chamber manufactured by BINDER (Shanghai, China). Dissolution apparatus PTWS 620I manufactured by PHARMA TEST (Hainburg, Germany).

3.3. Simulated nasal fluid preparation

The simulated nasal fluid was prepared by dissolving 14.196 g of di-sodium hydrogen phosphate (HNa_2PO_4); (molecular weight: $141.96 \text{ g.mol}^{-1}$) in 1 liter to achieve 0.1 molar phosphoric acid, which was adjusted to pH 6.5 using H_3PO_4 solution, and 8.77 g sodium chloride (NaCl), 2.98 g potassium chloride (KCl), 0.59 g calcium chloride (CaCl_2) was added to the phosphate buffer as mentioned in the work of (P. Pandey et al. 2017; Laffleur et al. 2018; Laffleur 2018).

3.4. Chromatographic method

3.4.1. Standard solution preparation

Standard solution of RvT for the chromatographic method was prepared by dissolving 40 mg of RvT in 100 ml of water, then 1 ml was diluted to 100 ml ($4 \mu\text{g.ml}^{-1}$).

3.4.2 First method

The mobile phase consists of mobile phase, Methanol (MeOH): acetonitrile (ACN): ammonium phosphate buffer (15:15:70). The ammonium buffer

consists of 0.065 molar di-basic ammonium phosphate which was adjusted with phosphoric acid (H_3PO_4) solution to pH 7.0. The detector was set at 215 nm; column, C18 (250 x 4.6 mm; 5 μm); flow rate, 1.5 mL/min; injection volume, 20 μL ; and column temperature 40°C.

3.4.3. Second method

The second method consists of mobile phase, MeOH: ACN: ammonium phosphate buffer (20:20:60). The phosphate buffer consists of 0.065 molar di-basic ammonium phosphate which was adjusted with H_3PO_4 solution to pH 7. The detector was set at 215 nm; column, C18 (250 x 4.6 mm; 5 μm); flow rate, 1.5 mL/min; injection volume, 20 μL ; column temperature, 40°C.

3.4.4. Third method

The third method consists of mobile phase, MeOH: ACN: ammonium phosphate buffer (25:25:50). The ammonium buffer consists of 0.065 molar di-basic ammonium phosphate which was adjusted with H_3PO_4 solution to pH 7. The detector was set at 215 nm; column, C18 (250 x 4.6 mm; 5 μm); flow rate, 1.5 mL.min⁻¹; injection volume, 20 μL ; column temperature, 40°C.

3.4.5. Fourth method

The fourth method consists of mobile phase, MeOH: ACN: ammonium phosphate buffer (30:30:40). The ammonium buffer consists of 0.065 molar di-basic ammonium phosphate which was adjusted with H_3PO_4 solution to

pH 7. The detector was set at 215 nm; column, C18 (250 x 4.6 mm; 5 μ m); flow rate, 1.5 mL.min⁻¹; injection volume, 20 μ L; column temperature, 40°C.

3.5. Validation of the optimum chromatographic method

3.5.1. Selectivity

Selectivity was assessed by preparing standard, tartaric acid and excipient solutions and injected each one into HPLC unit, then all the resulting chromatograms were compared to evaluate the interference.

3.5.1.1. Standard solution preparation

Standard solution of RvT was prepared by dissolving 20 mg of RvT in 100 ml of water, then 1 ml was diluted to 10 ml (20 μ g.ml⁻¹), the solution was injected into the HPLC unit and the chromatogram was obtained.

3.5.1.2. Tartaric acid solution preparation

Tartaric acid solution was prepared by dissolving 79 mg of tartaric acid in 100 ml of water, then 1ml was diluted to 100 ml (7.9 μ g ml⁻¹) which is equivalent to the concentration of tartaric acid in 20 μ g ml⁻¹ of RvT, the solution was injected to the HPLC unit and the chromatogram was obtained.

3.5.1.3. Excipient in the simulated nasal fluid sample preparation

Excipient solution was prepared equivalently to the maximum amount of each excipient in each one patch of formulations. An amount of each

excipient: 24 mg gelatin, 250 mg propylene glycol, 100 mg glycerol, 20 mg HPMC K4M, and 20 mg HPMC K15M, was dissolved in 100 ml of SNF with aid of stirring for 1 hour at 70°C, then 1 ml of the solution was diluted to 10 ml with SNF, the solution was filtrated and injected to the HPLC unit and the chromatogram was obtained.

3.5.2. System suitability

Standard solution of RvT was prepared by dissolving 20 mg of RvT in 100 ml of water, then 1 ml was diluted to 10 ml ($20\mu\text{g ml}^{-1}$), 5 injections of the sample solution was injected to the HPLC unit and the area under the curve (AUC) for each injection was obtained and RSD for all peaks injections.

3.5.3. Linearity

Linearity was performed by preparing 7 different concentrations of RvT, 8, 12, 16, 20, 24, 28 and $32\mu\text{g ml}^{-1}$ which are equivalent to 40%, 60% ,80% ,100% ,120% ,140% and 160% of the standard concentration, respectively. These solutions preparations were prepared from the same stock solution which was prepared by dissolving 20 mg of RvT in 100 ml, then a series dilution (0.4 ml, 0.6 ml, 0.8 ml, 1 ml,1.2 ml,1.4 ml and 1.6 ml) to 10 ml, and each solution was injected into the HPLC unit in triplicates.

3.5.4. Precision

The precision of the method was determined at two levels: repeatability and intermediate precision.

3.5.4.1. Sample solution preparation

The sample solution preparation for the precision evaluation was by preparing 6 artificial sample solutions following this procedure.

- Stock solution of RvT was prepared by dissolving 20 mg RvT in 100 ml SNF.
- Standard solution was prepared by dilution of 1 ml from stock solution up to 10 ml of SNF.
- Excipient solution was prepared by dissolving an equivalent amount of 10 nasal patches: 0.24 g gelatin, 2.5 g propylene glycol, 1 g glycerol, 0.2 mg HPMC K4M, and 0.2 mg HPMC K15M in 100 ml SNF.
- The artificial sample solution was prepared by transferring one ml of the excipient solution to 7 ml of SNF, stirred at 70 °C over a hot plate for one hour, then one ml of the stock solution was added and stirred at 70 °C over a hot plate for 15 minutes. Finally, the solution volume completed to 10 ml by SNF.

3.5.4.2. Repeatability

The repeatability was obtained by injecting 6 artificial sample solutions of 20 $\mu\text{g}\cdot\text{ml}^{-1}$ RvT containing excipient in SNF as described in 3.5.4.1. section, then each solution was filtrated using nylon syringe filter and injected to the

HPLC unit and the peak area was obtained, then the assay was calculated according to the following equation:

$$\% \text{Assay} = \frac{A_s}{A_{st}} * \frac{C_{st}}{C_s} * 100\% \dots \text{(1)}$$

A_s : Peak area of the artificial sample solution.

A_{st} : Peak area of the standard solution.

C_{st} : Standard concentration.

C_s : Artificial sample concentration

3.5.4.3. Intermediate precision

The intermediate precision was obtained by injecting 6 artificial sample solutions of $20 \mu\text{g}\cdot\text{ml}^{-1}$ RvT containing excipient in SNF as described in **3.5.4.2.** section, then each solution was filtrated using nylon syringe filter and injected to the HPLC unit and the peak area was obtained. This procedure is repeated in different days (inter-day), and then tested using different instruments; the automated HPLC and the manual HPLC (inter-Instrument), and by different persons; me and my lab partner Asmaa Abu Sa'aleek (inter-person). then assay was calculated according to the previously mentioned **equation (1)**.

3.5.5. Recovery

Recovery was studied at 50%, 100% and 150 % of standard solutions which is equivalent to 10, 20 and $30 \mu\text{g ml}^{-1}$ of RvT, respectively, where the preparation procedure described in **3.5.5.1.** section. Three replicates from

each level were prepared with excipient equivalent to one nasal patch, as described in section **3.5.5.1**, to have 9 determination solutions each, then each solution was filtrated using nylon syringe filter and injected to the HPLC unit, and the peak area was obtained to calculate the % recovery according to the following equation:

$$\% \text{ Recovery} = \frac{A_r}{A_{st}} * \frac{C_{st}}{C_r} * 100 \dots (2)$$

Ar: Peak area for recovery sample solution.

Ast: Peak area for standard solution.

Cr: Concentration of recovery sample.

Cst: Concentration of standard solution.

3.5.5.1. Sample solutions preparation

The sample preparation for the recovery test was achieved by preparing two stock solutions:

- The first stock solution was prepared by dissolving 20 mg of RvT in 100 ml SNF.
- The second stock solution was prepared by dissolving an excipient amount equivalent to 10 patches (0.24 g Gelatin, 2.5 g Propylene Glycol, 1 g Glycerol, 0.2 mg HPMC K4M, and 0.2 mg HPMC K15M) in 100 ml SNF.

- The standard solution was prepared by diluting 0.5, 1 and 1.5 ml of the first stock solution up to 10 ml SNF to achieve concentrations of 10, 20, and 30 $\mu\text{g}\cdot\text{ml}^{-1}$, respectively, of standard solution.
- The recovery sample solution was prepared by transferring 0.5, 1 and 1.5 ml of the first stock solution each to 10 ml volumetric flask, and 1 ml of the second stock solution was transferred to the same volumetric flask before diluting each up to 10 ml by SNF to achieve concentration of 10, 20, and 30 $\mu\text{g}\cdot\text{ml}^{-1}$, respectively, of artificial sample solution, then each solution was stirred for 15 min over a hot plat at 70°C.

3.5.6. Limit of detection

The limit of detection (LOD) of the HPLC method was determined using the SD and the slop (S) of the linearity curve according to the following equation (ICH guidelines Q2(R1) 2005):

$$\text{LOD} = 3.3 * \frac{\text{SD}}{\text{S}} \dots \text{(3)}$$

3.5.7. Limit of quantitation

The limit of quantification (LOQ) of the HPL C method was determined using the SD and the slop (S) of the linearity curve according to the following equation(ICH guidelines Q2(R1) 2005):

$$\text{LOQ} = 10 * \frac{\text{SD}}{\text{S}} \dots \text{(4)}$$

3.5.8. Robustness

The robustness of the chromatographic method was studied by preparing 20 $\mu\text{g}\cdot\text{ml}^{-1}$ solution of RvT and injected it to the HPLC unit with slight modifications on analytical method conditions. The modifications were on column oven temperature 38 $^{\circ}\text{C}$, 40 $^{\circ}\text{C}$, and 42 $^{\circ}\text{C}$, wavelength 214 nm, 215 nm, and 216 nm, flow rate 1.4 $\text{ml}\cdot\text{min}^{-1}$, 1.5 $\text{ml}\cdot\text{min}^{-1}$, and 1.6 $\text{ml}\cdot\text{min}^{-1}$, buffer pH 6.9, 7, and 7.1, mobile phase composition (44:28:28, 40:30:30, and 38:32:32) (ACN: MeOH: Buffer), then the RSD for the retention time (RT), area under the curve (AUC), tailing factor and number of theoretical plates (N) determined to check the robustness of the method.

3.6. Filtration compatibility

Filtration compatibility was investigated using 20 $\mu\text{g}\cdot\text{ml}^{-1}$ standard solution of RvT. The RvT solution was injected to HPLC unit without filtration, then the solution was filtrated using different syringe filter types; nylon, PTFE, and glass. 4 ml was filtrated and each ml was collected in a separated vial, three filter was assessed from each type to obtain 3 replicates for each sample, then each sample was injected to the HPLC unit and peak area was compared to the peak area of the non-filtrated solution according to the following equation:

$$\% \text{ Filtrated} = \frac{\text{Peak area of filtrate solution}}{\text{Peak area of non filtrate solution}} * 100\% \dots (5)$$

3.7. Stability in SNF

One nasal patch was dissolved in 100 ml SNF, then stored in room temperature inside amber and transparent container, in refrigerator inside amber and transparent container, and at temperature 35°C. Each solution was injected at a predetermined point: 24h, 48h and 72h and the peak area compared to freshly prepared standard solution each time point of RvT, then the % stability was calculated according to the following equation:

$$\% \text{ Stability} = \frac{P_s}{P_{ss}} * \frac{C_{ss}}{C_s} * 100\% \dots (6)$$

P_s : Peak area of standard solution.

P_{ss} : Peak area of freshly prepared standard solution.

C_s : Concentration of standard solution.

C_{ss} : Concentration of freshly prepared standard solution.

3.8. Nasal Mucosa Preparation

Sheep heads were obtained from a local slaughterhouse within 2 hours after the sheep were sacrificed. Firstly, the hair was removed using sharp knife, then the nose was removed from the head using electric bone sawing machine, then washed and stored in normal saline, then it was transported in an iced container. The sheep noses were stored in -80 °C freezer to avoid tissue damage. The nasal mucosa including the nerves was isolated carefully using surgical scalpel from each nostril (H. Y. Karasulu et al. 2008).

3.9. Nasal Patch Preparation

Nasal patches were prepared in a matrix form using gelation method based on quick melting step (Vasvári et al. 2018). This was achieved by mixing Water, glycerol and PG in the ratio 20:20:60 (v/v) respectively, then the mixture was degassed using vacuum pump for 2 hours with continuous magnetic stirring. The degassed mixture was added to the HPMC and gelatin mixture at percentages mentioned in **Table 3.1** up to volume 10 ml with continuous magnetic stirring for 1 hour on a hot plate at 70°C. After all ingredients were dissolved, RvT was added with continuous stirring for 15 min, then the solution was filled in a 1 ml syringe with internal diameter of 5 mm and sealed tightly using parafilm to avoid solvent loss. The mixture was left over night at room temperature to solidify. One nasal patch contains 0.4 ml of the solidified gel.

Table 3.1. Composition of the fabricated nasal patches

Formula Number	Gelatin (W/W)	HPMC K4M (W/W)	HPMC K100M (W/W)	Propylene Glycol (W/W)	Glycerol (W/W)	Water (W/W)	Drug (W/W)
F1	5.6%	1.9%	-	53.0%	21.8%	16.8%	0.9%
F2	3.7%	4.7%	-	52.4%	21.6%	16.7%	0.9%
F3	5.6%	-	1.9%	53.0%	21.8%	16.8%	0.9%
F4	3.7%	-	4.7%	52.4%	21.6%	16.7%	0.9%

3.10. Nasal Patch Characterization

3.10.1. Physical appearance

The physical appearance such as color, transparency and surface area roughness were assessed visually for every nasal patch. The odor was checked by smelling.

3.10.2. Diameter and length

The diameter and the length of the nasal patch was measured using electronic caliper for 6 samples from each formula.

3.10.3. pH determination of the patch surface

The surface pH was measured for 6 replicates of each formula using pH stripes with fix indicator, by spreading one drop of distilled water on the surface of the patch, then wait for one minute before contacting the strip with the witted patch. the color changing was compared with the manual of the strips to determine the pH value (Tedesco, Monaco-lourenço, and Carvalho 2016).

3.10.4. Mechanical properties assessment

3.10.4.1. %Elongation at Break

The elongation percentage at break was determined by using Texture Analyzer to measure the initial length of each formula. Each patch was fixed

horizontally to both probes of the texture analyzer using super glue. Both probes moved toward each other at 1 mm sec⁻¹ speed till rupture occurred. The length of the patch was recorded just before the break as length at break, the elongation percentage was calculated according to the following equation (Laffleur et al. 2018):

$$\% \text{Elongation} = \frac{(\text{Length at break} - \text{Initial Length})}{\text{Initial Length}} * 100\% \dots (7)$$

3.10.4.2. Tensile Strength

Tensile Strength was determined using Texture Analyzer by measuring the force needed to break the patch. It was performed by fixing the patch horizontally to each probe using super glue, then the upper probe moved onward in 10 mm sec⁻¹ speed, till the patch ruptured, the device measure the force (g) needed for the rupture, then the tensile strength was calculated according to the following equation (Laffleur et al. 2018):

$$\text{Tensile strength (N/mm}^2\text{)} = \frac{\text{Force required for rupture} * 9.81}{\text{Cross sectional area for patch}} \dots (8)$$

3.10.5. Mucoadhesive assessment

3.10.5.1. Detachment Force

The Detachment force was determined for 6 replicates of each formula using the texture analyzer. The nasal patch was attached to the lower probe, and the nasal mucosa was attached to the upper probe, after socking it in SNF

with 3% (w/w) mucin for 30 minutes, then the device parameter was set on 1 mm/sec^{-1} speed to move upward and the distance between the two probes was 4.5 mm. The nasal patch was allowed to attach for two minutes before each run starts this method inspired from the work of (Nižić et al. 2020).

3.10.5.2. Falling Liquid Test

The falling liquid test was performed by self-made falling liquid apparatus using syringe pump, which was set at 500 ml.h^{-1} to achieve a constant flow of SNF with 3% (w/w) mucin, then the syringe was linked to a glass condenser tube which was fixed downward by 10° , where the nasal mucosa was adhered inside the tube after cutting it to $1 \times 6 \text{ cm}$ pieces and soaking it in the same media, then the nasal patch was allowed to attach on the nasal mucosa. The temperature inside the tube was controlled (35°C), by attaching the condenser tube to aquarium pump, which was placed in water bath as represented in **Figure 3.1**. Finally, a camera was set in a holder and a ruler was fixed in the condenser tube to calculate the speed of which the patch moves by recording the time required for each patch to move 1 cm distance. This test was repeated to 3 replicates from each formula.

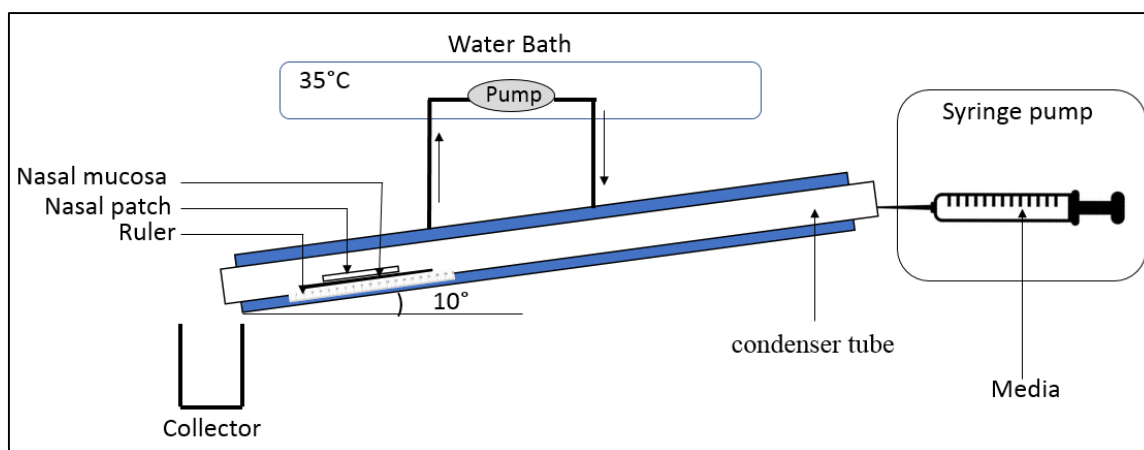


Fig. 3.1: Scheme draw for the falling liquid apparatus.

3.11. Content Uniformity

The content uniformity (CU) for formulations was assessed using 10 patches from each formula by dissolving each patch in 100 ml distilled water at 35 °C for 30 minutes, where 10 sample prepared from each then each sample was injected into HPLC unit (The United States Pharmacopeial Convention 2021).

3.12. Release Study

The release study was carried out in two different experiments:

- using 5 ml sample tubes filled with 5 ml of SNF, each nasal patch was filled in a dialysis bag (cut off ~ 5000 Dalton), before it was immersed in the media, since the media was set in a 35 °C water bath with a stirrer (200 rpm) in each sample tube, 0.2 ml of the sample was taken at a predetermined time point 0.5, 1, 2.5, 3.5, 4.5, 5.5, 6.5, 7.5, 20, 22, 24 hour, then each sample was completed up to 1 ml using SNF, and

centrifuged (5 min at 16000 rpm), then each sample was injected to HPLC unit.

- Using the basket dissolution apparatus, 6 vessels as every vessel filled in 500 ml SNF, temperature set at 35 °C and 50 rpm, samples obtained after one hour, then injected to HPLC unit.

3.13. Ex-vivo Permeation Study

The nasal permeation study of RvT was performed using Franz diffusion cell, with volume of 12 ml and diffusion effective area of 1.767 cm². The receptor compartment was filled with SNF at controlled temperature (35 °C), where the nasal patch was placed in the donor compartment over the sheep nasal mucosa which was prepared as mentioned previously in section **3.8** and soaked in SNF, then mounted between the donor and the acceptor compartment as shown in **Figure 3.2**. A 0.3 ml of sample was withdrawn at each time point 0.5, 1, 2,3,4,5,6,7,8, 24 hours and replaced with fresh SNF, then each sample placed in an Eppendorf tube and centrifuged for 10 min at 16000 rpm to eliminate the solid precipitate from the media, then the clear

solution of the sample placed in an 250 µl glass insert and injected to the HPLC (Abdelrahman et al. 2017).

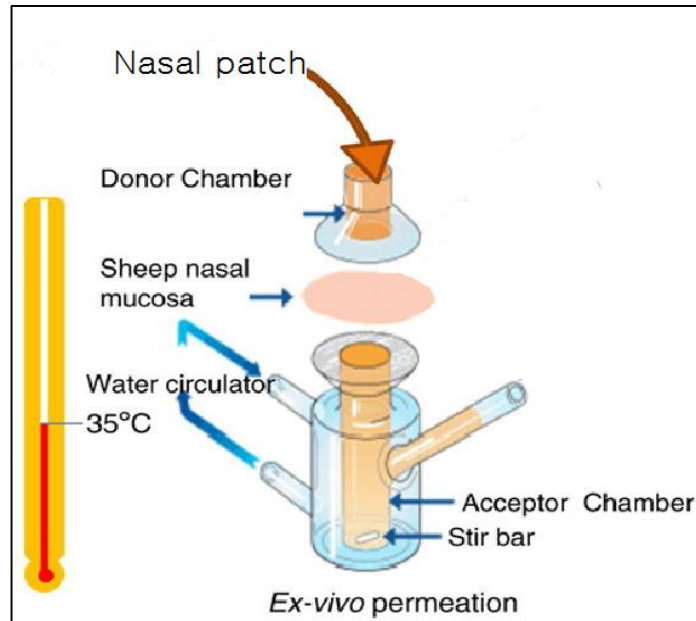


Fig. 3.2. Scheme draw to illustrate Franz cell parts and the mechanism of ex-vivo permeation study using Franz cell (Pund, Rasve, and Borade 2013).

The % cumulative amount of RvT permeated through the nasal mucosa %(Q) was plotted versus time (t). (Q) was calculated according to the following equation (Bruschi 2015a):

$$Q = (C_i V + \sum_{i=1}^{n-1} (C_i S)) \dots (9)$$

Q: Cumulative amount of drug permeated of membrane (mg.cm²).

C_n: Drug Concentration µg.ml⁻¹ determined at nth sampling interval.

V: Volume of the receiver solution in the Franz diffusion cell; 12 ml.

∑C_i: Sum of concentration of RvT mg.ml⁻¹ calculated at sampling intervals 1 through n-1.

S: Volume of the individual sample.

A: Surface area of Franz cell opening; 1.767cm².

The steady-state flux (J_{ss}); mg/cm²/hr was calculated from the slop of the linear portion of the (Q/A) versus (t) plot.

Permeability coefficient (P) cm.hr⁻¹ was calculated according to equation (Gouda, Baishya, and Qing 2017):

$$P = \frac{J_{ss}}{C} \dots (10)$$

P: Permeability coefficient (cm.hr⁻¹).

J_{ss}: The steady-state flux (mg/cm²/hr)

C: The drug concentration in the donor compartment (mg.ml⁻¹).

The concentration of drug in receiver compartment is considered negligible compared to the concentration of drug in the donor compartment, under sink condition (Patrick J. Sinko 2011).

3.14. Release Kinetics

The release kinetics was assessed using Lap Plot2 software version 2.8.1. LabPlot2 is a KDE-application for interactive graphing and analysis of scientific data. The model fitting was determined in terms of (K); the dissolution rate constant, (n); drug release exponent, (R²); correlation coefficients, (SSR); sum of squared residual, the residual data plotting.

Korsmeyer-Peppas model was investigated to understand the mechanism of drug release (Gouda, Baishya, and Qing 2017).

Korsmeyer-Peppas model equation (Bruschi, 2015):

$$Q_t = kt^n \dots (11)$$

Where:

Q_t : % Cumulative amount of drug at time.

K: Release rate constant.

T: Time.

n: Drug release exponent.

The residual data were calculated by subtracting the analysis data from the data obtained from the model application.

3.15. Stability Study

The stability study was carried out according to the (ICH guidelines Q1F 2021) in terms of content uniformity and physical appearance, by storing the nasal patch inside a nylon package in a stability chamber under controlled normal condition at 30 °C, and 65 RH for one, three and six months, and in accelerated condition 40 °C, and 75 RH for one month, then the content for 6 patches were re-assessed by dissolving one nasal patch in 100 ml to have 40 µg.ml⁻¹ RvT concentration and injecting each sample to HPLC unit, and determine the content (Assay) it was calculated as mentioned in **section 3.11**.

Chapter (4) Results

4.1. Chromatographic method optimization

The chromatograms and characteristics of each method are summarized in figures (4.1 - 4.4) and table 4.1.

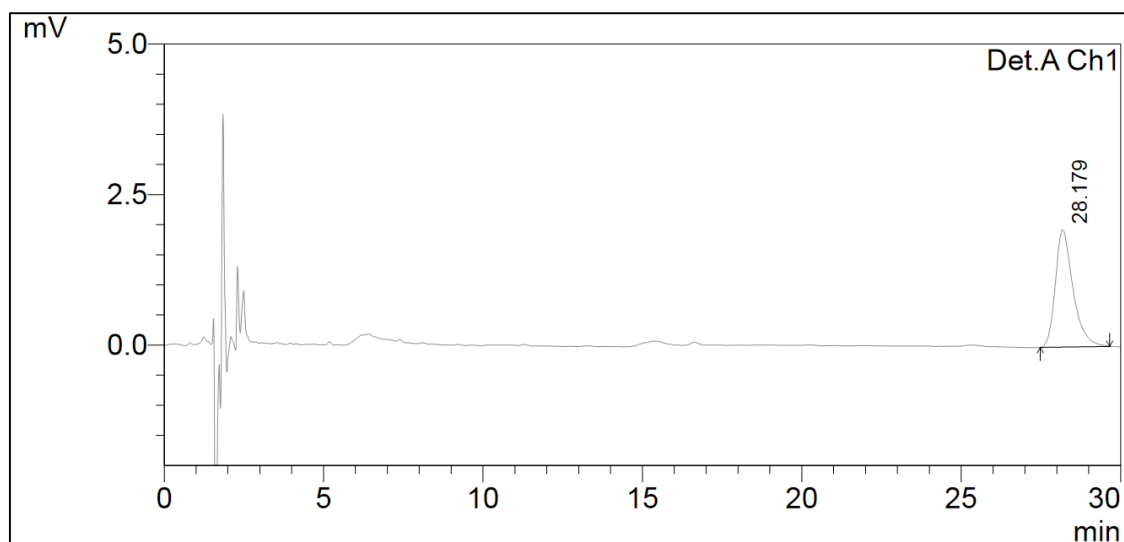


Fig.4.1: Chromatogram of the first method. Sample concentration, $4\mu\text{g ml}^{-1}$; mobile phase, MeOH: ACN: ammonium buffer (15:15:70); column, C18 250 x 4.6 mm, 5 μm ; column oven temperature, 40 °C; flow rate, 1.5 ml.min $^{-1}$; wavelength, 215 nm; injection volume, 20 μl .

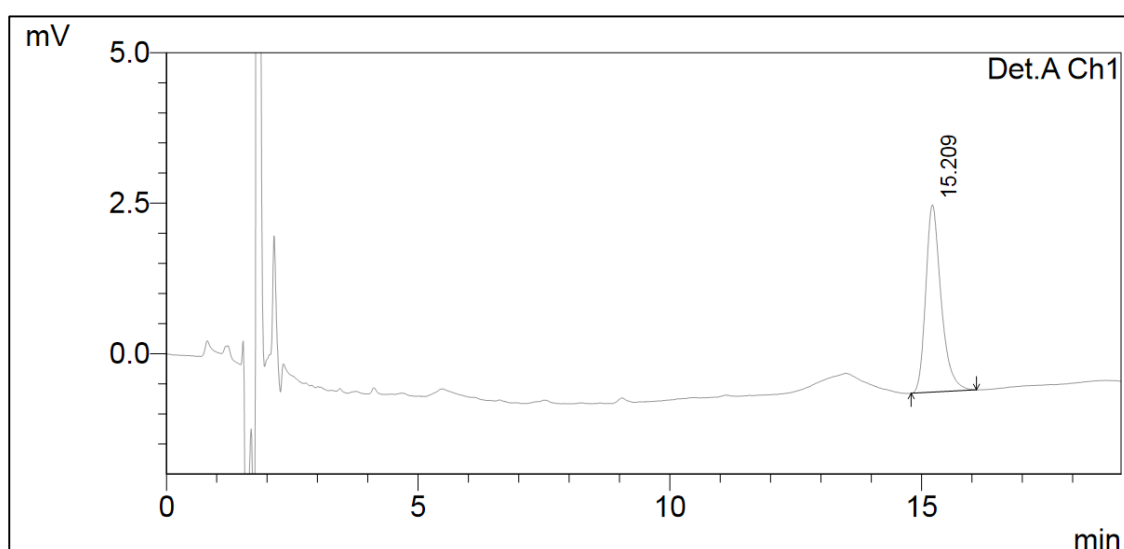


Fig.4.2: Chromatogram of the second method. Sample concentration, $4\mu\text{g ml}^{-1}$; mobile phase, MeOH: ACN: ammonium buffer (20:20:60); column, C18 250 x 4.6 mm, 5 μm ; column oven temperature, 40 °C; flow rate, 1.5 ml.min $^{-1}$; wavelength, 215 nm; injection volume, 20 μl .

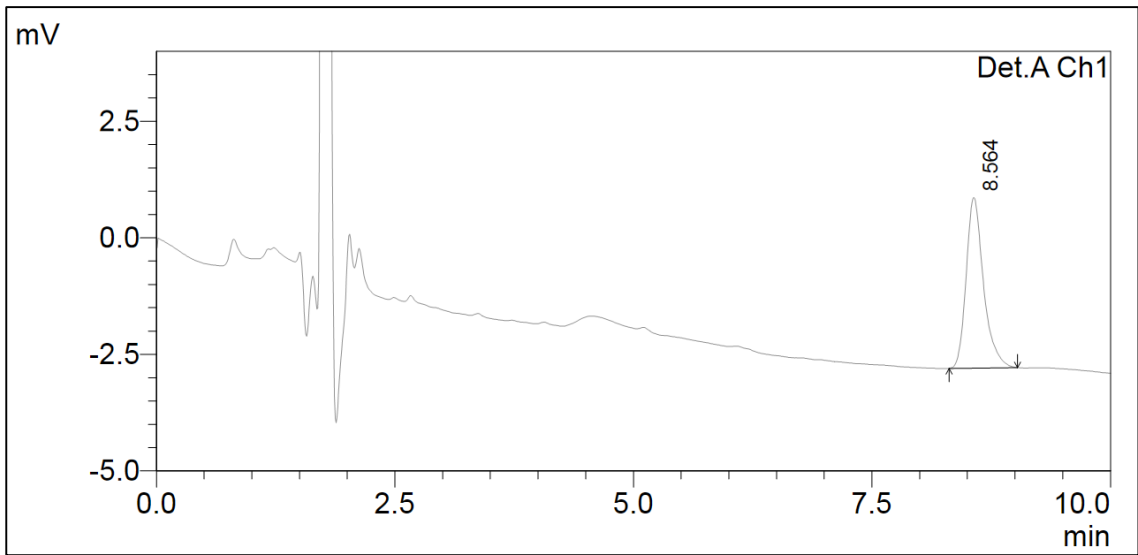


Fig.4.3: Chromatogram of the third method. Sample concentration, $4\mu\text{g ml}^{-1}$; mobile phase, MeOH: ACN: ammonium buffer (25:25:50); column, C18 250 x 4.6 mm, 5 μm ; column oven temperature, 40 °C; flow rate, 1.5 ml.min⁻¹; wavelength, 215 nm; injection volume, 20 μl .

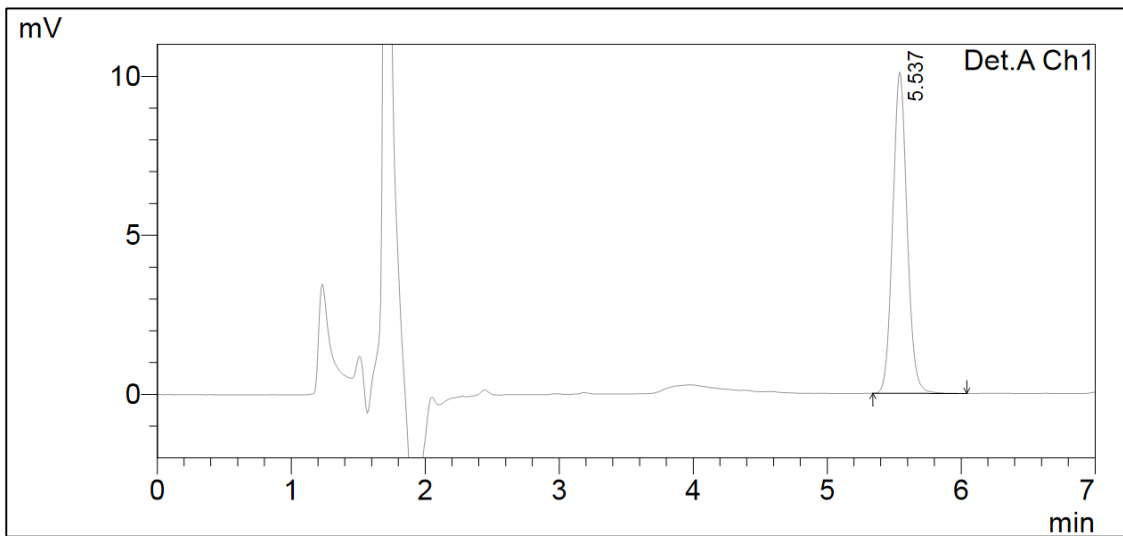


Fig.4.4: Chromatogram of the fourth method. Sample concentration, $4\mu\text{g ml}^{-1}$; mobile phase, MeOH: ACN: ammonium buffer (30:30:40); column, C18 250 x 4.6 mm, 5 μm ; column oven temperature, 40 °C; flow rate, 1.5 ml.min⁻¹; wavelength, 215 nm; injection volume, 20 μl .

Table 4.1: Characteristics the tested chromatographic methods.

Method Name	RT	TF	N	Mobile Phase Composition (v/v)
First method	28.2	1.40	11105	ACN:MeOH: Buffer (15:15:70)
Second method	15.2	1.35	12463	ACN:MeOH: Buffer (20:20:60)
Third method	8.6	1.36	10947	ACN:MeOH: Buffer (25:25:50)
Fourth method	5.5	1.13	11741	ACN:MeOH :Buffer (30:30:40)

4.2. Validation of analysis method

4.2.1. Selectivity

The selectivity results are presented in the chromatogram in **figure 4.6:**

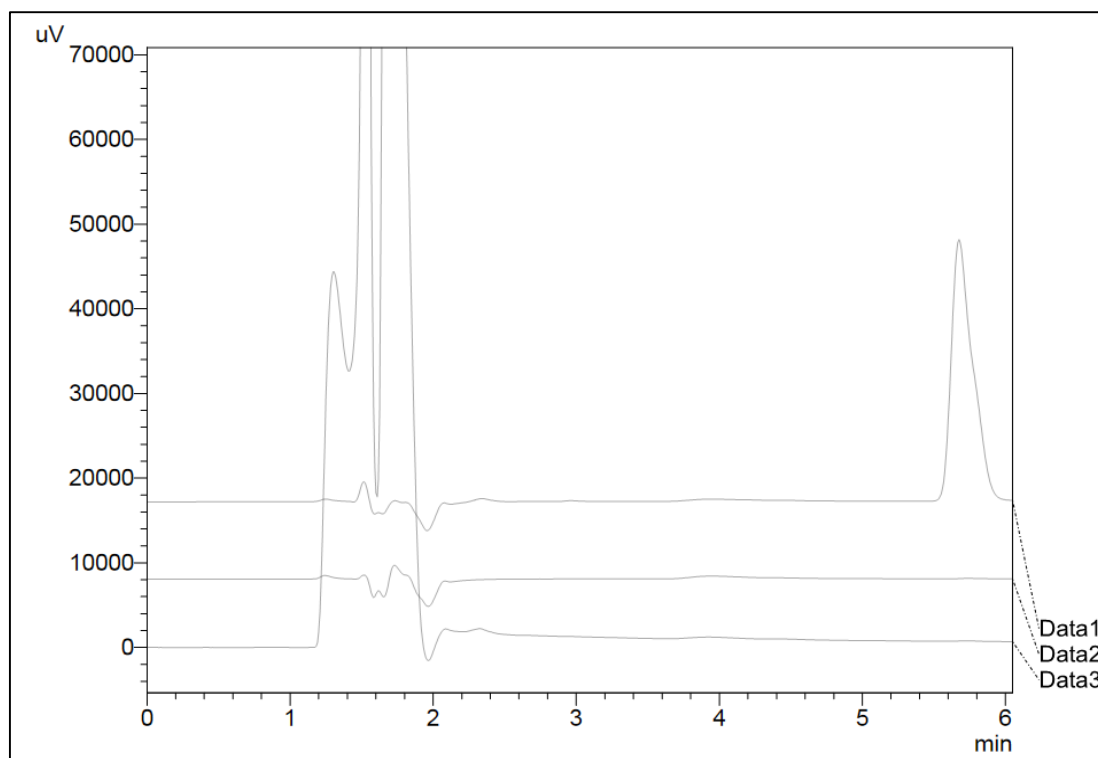


Fig. 4.5: The selectivity chromatograms of: Data 1, 20 $\mu\text{g.ml}^{-1}$ RvT standard; Data 2, 7.9 $\mu\text{g.ml}^{-1}$ tartaric acid; Data 3, SNF + excipients.

4.2.2. System suitability

The system suitability parameters are summarized in **table 4.2**:

Table 4.2 Peak area of 5 repeated injections of $20\mu\text{g ml}^{-1}$ standard solution of RvT

Injection Number	Peak area	N	TF	RT
1	316607	3850	0.98	5.80
2	314349	3753	0.97	5.79
3	317785	3732	0.98	5.79
4	315572	3756	1.00	5.79
5	313483	3752	0.98	5.79
Avg	315559	3769	0.98	5.79
RSD	0.54%	1.23%	1.12%	0.08%

4.2.3. Linearity

The linearity of the chromatographic for low concentration of RvT method was proved and presented in **table 4.3** and **figure 4.6**:

Table 4.3: The average peak area and the RSD% for the 3 replicates of the same concentration in the linearity curve, n=3.

Concentration ($\mu\text{g ml}^{-1}$)	%Level	Average Peak area	%RSD
8	40%	126100	1.60%
12	60%	192737	0.88%
16	80%	256820	0.33%
20	100%	320609	0.66%
24	120%	382544	0.10%
28	140%	449204	0.90%
32	160%	509363	0.25%

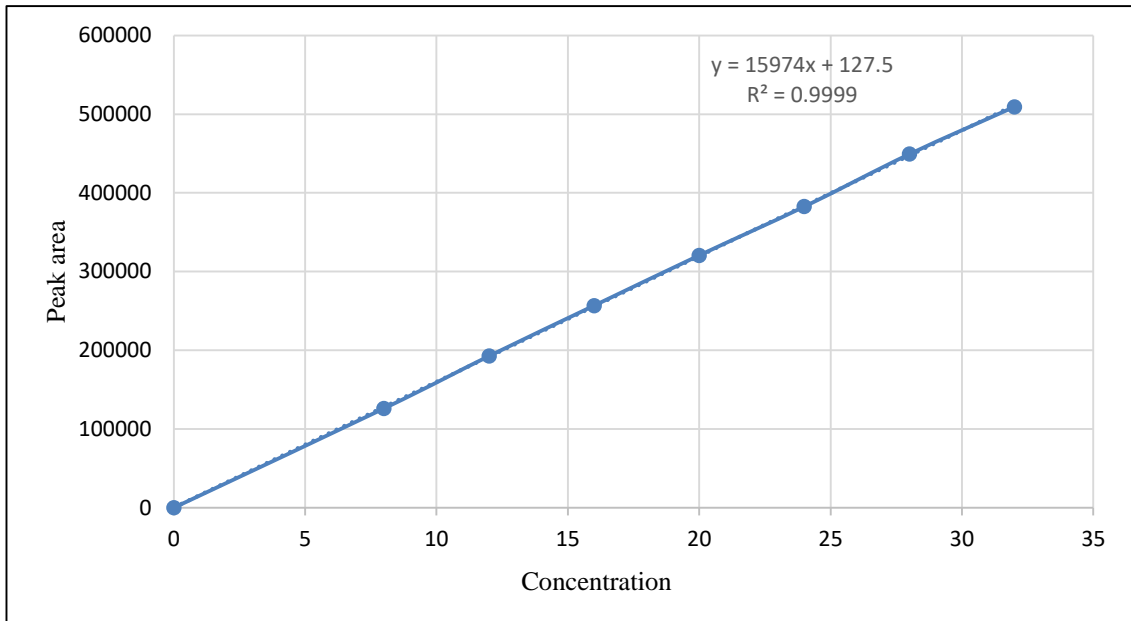


Fig.4.6: The linearity curve of RvT, n=3.

4.2.4. Precision

4.2.4.1. Repeatability

The assay results and the RvT of 6 artificial samples are presented in **table**

4.4:

Table 4.4: The assay for repeatability result for 6 artificial sample solution preparation under the same condition

Sample	Assay %	RT
1	101.6 %	5.59
2	101.3 %	5.59
3	101.4 %	5.60
4	100.7 %	5.60
5	101.2 %	5.59
6	101.9 %	5.59
Average	101.4 %	5.5915
SD	0.40	0.0035
RSD%	0.40 %	0.0627

4.2.4.2. Intermediate precision

The results of intermediate precision as inter-day, inter-instrument and inter-person are illustrated in table 4.5:

Table 4.5: The assay results for intermediate precision: inter-day, inter-instrument, and inter-person precision.

Sample	Assay		
	Inter-day	Inter- Instrument	Inter-person
1	101.1%	102.5%	100.4%
2	99.2%	100.3%	101.3%
3	100.2%	100.7%	98.5%
4	100.2%	100.1%	100.7%
5	100.0%	104.3%	100.0%
6	100.3%	101.6%	100.4%
Average	100.2%	101.6%	99.97%
SD	0.59	1.59	1.04
%RSD	0.59%	1.59%	1.04%

4.2.5. Recovery

The recovery was assessed and the results are presented in **table 4.6**:

Table 4.6: The recovery study results, n=3.

Level	Concentration ($\mu\text{g ml}^{-1}$)	Recovery	%RSD
50%	10	101.2%	1.63%
100%	20	100.0%	1.72%
150%	30	99.5%	1.07%

4.2.6. Limit of detection and Limit of quantitation

The LOD equals $0.246 \mu\text{g}\cdot\text{ml}^{-1}$.

The LOQ equals $0.745 \mu\text{g}\cdot\text{ml}^{-1}$.

SD value equals 1189.31.

S value equals 15966.45.

LOD and LOQ both were calculated from the linearity curve represented in section 4.2.3. using the equations (3 and 4) in section 3.5.6. and 3.5.7.

4.2.7. Robustness

4.2.7.1. Column oven temperature robustness

The column oven temperature robustness results are presented in **table 4.7**:

Table 4.7: Column oven temperature robustness results.

Sample	Temperature 38				Temperature 40				Temperature 42			
	Area	RT	TF	N	Area	RT	TF	N	Area	RT	TF	N
1	308945	5.81	1.09	3850	310228	5.97	0.98	4390	308697	5.80	1.06	3980
2	307908	5.83	1.11	3753	309938	5.96	0.97	4398	308419	5.79	1.06	3970
3	307788	5.83	1.11	3732	310601	5.95	0.98	4343	308470	5.79	1.06	3969
4	307787	5.84	1.10	3756	310311	5.94	1.00	4253	308883	5.79	1.07	3974
5	307514	5.84	1.11	3752	310309	5.93	0.98	4258	308261	5.79	1.08	3910
6	307811	5.84	1.12	3712	310317	5.92	1.01	4327	308281	5.79	1.08	3865
Average	307959	5.83	1.11	3759	310284	5.94	0.99	4328	308502	5.79	1.07	3945
%RSD	0.16%	0.21%	1.04%	1.26%	0.07%	0.32%	1.64%	1.44%	0.08%	0.07%	0.91%	1.18%

4.2.7.2. Wavelength robustness

The results of wavelength robustness are presented in **table 4.8**:

Table 4.8: Wavelength robustness results.

Sample	Lambda 214				Lambda 215				Lambda 216			
	Area	RT	TF	N	Area	RT	TF	N	Area	RT	TF	N
1	323929	5.84	1.03	3991	310228	5.97	0.98	4390	285461	5.83	1.06	3938
2	321603	5.84	1.04	4024	309938	5.96	0.97	4398	285322	5.83	1.06	3936
3	321589	5.83	1.05	4020	310601	5.95	0.98	4343	285485	5.82	1.08	3878
4	321520	5.84	1.04	4016	310311	5.94	1.00	4253	285168	5.82	1.07	3874
5	321827	5.83	1.05	4060	310309	5.93	0.98	4258	285067	5.82	1.07	3920
6	321447	5.83	1.05	3960	310317	5.92	1.01	4327	285250	5.82	1.07	3929
Average	321986	5.83	1.05	4012	310284	5.94	0.99	4328	285292	5.82	1.07	3912
%RSD	0.30%	0.05%	0.75%	0.84%	0.07%	0.32%	1.64%	1.44%	0.06%	0.06%	0.81%	0.74%

4.2.7.3. Flow rate robustness

The results of flow rate robustness are summarized in **table 4.9**:

Table 4.9: Flow rate robustness results.

Sample	Flow Rate 1.4				Flow Rate 1.5				Flow Rate 1.6			
	Area	RT	TF	N	Area	RT	TF	N	Area	RT	TF	N
1	332302	6.32	1.03	4248	310228	5.97	0.98	4390	291108	5.51	1.00	4015
2	332287	6.32	1.01	4281	309938	5.96	0.97	4398	290930	5.50	1.01	4053
3	332012	6.31	1.03	4270	310601	5.95	0.98	4343	291355	5.50	1.01	3990
4	332046	6.30	1.03	4254	310311	5.94	1.00	4253	291135	5.49	1.03	3929
5	331721	6.30	1.01	4325	310309	5.93	0.98	4258	290723	5.49	1.02	3910
6	331287	6.29	1.01	4305	310317	5.92	1.01	4327	289363	5.51	1.01	4021
Average	331943	6.31	1.02	4280	310284	5.94	0.99	4328	290769	5.50	1.01	3986
%RSD	0.12%	0.19%	1.06%	0.69%	0.07%	0.32%	1.64%	1.44%	0.25%	0.19%	0.94%	1.40%

4.2.7.4. Buffer pH robustness

The buffer pH robustness results are summarized in **table 4.10**:

Table 4.10: Buffer pH robustness results.

Sample	Buffer pH 6.9				Buffer pH 7				Buffer pH7.1			
	Area	RT	TF	N	Area	RT	TF	N	Area	RT	TF	N
1	305152	5.67	0.96	6799	310228	5.97	0.98	4390	303689	6.16	0.99	7000
2	305321	5.67	0.97	6619	309938	5.96	0.97	4398	304582	6.16	1.00	6959
3	305170	5.67	0.98	6522	310601	5.95	0.98	4343	305674	6.16	1.02	6971
4	319605	5.67	1.00	6389	310311	5.94	1.00	4253	302160	6.19	1.00	6866
5	303990	5.67	0.98	6503	310309	5.93	0.98	4258	303287	6.20	1.00	7009
6	305140	5.67	0.97	6412	310317	5.92	1.01	4327	303480	6.20	1.01	6991
Average	307396	5.67	0.98	6541	310284	5.94	0.99	4328	303812	6.18	1.00	6966
%RSD	1.95%	0.02%	1.53%	2.31%	0.07%	0.32%	1.64%	1.44%	0.39%	0.27%	1.08%	0.75%

4.2.7.5. Mobile phase composition robustness

Mobile phase composition robustness results are presented in **table 4.11**:

Table 4.11: Mobile phase composition (ACN: MeOH: Buffer) robustness results.

Sample	44:28:28				40:30:30				38:32:32			
	Area	RT	TF	N	Area	RT	TF	N	Area	RT	TF	N
1	285048	6.00	1.18	8980	310228	5.97	0.98	4390	310601	5.95	0.95	5343
2	286446	5.95	1.19	8943	309938	5.96	0.97	4398	309527	5.75	0.95	5725
3	285300	5.92	1.20	8893	310601	5.95	0.98	4343	309474	5.74	0.95	5565
4	285300	5.92	1.18	8893	310311	5.94	1.00	4253	309335	5.73	0.95	5461
5	285943	5.89	1.20	8812	310309	5.93	0.98	4258	310091	5.72	0.95	5326
6	285606	6.00	1.20	8903	310317	5.92	1.01	4327	309974	5.71	0.95	5213
Average	285607	5.94	1.19	8904	310284	5.94	0.99	4328	309834	5.77	0.95	5272
%RSD	0.20%	0.72%	0.08%	0.71%	0.07%	0.32%	1.64%	1.44%	0.15%	1.56%	0.31%	1.28%

4.2.8. Filtration compatibility

The filtration compatibility results are summarized in **table 4.12**:

Table 4.12: Filtration compatibility result for 20 $\mu\text{g ml}^{-1}$ RvT sample solution; filter size, 0.45 μm , 32mm for each type, n=3.

Volume (ml)	% Filtrated		
	Nylon	PTFE	Glass
1 ml	100.5%	100.2%	85.5%
2 ml	100.0%	100.3%	97.1%
3 ml	99.8%	100.2%	97.9%
4 ml	100.2%	100.3%	97.9%

4.2.9. Stability in SNF

The stability in SNF was assessed and presented in **table 4.13**:

Table 4.13: The % stability in SNF result for RvT standard solution of 20 $\mu\text{g.ml}^{-1}$ for 24 and 48 hours in different condition, n=3.

Time (hour)	% Stability				
	Refrigerated Light vial	Refrigerated Dark vial	Room Temperature Light vial	Room temperature Dark vial	Temperature 35°C
0	100.4%	100.3%	101.6%	100.2%	100.5%
24	100.7%	100.3%	99.7%	99.5%	99.5%
48	97.7%	98.5%	97.0%	97.2%	97.9%

4.3. Nasal patch characterizing

4.3.1. Physical appearance

The physical appearance of the fabricated nasal patches are illustrated in

Figure 4.7:

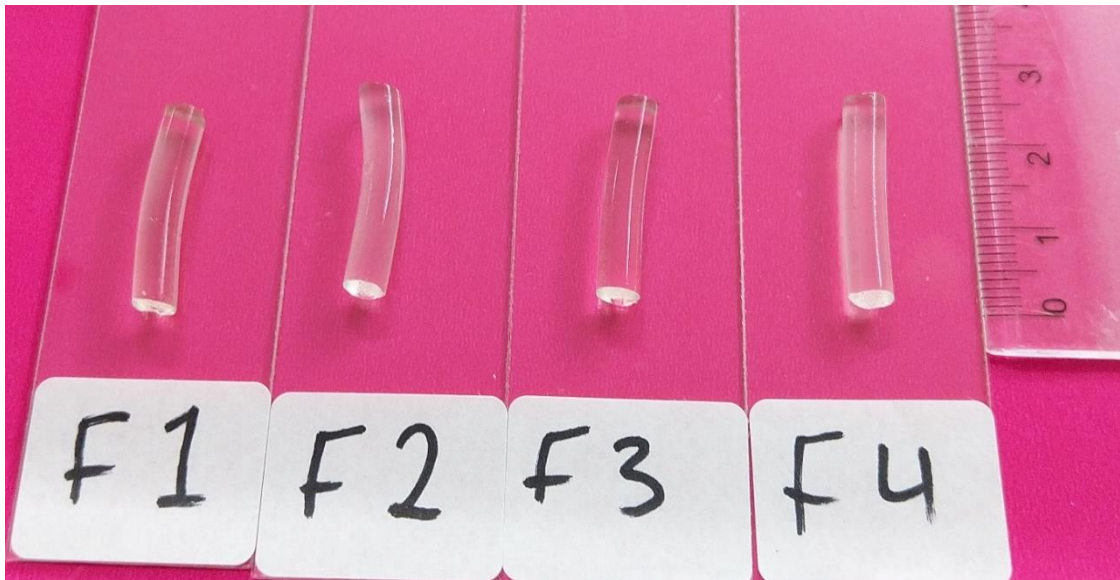


Fig. 4.7: Nasal Patches appears to be transparent and colorless, and no remarkable visual difference between formulas.

4.3.2. Diameter and length

The diameter and length measured for 6 replicates of each formula of nasal

patches are illustrated in **Table 4.14:**

Table 4.14: The Diameter and the length for the nasal patches, for F1, F2, F3, and F4, n=6.

	F1	F2	F3	F4
	Avg \pm SD	Avg \pm SD	Avg \pm SD	Avg \pm SD
Diameter	4.7 \pm 0.13	4.7 \pm 0.12	4.8 \pm 0.1	4.8 \pm 0.11
Length	23.6 \pm 0.8	23.2 \pm 0.7	23.0 \pm 0.8	23.1 \pm 0.55

4.3.3. Mechanical properties assessment

4.3.3.1. %Elongation at break

The % elongation at break result are summarized for 6 replicates of each formula in Figure 4.8:

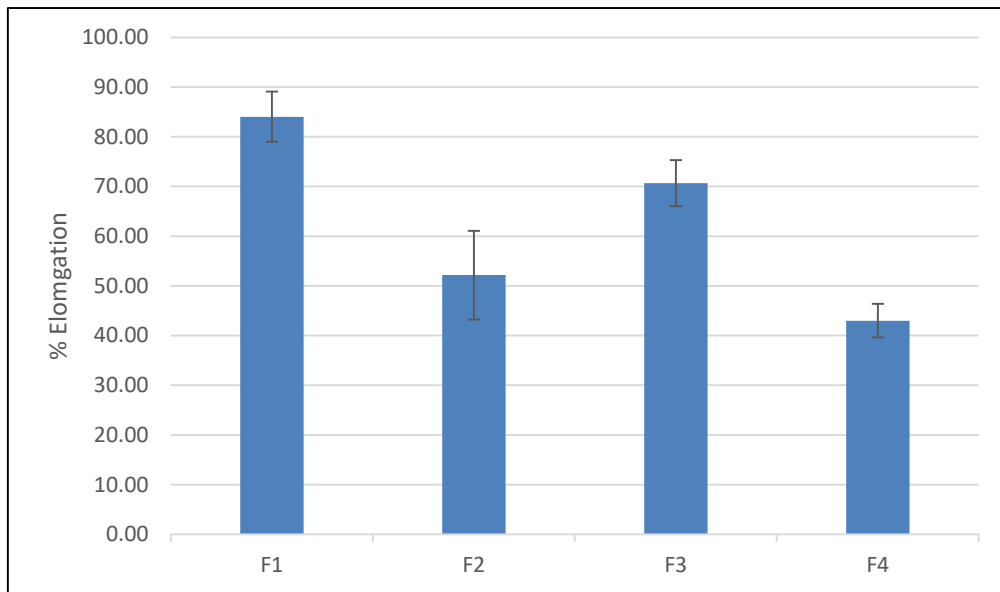


Fig. 4.8: Elongation percent result for each formula F1, F2, F3, and F4, calculated according to the **equation (7)** in section 3.10.4.1. and plotted as (Avg. ± SD) n=6.

4.3.3.2 .Tensile Strength

The tensile strength profile and the tensile strength force for all formulas, which was calculated according to **equation (8)**, and mentioned in section **3.10.4.2.** are illustrated in **Figure 4.9:**

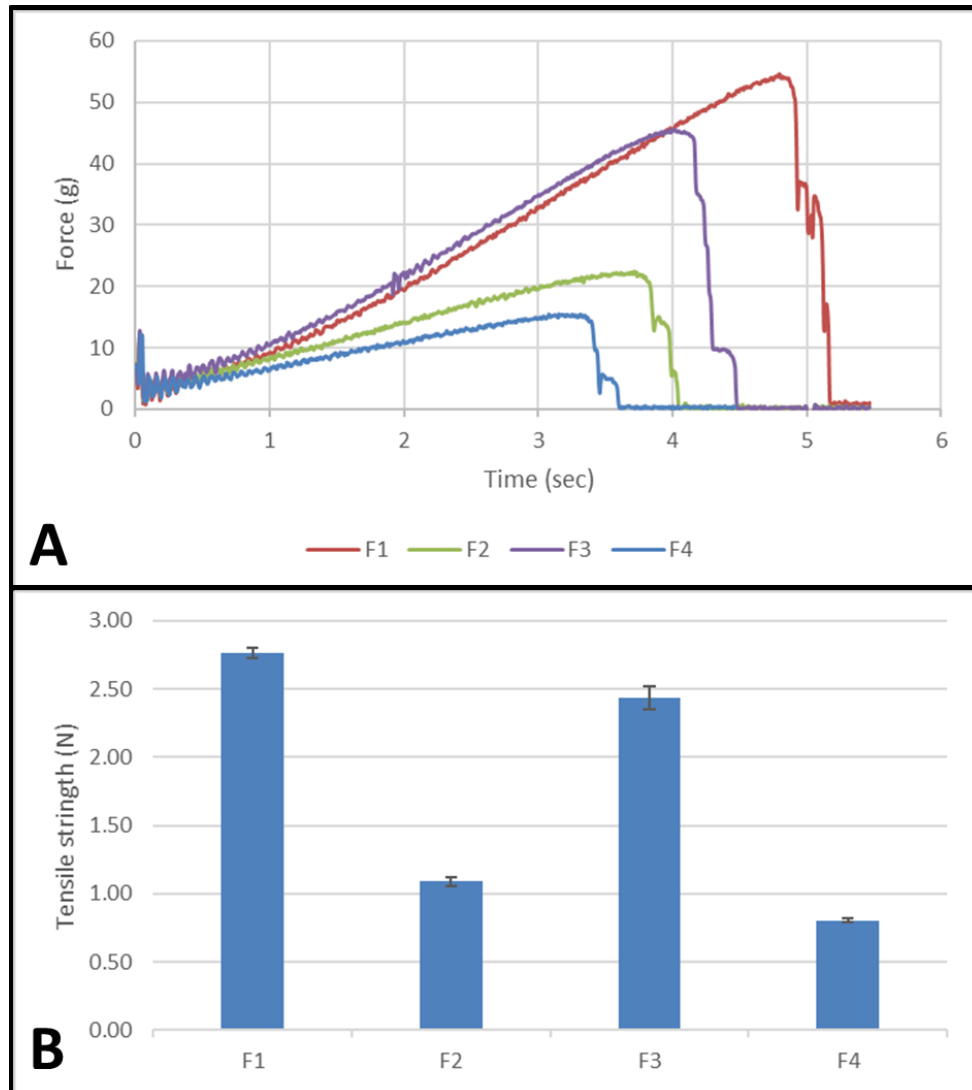


Fig. 4.9: Tensile Strength for each formula, A) Tensile profile, B) Tensile strength, n=6.

4.3.4. Mucoadhesive assessment

4.3.4.1. Detachment Test

The detachment force results for all formulas are summarized in **Figure 4.10**:

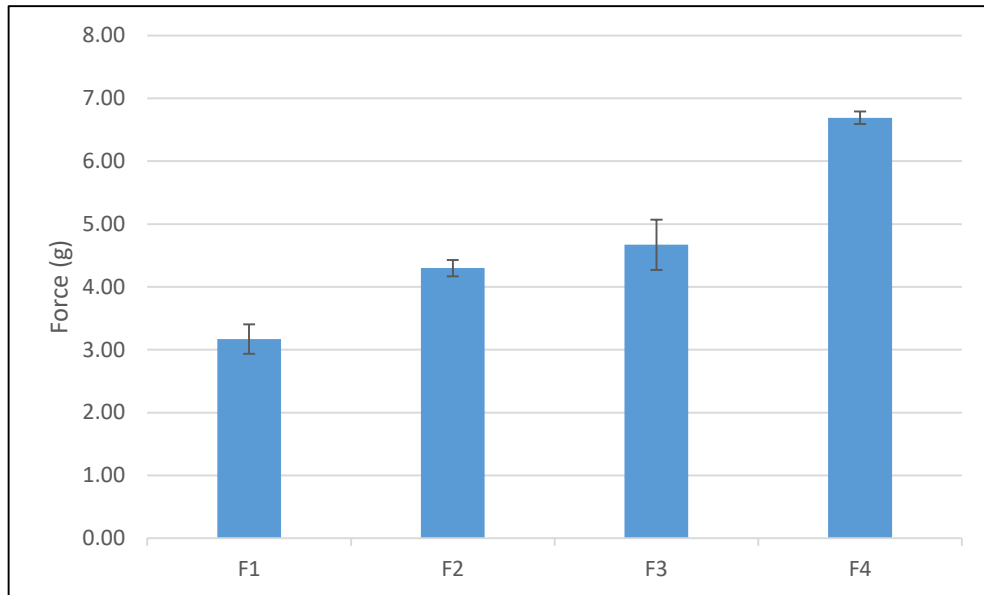


Fig. 4.10: The detachment force (N) between the nasal patch and the nasal mucosa for each formula F1, F2, F3, and F4 using texture analyzer, n=6.

4.3.4.2 .Falling Liquid Test

The falling liquid test results are summarized in **Figure 4.11**.

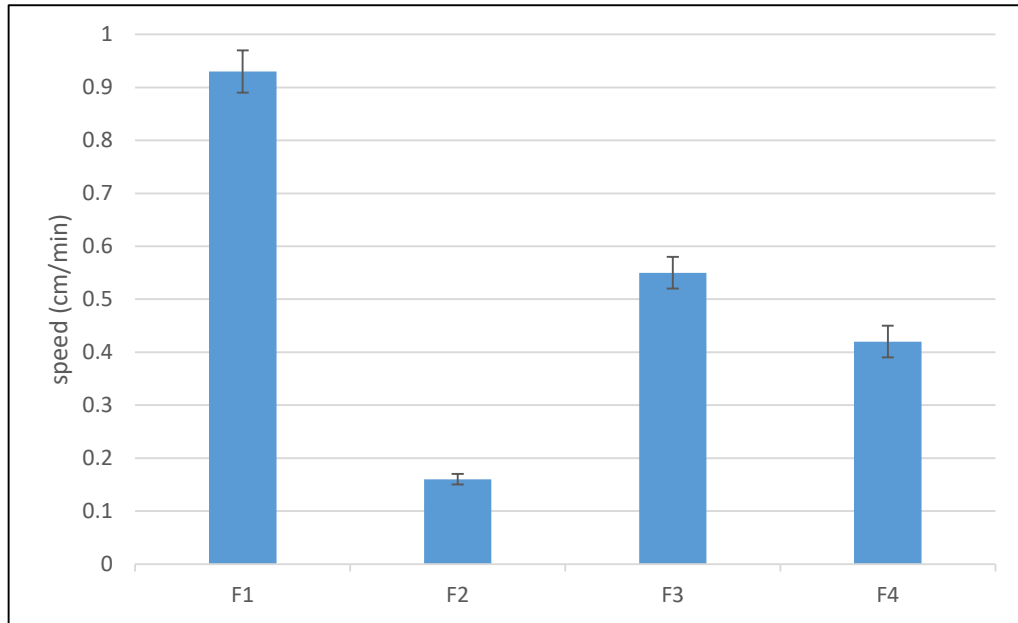


Fig. 4.11: Falling liquid test; flow, 0.5 l.h^{-1} , $n=3$.

4.4. Content Uniformity

The uniformity of nasal patches content, which was calculated according to **equation (9)**, mentioned in section **3.15**. are illustrated in **Table 4.15**.

Table 4.15: The content uniformity result for each formula, $n=10$.

	% Amount			
	F1	F2	F3	F4
Average	100.2%	99.9%	100.3%	98.9%
SD	1.17	1.33	1.13	0.96
RSD	1.17%	1.33%	1.12%	0.97%

4.5. Release study

The release study result of RvT from each formula carried out in 5 ml SNF at 35 °C water bath are summarized in **Figure 4.12**:

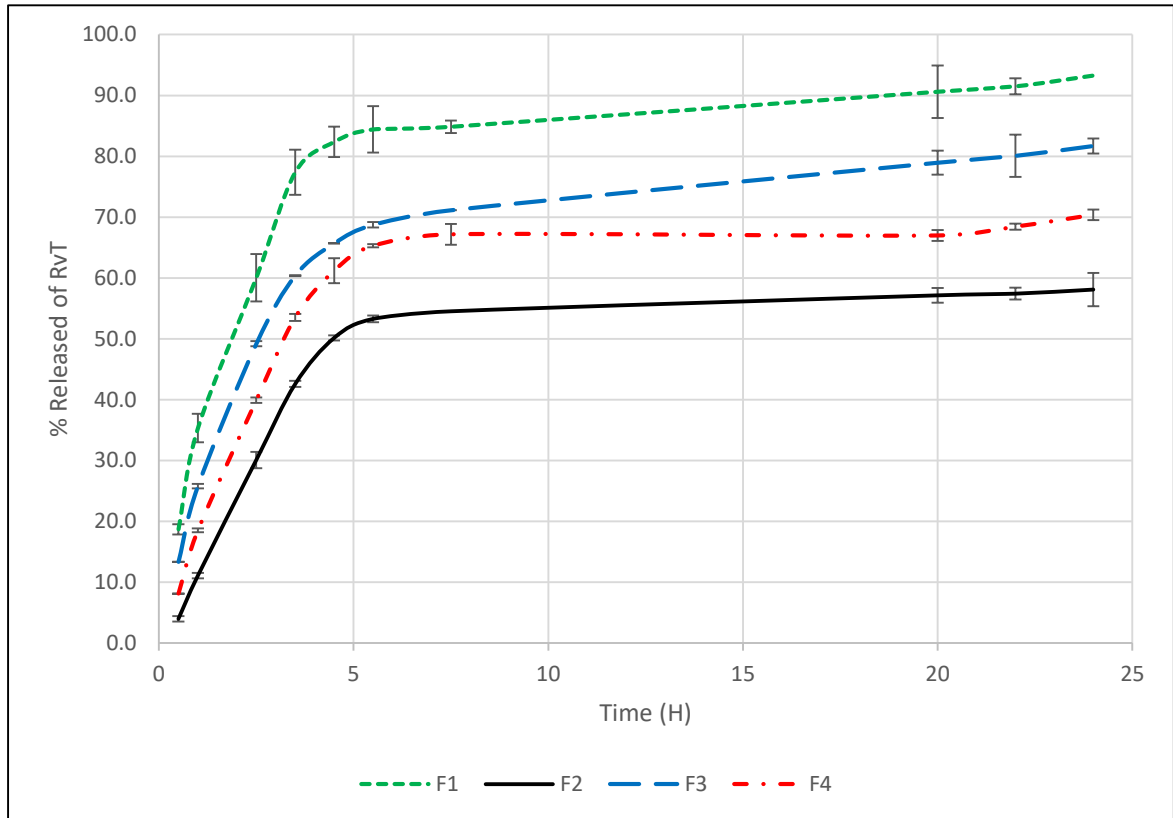


Fig. 4.12: The release result carried out using sample tubes filled with 5 ml of SNF at 35 °C, result plotted in term of % released of RvT vs. time for F1, F2, F3, and F4, n=3.

4.6. Ex-vivo Permeation study

The permeation of RvT result through nasal mucosal tissue summarized as % permeated amount in **Figure 4.13**. and the drug permeation parameters are summarized in **Table 4.16**:

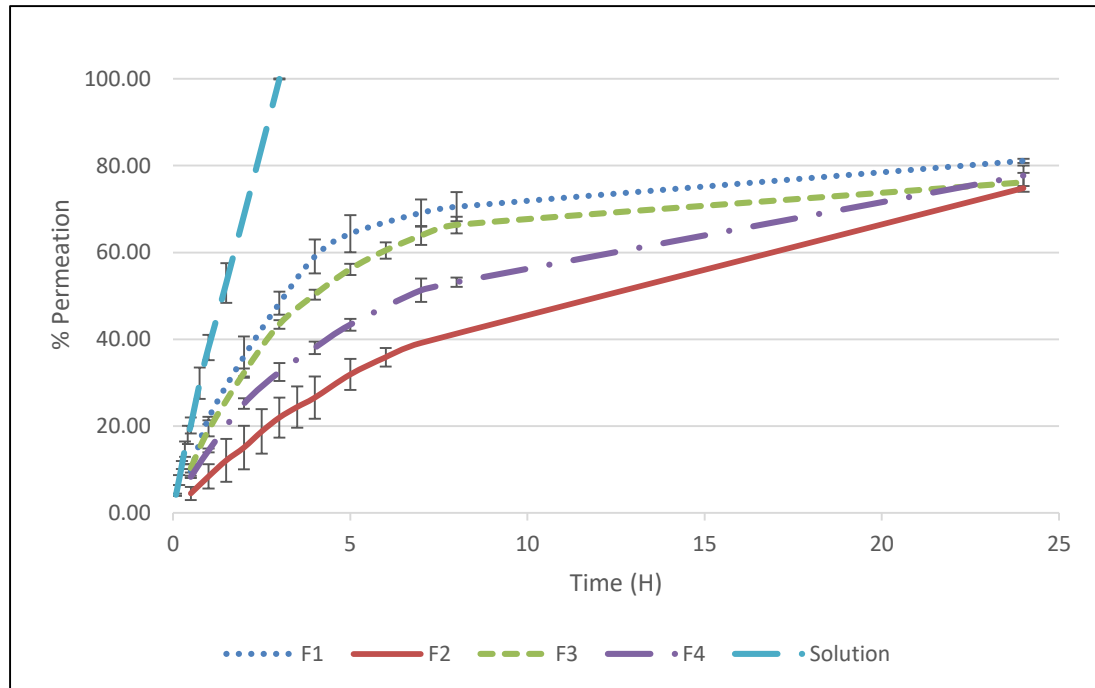


Fig. 4.13: The result for Ex-vivo permeation study of RvT through nasal mucosa tissue using Franz cell filled with 12 ml SNF at 35 °C with effective permeation area 1.767 cm², n=3.

Table 4.16: Permeation parameters for RvT in each formula.

Formula	Q/A (mg/cm ²)	J _{ss} (mg/cm ² /h)	P (cm/h)
	Avg ± SD	Avg ± SD	Avg ± SD*10 ⁻⁵
F1	1.83 ± 0.01	0.19 ± 0.009	15.12 ± 0.6
F2	1.69 ± 0.06	0.11 ± 0.007	8.01 ± 0.4
F3	1.7 ± 0.04	0.15 ± 0.01	14.27 ± 0.7
F4	1.75 ± 0.05	0.13 ± 0.003	10.64 ± 0.21

4.7. Release Kinetics

The release of kinetic model fitting represented in **Figure 4.14**, the summary of model fitting values are summarized in **Table 4.17** and the residual plotting is illustrated in **Figure 4.15**.

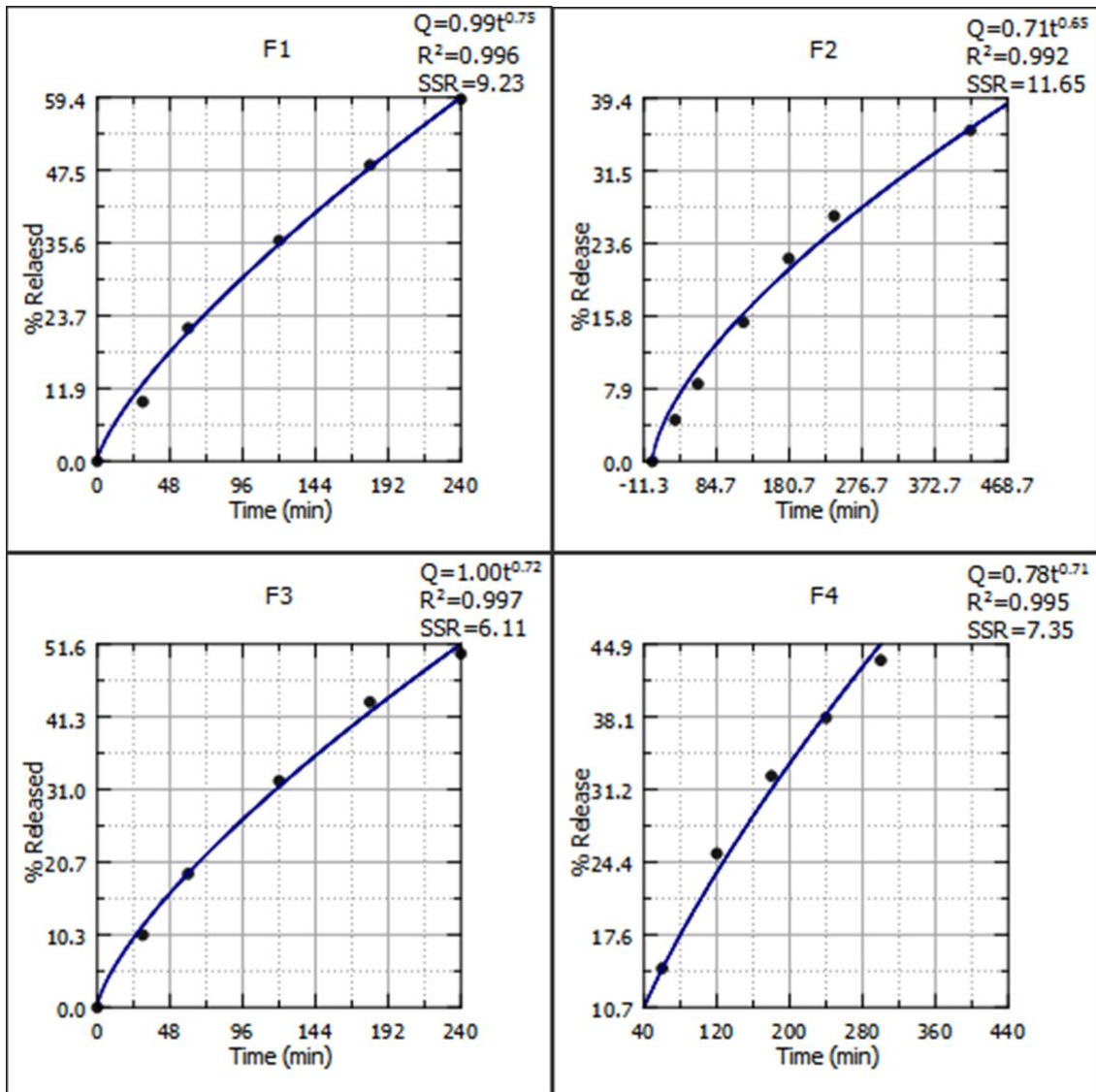


Fig. 4.14: The models fitting result for F1, F2, F3, and F4.

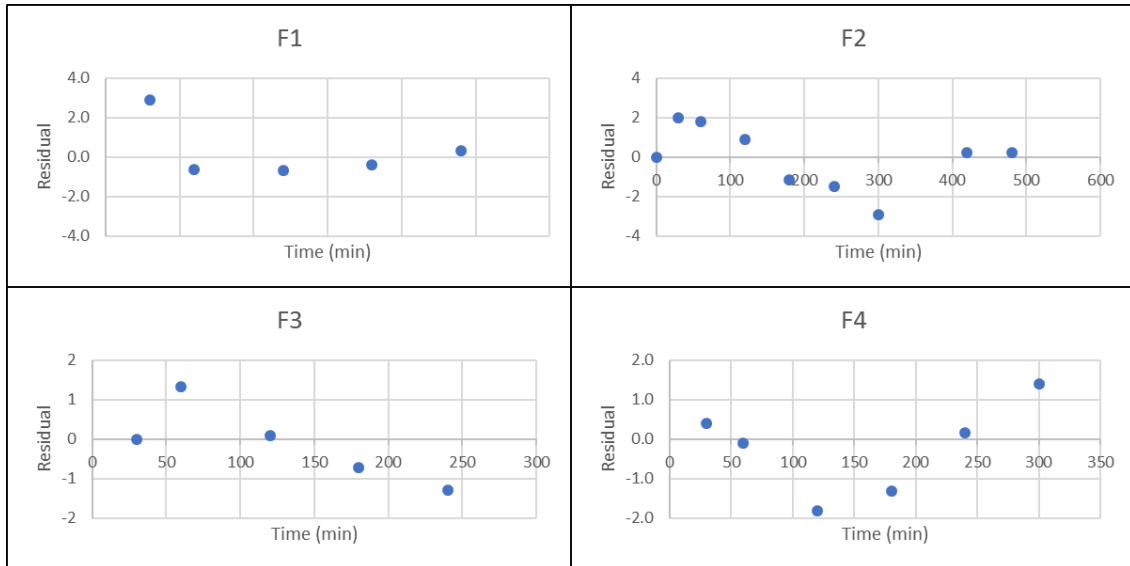


Fig. 4.15: Plotting of residual data.

Table 4.17: Summary for model fitting values.

	F1	F2	F3	F4
K	0.99	0.71	1.00	0.78
n	0.75	0.65	0.72	0.71
SSR	9.23	11.65	6.11	7.35
R ²	0.996	0.992	0.997	0.995

The release of RvT for 1 hour using USP I dissolution apparatus result

illustrated in **Figure 4.16:**

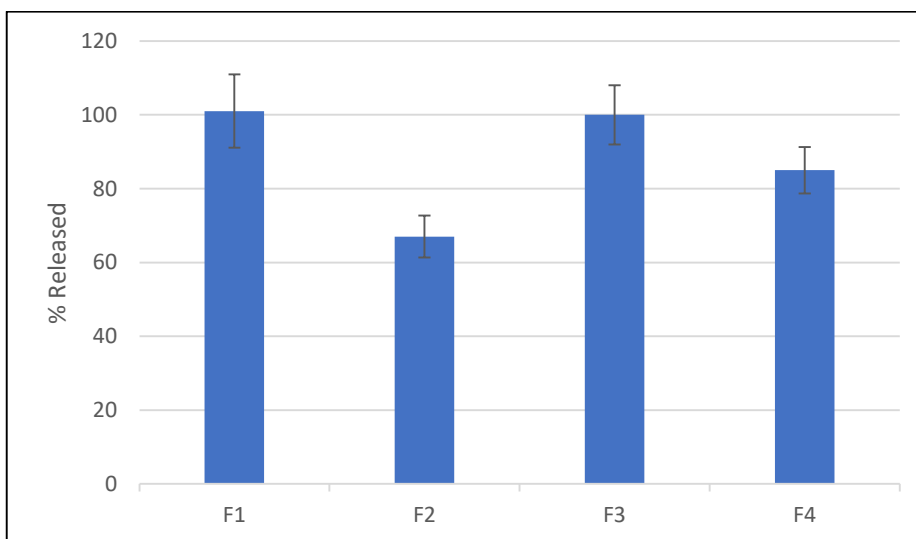


Fig. 4.16: The % released of rivastigmine F1, F2, F3, and F4 for each formula in basket dissolution apparatus for 1 hour.

4.8. Stability Study

The content uniformity of nasal patches reassessed after one, three and six months by comparing each nasal patch amount to the theoretical amount (4 mg) and summarized in **table 4.18:**

Table 4.18: The result for stability study of RvT in the formulation under controlled normal condition (30 °C, 65 RH), n=5.

Time (month)	% Amount			
	F1	F2	F3	F4
Zero	102.5%	102.8%	101.2%	100.9%
One	100.7%	100.7%	100.5%	99.1%
Three	98.4%	99.0%	100.9%	101.7%
Six	98.2%	98.3%	101.7%	100.5%

The physical appearance for each formula has no difference after long term storage; one, three and six months in the normal condition. Separation was noticed at the accelerated condition.

Chapter (5) Discussion

5.1. Method Optimization

The chromatographic method for the analysis of RvT in nasal patches was developed. The method was optimized to check its suitability for the determination of RvT in the preparation.

The first analysis method tested was according to the USP monograph of RvT raw material analysis method (The United States Pharmacopeial Convention 2021), which states that the mobile phase is MeOH: ACN: ammonium phosphate buffer pH 7 (15:15:70). For the lack of availability of C8 column, we used C18 column to have the first chromatographic method. Changing the column type increases the RT of RvT peak from 6 minutes, as proposed in the USP monograph, to 28 minutes as shown in **Figure 4.1**. This RT appears to be time and chemical consuming. Therefore, we slightly modify the mobile phase composition by increasing the MeOH and ACN composition to speed up the analysis.

The mobile phase of the second chromatographic method consists of MeOH: ACN: ammonium phosphate buffer pH 7 (20:20:60) which has a higher organic ratio than the first method. As shown in **Figure 4.2** the RT of RvT peak was around 15 minutes, which is still considered a relatively high RT. Therefore, the mobile phase of the second chromatographic method was modified to the third chromatographic method which consists of MeOH:

ACN: ammonium phosphate buffer pH 7 (25:25:50). As shown in **Figure 4.3**, the RT of rivastigmine peak was about 8.5 minutes. Further modification to the third method was applied to reach the fourth method which appeared to be the optimum method, where the retention time appeared to be around 6 min.

The fourth method which was the optimum method that is used in this project, which composed of the mobile phase, MeOH: ACN: ammonium phosphate buffer pH7 (30:30:40), gave a RT of the RvT peak around 6 min as appeared in **Figure 4.4**. Despite the low RT attained in this method, the selectivity of the method was still preserved, since there were no any interfering peaks around the RvT peak. Furthermore, this method showed good peak characteristics, since the N value was 11741, which was the highest value from the other methods, and TF value was 1.13, which was the least value from the other methods as presented in **Table 4.1**. These values are considered accepted values according to (Center for Drug Evaluation and Research 1994), since the N was > 2000 and the TF was < 2 .

5.2. Method Validation

The validation of the analytical method was performed in this project according to (ICH guidelines Q2(R1) 2005). Selectivity, system suitability, linearity, precision, intermediate precision, recovery, robustness, range, and limit of detection were evaluated.

5.2.1 Selectivity

Selectivity is the ability to assess the unequivocally of the analyte in the presence of other components, which may be expected to be present such as impurities, degradants, matrix, and excipient. Selectivity could be expressed as specificity in many references such as (ICH guidelines Q2(R1) 2005).

Rivastigmine peak appears around 6 minutes. On the other hand, there is no interfering peaks of excipient, tartaric acid or SNF appear around 6 minutes as observed in **Figure 4.5**, which indicates a good selectivity of the chromatographic method for Rivastigmine.

5.2.2. System Suitability

System suitability is an integral part of HPLC method. It is used to evaluate performance of the chromatographic system for the analysis (ICH guidelines Q2(R1) 2005). System suitability was evaluated by 5 replicate injections of a standard preparation, where the RSD% for AUC of the 5 injections was 0.55% as presented in **Table 4.2**, which is considered suitable according to Chromatography chapter <621> (The United States Pharmacopeial Convention 2021) since the accepted criteria is for the RSD% is NMT 2.

5.2.3. Linearity

The linearity of an analytical method is the ability to obtain directly proportional test results to the concentration or amount of analyte in the sample (ICH guidelines Q2(R1) 2005). The linearity performed by

preparation of 3 replicates of 7 different concentrations (8, 12, 16, 20, 24, 28, 32) $\mu\text{g ml}^{-1}$ of RvT, where each concentration level result of RSD NMT 2% as shown in **Table 4.3**, where the R^2 equals 0.9999 and the linear equation was ($y = 15974x + 127.5$) as shown in **Figure 4.6**. These results are considered acceptable since the concentrations have linear relation according to the Center of Drug Evaluation and Research (CDER) and (ICH guidelines Q2(R1) 2005), since the accepted criteria for the R^2 is ≥ 0.995 .

5.2.4. Precision

The precision of a chromatographic method expresses the closeness between a series of measurements obtained from multiple artificial sample solutions under the prescribed conditions. It is usually expressed as the variance, standard deviation, or coefficient of variation of 6 repeated measurements. The precision of this method was determined at two levels: Repeatability and Intermediate precision (ICH guidelines Q2(R1) 2005).

5.2.4.1. Repeatability

Repeatability represents the precision under the same conditions over a short time interval. Repeatability is also determined as intra-assay precision. Repeatability was determined by assaying 6 replicate of artificial sample solution in the same day, the same laboratory condition, and the same person, as documented in **Table 4.4**, the RSD% for 6 samples NMT 0.4. This considered precise according to acceptance criteria of the general chapter

<1225>, since the RSD% NMT 2 (The United States Pharmacopeial Convention 2021).

5.2.5.2. Intermediate Precision

Intermediate precision mainly expresses variations within-laboratories: different days, different analysts, different equipments, etc. (ICH guidelines Q2(R1) 2005). The intermediate precision was assessed in three different levels: same procedure of the precision was repeated after three days (inter-day), using different HPLC instrument; the automated HPLC and the manual HPLC (Inter-Instrument), and by different persons; me and my lap partner, Asmaa Abu Sa'aleek (inter-person). The degree of closeness of the result represented using RSD%, the result as shown in **Table 4.5** as the RSD% was 0.59%, 1.59%, and 1.04% In row which is considered precise according to the general chapter <1225> (The United States Pharmacopeial Convention 2021) since the acceptance criteria of $RSD\% \leq 2$.

5.2.5. Recovery

Recovery could be used to express the accuracy of the method, where it is sometimes termed as trueness. The accuracy of an analytical procedure expresses the closeness of the value which is accepted as an accepted reference value, and the value found (ICH guidelines Q2(R1), 2005), and how close the experimental value, to the true value (Center for Drug Evaluation and Research, 1994). It was attended at three different levels

(50%, 100%, and 150%) of the total quantity of a substance recoverable with all the excipient used in the formulation. This was covering the levels (80%, 100%, and 120%) according to (Center for Drug Evaluation and Research, 1994). Different levels were evaluated as shown in **Table 4.6**, where the % recovery was between (99.5 - 101.2) % and the %RSD for each level was NMT 1.72% which is considered recoverable according to the acceptance criteria in the monograph of RvT in the (The United States Pharmacopeial Convention, 2021): % recovery (98%-102%), %RSD \leq 2.

5.2.6. Limit of detection and limit of quantitation

The LOD of the method is the lowest amount of the analyte in the sample that can be detected but not necessarily quantitated as an exact value, where the LOQ of the method is the lowest amount of the analyte in the sample that can be determined quantitatively with suitable precision and accuracy of the method (ICH guidelines Q2(R1) 2005). Even that LOD and LOQ are not normally evaluated for the assay, dissolution, content, and potency according to (ICH guidelines Q2(R1) 2005). The LOD was calculated according to **equation (3)** in section **3.5.6**. from the residual standard deviation of the regression line (1189) and the slope (15947) of the calibration curve that was obtained from the linearity data in section **4.2.3**. The LOD value was 0.246 $\mu\text{g}.\text{ml}^{-1}$ which represents 3.07% of the lowest used concentration in this project ($8\mu\text{g}.\text{ml}^{-1}$).

The LOQ is a parameter of quantitation for the analytes in low levels in the sample matrices. The LOQ was determined according to **equation (4)** in section **3.5.7**. from the residual standard deviation of the regression line (1189) and the slope (15947) of the calibration curve that was obtained from the linearity data in section **4.2.3**. The LOQ value was $0.745 \mu\text{g}\cdot\text{ml}^{-1}$ which represents 8.75% of the lowest tested concentration in this project ($8\mu\text{g}\cdot\text{ml}^{-1}$). All concentrations of RvT used in this project were above the LOD and LOQ.

5.2.7. Robustness

Robustness of an analytical procedure indicates its reliability during normal usage as it is a measure of its capacity to remain unaffected by small, but deliberate variations in method parameters (ICH guidelines Q2(R1) 2005), such as variations in Column oven temperature, wavelength, Flow rate, Buffer pH and Mobile phase composition, the reliability was expressed in terms of %RSD.

Column oven temperature robustness was studied at 38°C, 40°C, and 42°C, as documented in **Table 4.7**. All the %RSD for RT, AUC, N, and TF were in the range of (0.07-1.64) %.

Wavelength robustness was studied at 214nm, 215nm, and 216nm, as documented in **Table 4.8**, the %RSD for RT, AUC, N, and TF were in the range of (0.05-1.64) %.

Flow rate robustness was studied at 1.4 ml min⁻¹, 1.5 ml min⁻¹, 1.6 ml min⁻¹ as documented in **Table 4.9**, the %RSD for RT, AUC, N, and TF were in the range of (0.07-1.64) %.

Buffer pH robustness was studied at 6.9, 7, 7.1 as documented in **Table 4.10** the %RSD for RT, AUC, N and TF were in the range of (0.02-1.64) %.

Mobile phase composition robustness was studied in range of (44:28:28), (40:30:30), and (38:32:32) of (ACN: MeOH: Buffer), as documented in **Table 4.11** the %RSD for RT, AUC, N and TF were in the range of (0.07-1.64) %.

As a result, all % RSD values for all circumstances were less than 2%, and according to the (Center for Drug Evaluation and Research 1994), which indicates that the system suitability criteria was met in all experiments and will not be affected by the deliberate variations that could be uncounted in any routine analysis

5.3. Filtration Compatibility

Filtration of the samples is usually necessary to prevent undissolved drug particles from entering the analytical sample and to remove the insoluble excipients that may otherwise cause high background or turbidity. As the SNF contains turbid particles <1092> the Dissolution Procedure chapter (The United States Pharmacopeial Convention 2021). Filtration compatibility was important to be evaluated for three different syringe filter

types (Nylon, PTFE, Glass) in order to compare and choose the best filter type. The % filtrated was calculated by comparing the filtrate solution to the non-filtrate solution following **equation (5)** mentioned in section **3.6**. According to **Table 4.12** the first ml of each syringe filter: nylon, PTFE, and GF has filtrated 100.5%, 100.2%, and 85.5% respectively of the RvT concentration. This could be due to the hydrophilicity of the PTFE syringe filter which is compatible with the hydrophilicity of RvT. As a result, discard the First 1ml if GF intended to be used or directly take the sample if Nylon or PTFE syringe filter used.

5.4. Stability in SNF

The stability of RvT in SNF was investigated to determine the stability of the samples after preparation. and during the release time of the formulas. Furthermore, samples were in solution for multiple hours in the laboratory environment before testing it to the HPLC unit. Based on that, the stability in solution should be tested. The stability in solution was calculated by **equation (6)** mentioned in section **3.7**. where the result represented in **Table 4.13** shows that RvT in the SNF is stable for 48 hours, where it appears to start degradation after 48 hours for the slight decrease in % stability. It is noteworthy to mention that the stability of RvT is not affected significantly by the environmental condition for 48 hours, even that it is suggested to keep the samples in an amber container at refrigerated temperature.

5.5. Nasal tissue preparation

The sheep heads used in this project were taken from Australian whether sheep which has a lifespan of about one year - to ensure the full development of the olfactory region - (Barrios, Quinteiro, and Salazar 2014). The olfactory epithelium is located in the ethmoturbinates mainly in their posterior and medial areas, which was also observed in (Barrios, Quinteiro, and Salazar 2014) work.

Through the experience and the study conducted, the Australian sheep appears to have the largest olfactory region in relation to its large head size in comparison with Roman and Domestic sheep. Therefore, the Australian sheep provides more tissue than other races.

Out of distinction, the olfactory region was observed as a yellow region as it contains a carotenoid pigment, even that it is not distinguished clearly by its color, which was also observed by other research groups such as (Barrios, Quinteiro, and Salazar 2014). While the respiratory region notably appears as red to purple region as it is a highly vascularized region as appears in Figure 3.1. In addition, the olfactory nerve bundle, the trigeminal nerve bundle, and the ethmoid bone were clearly observed in the olfactory region during the work.

Some research groups suggest one additional final step, which is delipidation of the tissue using chloroform or methanol such as (E. Karasulu et al. 2008),

notwithstanding that this step could cause a dramatic change on the absorption properties of the mucosa.

Because of the limited availability of human nasal mucosa, which can be obtained from patients undergoing surgery for nasal obstruction (P. Pandey et al. 2017), the need for another species for nasal tissue donor arises, that is why variant of animals was studied as a model for nasal drug delivery study.

Sheep is the best animal model that presents permeation and mucoadhesive proprieties similar to humans (Salade et al. 2019), as the study of the morphology and the histology of the sheep nasal mucosa shows it to be nearly identical to human nasal mucosa (Shaw et al. 2000). Sheep were used as a promising in-vivo model to deliver insulin to the brain (Silver, Carey, and Dueovi 1987).

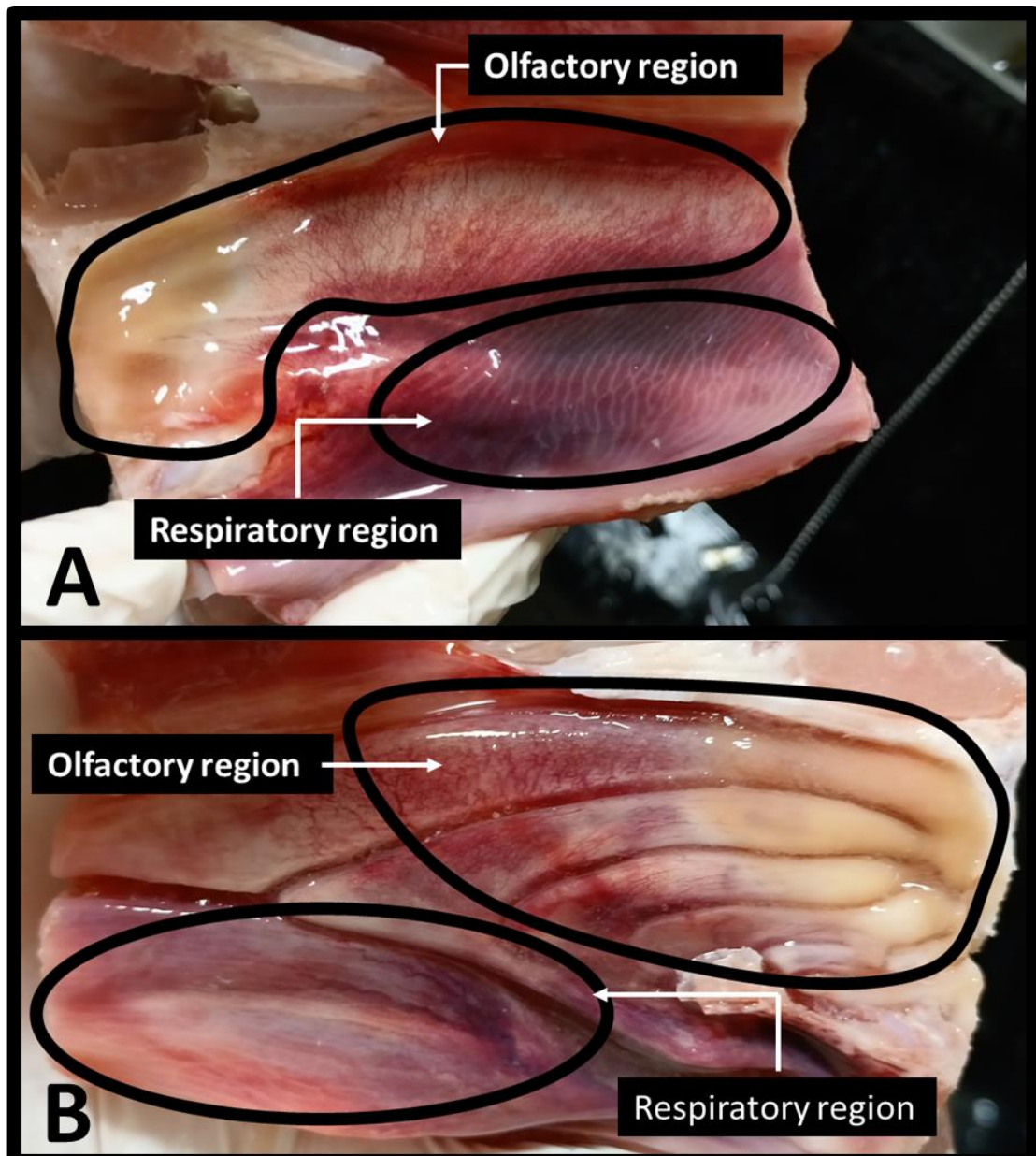


Fig. 5.1. A) the olfactory and the respiratory region in the medial part of the sheep nasal cavity. B) the olfactory and the respiratory region of the lateral part of the sheep nasal cavity.

Another study group reveals that dogs olfactory mucosa and the core of the olfactory nerve bundle appear to be thicker than sheep, since a blood vasculature was observed in the core of the olfactory nerve (Kavoi et al. 2010).

Even that monkeys could be more representative as a model for human olfactory mucosa as it occupies around 5% of the nasal cavity and it contains similar enzymatic activity (Chamanza and Wright 2015), from the standpoints of the cost, the controversy surrounding their use in experiments, and the use in a conscious state, in a comparison of the good correlation for the results obtained from the human and sheep, sheep is considered an excellent model (Illum 1996).

Rabbits and rats, both showed a variety of results, widely different plasma profiles in comparison with a human volunteer for nasal administration, especially for drugs with absorption issues (Illum 1996).

Overall, the sheep is the most suitable animal model for nasal ex-vivo and in-vivo study, for its availability, relatively low cost and good correlation for absorption, and mucoadhesive properties which also corresponded to (Illum 1996) and (Chamanza and Wright 2015) works.

5.6. Nasal Patch preparation

Nasal patch was prepared using gelation method based on a quick melting step as mentioned in section 3.9. The simplicity of this method makes it suitable for large scale production.

Gelatin is a biocompatible, highly available, with low cost protein, which is derived from controlled hydrolysis of collagen (Lobo 2016). It is one of the

most popular fibrous proteins with excellent film-forming properties (Barbosa et al. 2021). The melting point of the gelatin matrix is similar to the body temperature (Liu et al. 2020; Tedesco, Monaco-lourenço, and Carvalho 2016) Gelatin has thermo-reversible gel-forming properties around 35 °C, which is considered a unique temperature as it is close to the body temperature (Babin and Dickinson 2001; Yavari et al. 2021).

Generally, Hydroxypropylmethylcellulose (HPMC) is used as a coating agent, dispersing agent, emulsifying agent, emulsion stabilizer, film-forming, foaming agent, granulation, solubilizing agent, tablet binder, thickening agent, stabilizing agent, and suspending agent. HPMC was used in this work for its modified-release, mucoadhesive, and viscosity-increasing properties (Rowe, Sheskey, and Quinn 2009).

Both Gelatin and HPMC possess good film or gel-forming (matrix-forming) ability, chemical compatibility, great biocompatibility, biodegradability (Ding, Zhang, and Li 2015).

Glycerol and PG were used mainly in this preparation as a plasticizer, preservative, emollient, humectant, and cosolvent (Rowe, Sheskey, and Quinn 2009).

Since the olfactory nasal mucosa is considered as a sensitive region for containing the olfactory nerve, emollient and humectant properties for PG and glycerol consider important to preserve the nasal mucosal humidity and

to prevent drying. PG provides a dense, compact, smooth structure in the gelatin/HPMC film, properly due to the hydrogen bonding between PG and gelatin/HPMC, which decreases the interspace between gelatin and HPMC, thus increases the homogeneity and miscibility as it is described in Ding, Zhang and Li work which investigates the collagen/HPMC film behavior with and without PG. Therefore, adding PG to the formulas making it exhibit a uniform and reproducible results and suitable for large scale production (Ding, Zhang, and Li 2015).

Glycerol was used in this formulation as a physical stabilizer. A research article by (Morsy et al. 2017) reported that incorporation of glycerol in gelatin-based formulations causes changes to its secondary structure, which was attributed to the formation of hydrogen bonds between the glycerol-gelatin matrix. In the work presented herein, it was observed that increasing the amount of glycerol would result in a gel that is too viscous to be injected from the syringe. At lower concentrations, however, glycerol was found to increase the viscosity sufficiently to allow for a rigid matrix, without introducing difficulty in processing.

The formulas were prepared from 10% (gelatin/HPMC) mixture and 90% (60% PG, glycerol 20%, water 20%). The initial formulations using different concentrations of HPMC were inspired from (Liu et al. 2020) work and the handbook for pharmaceutical excipient (Rowe, Sheskey, and Quinn 2009).

It was covering (2-8% W/W%) of HPMC (K15M) grade. The ratios of gelatin/HPMC in the formulas G1, G2, G3, and G4 w (8:2), (6:4), (4:6), and (2:8) respectively. It was observed that the low ratio of gelatin as G4 resulted in a formula with a loos physical consistency, which is not suitable for further investigation. On the other hand, the high ratio of gelatin as in G1 was observed to have a firm structure, which resulted in a difficulty in injecting the formula from the syringe.

The best formulas observed in the term of physical properties were G2 and G3. Further investigation was performed to optimize the HPMC concentration in order to achieve the best adhesion. Each gelatin concentration was prepared with different HPMC concentration to get the formulas H1, H2, H3, H4, H5, H6, H7 and H8, which have the gelatin/HPMC concentrations of (6%-2%), (6%-3%), (6%-4%), (6%-5%), (4%-2%), (4%-3%), (4%-4%), and (4%-5%) respectively. It was observed that all these fabricated formulas have a good physical consistency since it was governed mainly by gelatin. Based on that, these formulas were subjected to simple initial mucoadhesive test to choose the most suitable formula on the basis of adhesion. The nasal mucosa which was soaked previously in mucin for 1 hour was adhering on a glass rod. All formulas were aligned parallel to each, and the nasal mucosa was allowed to attach the formulas for 0.5 minute then it was pulled over. It was observed that there was no significant difference

in the adhesion in all these formulas. Based on that, we decided to choose the formulas that contain the least and the highest ratio of HPMC to gelatin which were H1 and H8. Furthermore, the same ratios of gelatin/HPMC were used with both grades of HPMC (K4M and K15M) to get 4 preparations F1, F2, F3, and F4 which their composition is illustrated in **Table 3.1**. These formulas were considered to be suitable for further investigation.

Finally, every preparation was prepared in term of weight per volume to achieve the final nasal patch was considered per volume. It was considered that each 0.4 ml formula contains 4 mg of RvT.

F1, F2, F3, and F4 were the best initially adhesive formulas visually, and suitable for further investigation.

5.7. Nasal Patch Characterization

5.7.1. Physical Appearance

All patches appear to be colorless and transparent with a smooth surface with no visual difference between formulas (F1 – F4), as shown in **Figure 4.7**. As mentioned before PG and glycerol introduce smooth and dense structure for the formulas. Predictably, all formulas appear to be acceptable for patient administration for being clear and smooth (Tamasree Majumder, Gopa Roy Biswas, and Sutapa Biswas Majee 2016). Finally, all formulas appear to be odorless which is expected to be more suitable if we take into consideration

that the administration site of the formulas will be close to the olfactory nerves.

5.7.2. Diameter and length

The diameter and the length of all formulas were measured to estimate the symmetry of the nasal patch and the nasal cavity dimension, as represented in **Table 4.14**. The results for the length of all formulas were ($23.0 \pm 0.8 - 23.6 \pm 0.8$) mm, which facilitates its introduction to the nasal cavity easily, since the nasal anatomy has about (120-90) mm length (Pandey *et al.*, 2019) mm. It is estimated that the human olfactory region width is about 6 mm (Valtonen *et al.*, 2020), therefore the diameter for all formulas (F1-F2) ($4.7 \pm 0.12 - 4.8 \pm 0.11$) mm is considered suitable for human administration.

5.7.3. pH determination of the patch Surface

The surface pH of all formulas (F1 - F4) was estimated to predict the incidence of irritation after the application of the formula in the nasal cavity, as the pH of the normal nasal fluid is about ~6.5-5.5 (Salade et al. 2019). The surface pH was about 6 in all formulas, which resembles another group work (Tedesco, Monaco-lourenço, and Carvalho 2016) that observed a surface pH for gelatin/HPMC film between 6.21 and 6.73. Based on that, the surface pH of the formulas is considered acceptable and expected to induce no irritation.

5.7.4. Mechanical properties assessment

The mechanical properties of film materials are important for their practical applications and for deeper understanding of their behavior. The interaction between polymers notably influences the mechanical properties of the blended polymers (Fan et al. 2007).

5.7.4.1. % Elongation at break

The % elongation at break is the percentage of length that increased just before breaking of patch occurs to the initial length, which is also known as fracture strain (Petroudy 2017).

The % elongation at break test was performed to evaluate the elasticity and mechanical stability of each formula. The higher elongation of the formula, the more elasticity of it (Takeuchi et al. 2020), which is clearly represented in **Figure 4.8**. Formulas show an elongation behavior as $F1 > F3 > F2 > F4$. It was noticed that the elongation of patches in the formulas which have low concentration of HPMC as in F1 and F3 (the percent elongation was 88.91% and 71.98%, respectively, and HPMC concentration was 1.9%), is affected by the length of HPMC chain, since F1 which was composed of the HPMC K4M grade which is shorter than the HPMC chain in F3 that was composed of HPMC K15M. Therefore, the shorter the chain length of HPMC, the higher elongation will be observed. This behavior refers to the plasticizing

effect of HPMC to the gelatin matrix, as HPMC polymer interrupts the gelatin-gelatin bond as it was illustrated in **Figure 5.2**. Generally, gelatin films exhibit high tensile strength. Increasing gelatin concentration increases the tensile strength, probably due to adjacent polymer interactions (Tedesco, Monaco-lourenço, and Carvalho 2016). The structure of HPMC may hinder the junction zones results of the gel formation (Tedesco, Monaco-lourenço, and Carvalho 2016). This reduces the cohesiveness of the formed polymer matrix. Notably, it was found that myofibrillar proteins are relatively rich in a polar non-ionized amino acids, that form numerous protein-protein hydrogen bonds resulting in low flexibility and high cohesion of unplasticized films. These bonds saturated in the use of high concentration of HPMC such as F2 and F4 ($52.96\% \pm 10.00$ and $42.28\% \pm 6.83$), since the change of the elongation is not significant (Cuq, Gontard, and Cuq 1997).

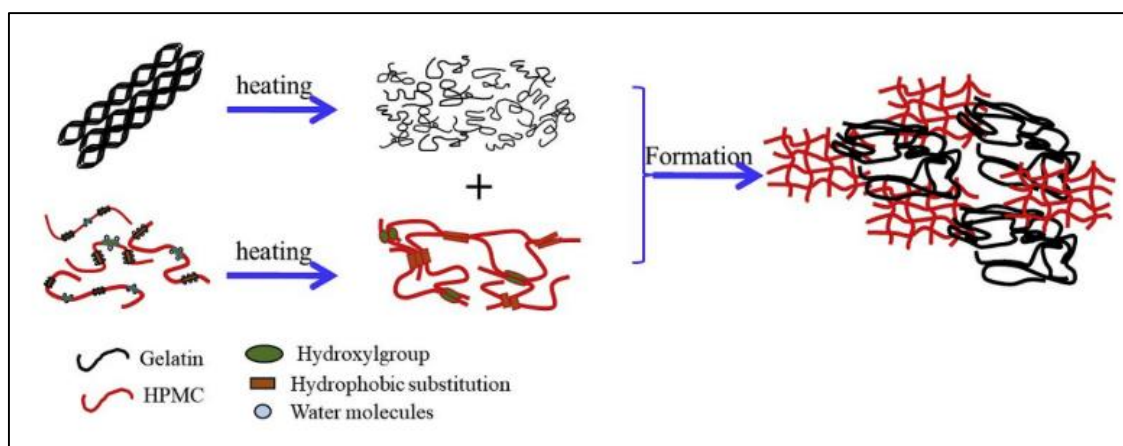


Fig. 5.2 A schematic representation of the mechanism for the HPMC/gelatin film and the plasticizing effect of HPMC (Liu et al. 2020).

5.7.4.2. Tensile strength

Tensile strength is the force needed to break material. The tensile strength test was performed to determine the maximum force that the patch can hold just before break or rupture (Malaiya et al. 2018). Tensile test results stress-strain curve. As illustrated in **Figure 4.9.(A)**, the stress–strain curve has a linear region at the initial part, which represents the elastic deformation. Then, it gradually loses its linearity, which represents the deformation from elastic behavior to plastic behavior. Finally, it reaches the maximum stress, followed by a slight decrease just before the rapid decrease stress which represented the breaking of the films. These features for the stress-strain curve determine that all formulas have a ductile behavior (Takeuchi et al. 2020).

According to **Figure 4.9.(B)**, it was found that the tensile strength was in the order $F1 > F3 > F2 > F4$. The tensile strength was higher in F1 (52.66 N) and F3 (45.18 N), due to the high concentration of gelatin (5.6 % w/w) and low concentration of HPMC (1.9% w/w) in those formulas. On the other hand, when the same gelatin concentration was used as in F1 and F3 (5.6% w/w), or F2 and F4 (3.7% w/w) the tensile strength was affected mainly by the plasticizing effect of HPMC, since either increasing the concentration or the grade of HPMC resulted in a decrease in the tensile strength. It is noteworthy that these results are in a good agreement with the percent elongation results.

5.7.5. Mucoadhesive test

Mucoadhesive tests were performed to evaluate the bio-adhesive force between nasal mucosa and the nasal patches (Laffleur 2018). Mucociliary clearance is the main limitation for the nasal drug delivery (Trotta et al. 2018). Furthermore the mucoadhesive properties increase the residence, therefore increase the time allowed for absorption (Yarragudi et al. 2017). Mucoadhesion depends on various factors such as cohesiveness, swelling capacity, and mechanism of interaction between polymers and mucosa. Therefore, two mucoadhesive tests were performed on nasal mucosa under different conditions to have a deeper understanding of the mucoadhesion mechanism (Tangri and Madhav 2016).

5.7.5.1. Detachment test

The detachment test was performed to assess the mucoadhesive force of each formula just after the insertion at room temperature and under normal atmospheric pressure, as represented in **Figure 4.10**. Formula ranking was following the order ($F4 > F3 > F2 > F1$), where F4 (6.69 g) results the maximum attachment, increasing both HPMC grade - chain length - and concentration obviously increases the detachment force of the patch, the adhesion mechanism was following the adsorption theory, for adhesion to begin the surface of the matrix should be wetted. Thus, the entanglement of the polymeric chain on the surface will be unwarp, resulting more chance to

interact with mucin and mucus, mainly by hydrogen bond and Van der Waals forces as shown in **Figure 5.3**. This concurs with the work of (Škrovánková, Mišurcová, and Machů 2012; Cook et al. 2017; Laffleur et al. 2018).

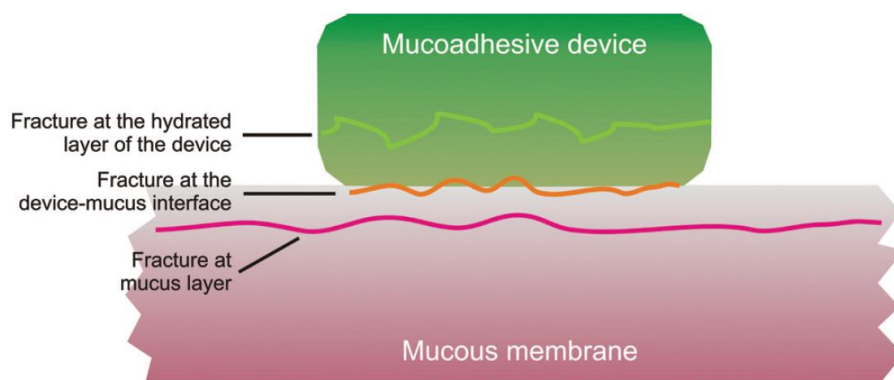


Fig. 5.3: description for the adsorption theory and the regions of interaction between mucin protein and HPMC polymer at room temperature and under normal atmospheric pressure (Tangri and Madhav 2016).

5.7.5.2. Falling liquid test

The falling liquid test was performed to evaluate the mucoadhesive force and to determine the formulas' resistance to the mucociliary clearance shear force between the formula and the nasal mucosa at 35 °C which represents the normal temperature of the nasal cavity. Falling liquid apparatus was inspired from the work of other research groups (Carvalho *et al.*, 2010; Prajapati Twinkle Kantibhai, 2015; Laffleur, 2018; Salade *et al.*, 2019; Alexander *et al.*, 2020), which was simulating the nasal mucocilliary clearance and the conditions in the nasal cavity. From the results shown in **Figure 4.11**, it was noticed that the detachment speed followed the rank of $F1 > F3 > F4 > F2$. It's noteworthy that these results did not follow the detachment results' order,

which means obviously that changing the test's condition especially the temperature, resulted in a remarkable change in the mucoadhesive mechanism. The gelatin solution forms a reversibly cross-linked network that was held together by hydrogen bond. These bonds were affected by temperature, since it was stated in the work of (Babin and Dickinson, 2001) that the gelatin matrix started to lose its firm texture above 35 °C, as it starts to lose the hydrogen bond, and thus the triple helix conformation of gelatin. Therefore, the viscosity will decrease till the complete deformation of the triple helix occurred as illustrated in **Figure 5.4**. This transformation of the physical state increases the mobility of the HPMC in the gelatin matrix, since the mobility of HPMC is inversely related with the chain length and directly with the temperature. As a result, the mucoadhesive theory suggested in this behavior is mainly the diffusion theory, since the F2 formula had a high concentration of low grade – low molecular weight- HPMC, which gave it the best chance to diffuse to the surface and interact with the mucin in the SNF as it is explained in **Figure 5.5** (Alipal et al. 2019; Babin and Dickinson 2001; Tekade et al. 2019).

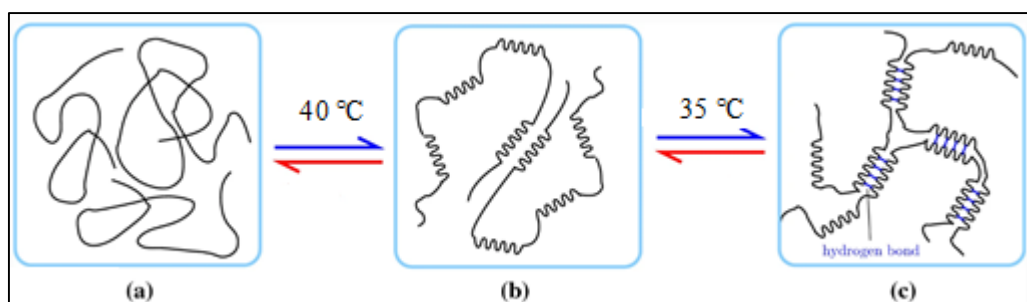


Fig. 5.4: The physical state of the gelatin solution according to the change of temperature, as the viscosity of the solutions $a < b < c$ (Zhou et al. 2018).

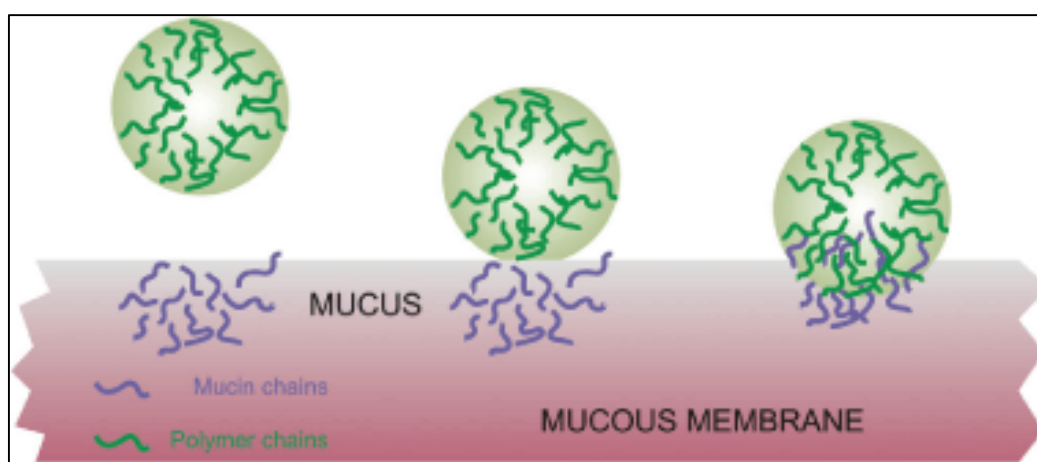


Figure 5.5: Scheme draw illustrates the diffusion and the adsorption theory for the interaction between the mucin protein and HPMC polymer (Tekade et al. 2019).

5.8. Content Uniformity

Content uniformity of the patches was assessed to determine whether the theoretical amount individual patches is within the acceptance limits and to evaluate the distribution of the drug in the patches. As shown in **Table 4.15**, all formulas were uniform as the %RSD was in the range 0.97 % -1.33 %, and the assay was 98.9% - 100.3%. Since all values of RSD are not more than 2% and the assays are within (70-130)% of the targeted amount, all formulas are considered within the accepted limit according to chapter <1225> (The United States Pharmacopeial Convention 2021).

5.9. Release and ex-vivo permeation study

The drug release from any dosage form is affected by several factors; the drug molecule, the formula composition, formulation processes, and the media (Tahara, Yamamoto, and Nishihata 1996). The release study was assessed using three different apparatus; basket dissolution apparatus, Franze cell, and dialysis bag, in order to study the effect of the hydrodynamic environment (the media volume and stirring speed) on the release of the fabricated nasal patches. Thus, highlighting the polymer media interaction. In each apparatus different volumes of SNF were used, therefore, different release profile was observed, since in the basket dissolution apparatus it was found that the % released of RvT at 1 hour for the formulas F1, F2, F3, and F4 was 100%, 65%, 100%, 85% respectively, while in the franze cell apparatus, the % released of RvT at 8 hours was 70.54%, 38.17%, 66.3%, and 53.2% respectively, and when using the dialysis bag for release evaluation, the % released of RvT at 8 hours was 84.9%, 54.5%, 71.1%, and 67.2% respectively. This difference ensures that the rate of the release is highly affected by the hydrodynamic environment. That was a confirmation that these formulas did not follow the zero-order kinetic model since this model defines the process of constant drug release only as function of time and the release takes place at a constant rate independent of active agent concentration from a drug delivery system.

In addition, it was noticed that all formulas exhibit a change in dimensions and size at temperature 35 °C in the presence of water as shown in **Figure 5.6**. This observation assures that Higuchi model is not suitable to fit the release kinetics as it mainly fits the release that is governed mainly by Fickian diffusion. Fickian diffusion assumes no change in the dimensions of the membrane across the drug is diffusing (Bruschi 2015a). Seeing as the formula exhibits clear deformation throughout release, Fickian diffusion cannot be the mechanism through which drug is released.



Fig. 5.6: The nasal patch shape after exposure to 35 °C.

Furthermore, the first order model is not a suitable model (Bruschi 2015a), as it involves a constant rate of release, which is not observed in the formula

as the change in the size caused a change in the rate of drug release in the formula.

As a result, these data indicate that RvT release from our fabricated nasal patches follows a hybrid mechanism, which is governed by swelling and erosion mainly.

Drug release kinetics were investigated by fitting the data to the Korsmeyer-Peppas model to calculate K and n values using Labplot2 (Version 2.0.8) software. The results are illustrated in **Figure 4.14**.

It was found that the n value in the fabricated nasal patches between 0.5 and 1 as illustrated in **Table 4.17**. It was observed also that the least n value was for F2 as it equals 0.65. When the n exponential value is deviated toward 0.5, the more diffusion mechanism will be predominant. While when the deviation is toward 0.89 the erosion mechanism will be predominant based on that diffusion mechanism is more predominant in F2. While the other formulas appeared to be deviated toward 0.89 this indicates that the erosion is the predominant mechanism in these formulas. The random distribution of the residual values as it is observed in **Figure 4.15** and having SSR values for all models NMT 11.65, indicates a good fitting for the model. (Nasereddin et al. 2018).

The permeation study was assessed using Franz cell apparatus, with a sheep nasal musoca as a membrane and SNF in the acceptor compartment media to

evaluate the permeability of RvT. As illustrated in **Figure 4.13**, the permeation results of RvT were in the order of $F1 > F3 > F4 > F2$, which were in a great agreement with the release result.

Statistical analysis of difference parameters such as cumulative amount of RvT per unit area (Q/A), steady state flux (J_{ss}) and permeability coefficient (P) among predetermined interval between formulations was performed. Significant difference in these parameters between the formulas was observed except for the (Q/A).

5.10. Stability Study

The stability study was achieved to evaluate the chemical stability of RvT in the nasal patch and the physical stability of the nasal patches under long term storage (normal and accelerated) conditions.

The content of 6 nasal patches from each formula for the same preparation was studied at previously determined time point: at the day of preparation, after one month, after three months, after six months.

At the normal long-term storage conditions, RvT appeared to be stable in the nasal patch formulations and compatible with the excipient.

The low degradation rate may be referred to the low concentration of water, therefore, low hydrolysis. The stability of the physical appearance was clearly observed.

At the accelerated storage conditions, RvT appeared to be stable in the nasal patch formulations, but the physical stability was not observed as a separation of HPMC and gelatin occurs, which could be referred to the low glass transition of gelatin as shown in Figure 5.4.

5.11. Conclusion

RvT analysis method was successfully validate in terms of selectivity, linearity, precision, recovery, robustness, and system suitability according to the ICH guidelines.

It was observed that all formulated nasal patches have the same physical appearance and surface pH, where the dimensions of the nasal patches depend on the mold since changing the composition of polymers has no significant effect on the dimensions. The fabricated formulas F1, F2, F3, and F4 appeared to have different characteristics in term of mechanical properties as F1 and F3 show the best % elongation and tensile strength rendering it more suitable for patch handling. While F4 provided the best adhesion properties for the insertion of the nasal patch and F2 provided the best mucoadhesive characteristics in the nasal cavity conditions. The content for all formulas was uniform with no significant difference. The release of RvT from the fabricated nasal patches appears to follow a hybrid model as gelatin swells and HPMC dissolved. F2 formula appeared to have release profile that is more sustained and constant release.

After weighing the pros and cons and a deeper understanding to the full vision of the purpose of the dosage form, it was suggested that F2 is the most promising formula among all formulas. for being the most adhesive formula in the nasal condition as the mucocilliary clearance is the main challenge for the nasal drug delivery and for it is sustained release profile.

Nasal patches were fabricated for the first time for nose-to-brain delivery of rivastigmine. The optimized HPLC method for rivastigmine analysis was validated according to ICH guideline. The fabricated formulas were successfully examined in terms of mechanical properties, physical appearance, dimension measurements, surface pH, mechanical properties, mucoadhesive properties, content uniformity, release and permeation, based on that F2 formula appeared to be a promising formula which was successfully provided the best characteristics to be suitable for further in-vivo study.

5.12. Further work

The nasal drug delivery is a promising and interesting area for research. We would recommend studying a dissolution apparatus that could suit the large-scale production and further in-vivo study for formulas. We would recommend studying an apparatus that mimics all the nasal condition in-vitro. Nasal drug delivery could provide a solution many CNS disorders especially the chronic diseases and meningitis. More studies could serve elderly, kids, unconscious, and pregnant patients. Additionally, nasal drug delivery could be an effective route to avoid many drug-drug interactions and drug-food interactions.

Chapter (6) References

- Abdelrahman, Fatma Elzahraa, Ibrahim Elsayed, Mary Kamal Gad, Ahmed Hassen Elshafeey, and Magdi Ibrahim Mohamed. 2017. "Response Surface Optimization, Ex Vivo and In Vivo Investigation of Nasal Spanlastics for Bioavailability Enhancement and Brain Targeting of Risperidone." *International Journal of Pharmaceutics* 530 (1–2): 1–11. <https://doi.org/10.1016/j.ijpharm.2017.07.050>.
- Abouhussein, Dalia M N, Abeer Khattab, Noha A Bayoumi, Ashgan F Mahmoud, and Tamer M Sakr. 2018. "Brain Targeted Rivastigmine Mucoadhesive Thermosensitive In Situ Gel: Optimization, in Vitro Evaluation, Radiolabeling, in Vivo Pharmacokinetics and Biodistribution." *Journal of Drug Delivery Science and Technology* 43: 129–40. <https://doi.org/https://doi.org/10.1016/j.jddst.2017.09.021>.
- Agrawal, Mukta, Swarnlata Saraf, Shailendra Saraf, Sophia G. Antimisiaris, Mahavir Bhupal Chougule, Sunday A. Shoyele, and Amit Alexander. 2018. "Nose-to-Brain Drug Delivery: An Update on Clinical Challenges and Progress towards Approval of Anti-Alzheimer Drugs." *Journal of Controlled Release* 281 (April): 139–77. <https://doi.org/10.1016/j.jconrel.2018.05.011>.
- Akel, Hussein, Ruba Ismail, and Ildikó Csóka. 2020. "Progress and Perspectives of Brain-Targetin1. Akel H, Ismail R, Csóka I. Progress

- and Perspectives of Brain-Targeting Lipid-Based Nanosystems via the Nasal Route in Alzheimer's Disease. *Eur J Pharm Biopharm* [Internet]. 2020;148:38–53. Available from: Http.” *European Journal of Pharmaceutics and Biopharmaceutics* 148: 38–53. <https://doi.org/https://doi.org/10.1016/j.ejpb.2019.12.014>.
- Alexander, Amit, Mukta Agrawal, Mahavir Bhupal Chougule, Shailendra Saraf, and Swarnlata Saraf. 2020. *Nose-to-Brain Drug Delivery: An Alternative Approach for Effective Brain Drug Targeting. an Alternative Approach for Effective Brain Drug Targeting. Nanopharmaceuticals: Volume 1: Expectations and Realities of Multifunctional Drug Delivery Systems*. Elsevier Inc. <https://doi.org/10.1016/B978-0-12-817778-5.00009-9>.
- Alipal, J., N. A.S. Mohd Pu'ad, T. C. Lee, N. H.M. Nayan, N. Sahari, H. Basri, M. I. Idris, and H. Z. Abdullah. 2019. “A Review of Gelatin: Properties, Sources, Process, Applications, and Commercialisation.” *Materials Today: Proceedings* 42: 240–50. <https://doi.org/10.1016/j.matpr.2020.12.922>.
- Alshweiat, Areen, Ildikó I. Csóka, Ferenc Tömösi, Tamás Janáky, Anita Kovács, Róbert Gáspár, Anita Sztojkov-Ivanov, et al. 2020. “Nasal Delivery of Nanosuspension-Based Mucoadhesive Formulation with Improved Bioavailability of Loratadine: Preparation, Characterization, and in Vivo Evaluation.” *International Journal of Pharmaceutics* 579:

119166. <https://doi.org/10.1016/j.ijpharm.2020.119166>.

Articus, Konstantin, Klaus Hechenbichler, and Klaus Bornholdt. 2011.

“EXPECT (EXelon Patch EffeCtiveness Trial): Effectiveness and Tolerability of Transdermal Rivastigmin in Daily Practice.” *Alzheimer’s & Dementia* 7 (4, Supplement): S777.

<https://doi.org/https://doi.org/10.1016/j.jalz.2011.05.2235>.

Babin, Á, and Eric Dickinson. 2001. “Influence of Transglutaminase Treatment on the Thermoreversible Gelation of Gelatin” 15: 271–76.

Barbosa, Quinta, Palmer Vicente Pulla-huillca, Andresa Gomes, M Ana, Rodrigo Vinícius Lourenço, and Paulo Jos. 2021. “Wettability of Gelatin-Based Films: The Effects of Hydrophilic or Hydrophobic Plasticizers and Nanoparticle Loads” 297 (October 2020). <https://doi.org/10.1016/j.jfoodeng.2021.110480>.

Barnabas, Wilson. 2019. “Drug Targeting Strategies into the Brain for Treating Neurological Diseases.” *Journal of Neuroscience Methods* 311: 133–46. <https://doi.org/10.1016/j.jneumeth.2018.10.015>.

Barrios, Arthur William, Pablo Sanchez Quinteiro, and Ignacio Salazar. 2014. “The Nasal Cavity of the Sheep and Its Olfactory Sensory Epithelium” 1059 (July): 1052–59. <https://doi.org/10.1002/jemt.22436>.

Bruschi, Marcos Luciano, ed. 2015a. “Mathematical Models of Drug Release.” In *Strategies to Modify the Drug Release from Pharmaceutical*

- Systems*, 63–86. Elsevier. <https://doi.org/10.1016/b978-0-08-100092-2.00005-9>.
- . 2015b. “Mathematical Models of Drug Release 5.” <https://doi.org/10.1016/B978-0-08-100092-2.00005-9>.
- Carvalho, Flávia Chiva, Marcos Luciano Bruschi, Raul Cesar Evangelista, Maria Palmira, and Daflon Gremião. 2010. “Mucoadhesive Drug Delivery Systems” 46 (2008): 1–18.
- Center for Drug Evaluation and Research. 1994. *Reviewer Guidance Validation of Chromatographic Methods*.
- Chamanza, R, and J A Wright. 2015. “A Review of the Comparative Anatomy , Histology , Physiology and Pathology of the Nasal Cavity of Rats , Mice , Dogs and Non-Human Primates . Relevance to Inhalation Toxicology and Human Health Risk Assessment.” *Journal of Comparative Pathology*. <https://doi.org/10.1016/j.jcpa.2015.08.009>.
- Chatterjee, Bappaditya, Bapi Gorain, Keithanchali Mohananaidu, Pinaki Sengupta, Uttam Kumar Mandal, and Hira Choudhury. 2019. “Targeted Drug Delivery to the Brain via Intranasal Nanoemulsion: Available Proof of Concept and Existing Challenges.” *International Journal of Pharmaceutics* 565 (May): 258–68. <https://doi.org/10.1016/j.ijpharm.2019.05.032>.
- ChemicalBook. 2021. “Rivastigmine Tartrate.” 2021.

https://www.chemicalbook.com/ChemicalProductProperty_EN_CB9500851.htm.

Chen, Jia Chen, Li Ming Li, and Jian Qing Gao. 2019. "Biomaterials for Local Drug Delivery in Central Nervous System." *International Journal of Pharmaceutics* 560 (January): 92–100. <https://doi.org/10.1016/j.ijpharm.2019.01.071>.

Chen, Jian, Xiaomei Wang, Juan Wang, Guangli Liu, and Xing Tang. 2008. "Evaluation of Brain-Targeting for the Nasal Delivery of Ergoloid Mesylate by the Microdialysis Method in Rats." *European Journal of Pharmaceutics and Biopharmaceutics* 68 (3): 694–700. <https://doi.org/https://doi.org/10.1016/j.ejpb.2007.08.013>.

Chen, Tzu Hua, Mei Chuan Chou, Chiou Lian Lai, Shyh Jong Wu, Chia Ling Hsu, and Yuan Han Yang. 2017. "Factors Affecting Therapeutic Response to Rivastigmine in Alzheimer's Disease Patients in Taiwan." *Kaohsiung Journal of Medical Sciences* 33 (6): 277–83. <https://doi.org/10.1016/j.kjms.2017.04.006>.

Chokshi, Ashish, Ravi Vaishya, Rachana Inavolu, and Thrimoorthy Potta. 2019. "Intranasal Spray Formulation Containing Rizatriptan Benzoate for the Treatment of Migraine." *International Journal of Pharmaceutics* 571: 118702. <https://doi.org/10.1016/j.ijpharm.2019.118702>.

Christian, H. 2014. "First Clinical Data of the Neuroprotective Effects of

- Nasal Insulin Application in Patients with Alzheimer ' s Disease” 10: 33–37. <https://doi.org/10.1016/j.jalz.2013.12.006>.
- Citrome, Leslie, Allitia DiBernardo, and Jaskaran Singh. 2020. “Appraising Esketamine Nasal Spray for the Management of Treatment-Resistant Depression in Adults: Number Needed to Treat, Number Needed to Harm, and Likelihood to Be Helped or Harmed.” *Journal of Affective Disorders* 271 (November 2019): 228–38. <https://doi.org/10.1016/j.jad.2020.03.106>.
- Cook, Sarah L, Stephanie P Bull, Lisa Methven, Jane K Parker, and Vitaliy V Khutoryanskiy. 2017. “Mucoadhesion : A Food Perspective.” *Food Hydrocolloids* 72: 281–96. <https://doi.org/10.1016/j.foodhyd.2017.05.043>.
- Crowe, Tyler P., M. Heather West Greenlee, Anumantha G. Kanthasamy, and Walter H. Hsu. 2018. “Mechanism of Intranasal Drug Delivery Directly to the Brain.” *Life Sciences* 195: 44–52. <https://doi.org/10.1016/j.lfs.2017.12.025>.
- Cuq, Bernard, Nathalie Gontard, and Jean-louis Cuq. 1997. “Selected Functional Properties of Fish Myofibrillar Protein-Based Films As Affected by Hydrophilic Plasticizers,” 622–26.
- Davergaon, Channamallikarjun A, and New V V Nagar. 2017. “CRITICAL REVIEW OF PHANA MARMA WITH SPECIAL REFERENCE TO”

5 (10).

Değirmenci, Yıldız, and Hulusi Keçeci. 2016. “Visual Hallucinations Due to Rivastigmine Transdermal Patch Application in Alzheimer’s Disease; The First Case Report.” *International Journal of Gerontology* 10 (4): 240–41. <https://doi.org/10.1016/j.ijge.2015.10.010>.

Dehpour, Ahmad Reza. 2021. *Naturally Occurring Chemicals against Alzheimer ’ s Disease*.

Dinç, Mehmet Emre, Nuray Bayar Muluk, and Becky M Vonakis. 2020. “Physiology of the Nose and Paranasal Sinuses BT - All Around the Nose: Basic Science, Diseases and Surgical Management.” In , edited by Cemal Cingi and Nuray Bayar Muluk, 57–63. Cham: Springer International Publishing. https://doi.org/10.1007/978-3-030-21217-9_6.

Ding, Cuicui, Min Zhang, and Guoying Li. 2015. “Preparation and Characterization of Collagen / Hydroxypropyl Methylcellulose (HPMC) Blend Film.” *Carbohydrate Polymers* 119: 194–201. <https://doi.org/10.1016/j.carbpol.2014.11.057>.

Djupesland, Per G., John C. Messina, and Ramy A. Mahmoud. 2014. “The Nasal Approach to Delivering Treatment for Brain Diseases: An Anatomic, Physiologic, and Delivery Technology Overview.” *Therapeutic Delivery* 5 (6): 709–33. <https://doi.org/10.4155/tde.14.41>.

Dong, Jingliang, Yidan Shang, Kiao Inthavong, Hak Kim Chan, and Jiyan

- Tu. 2018. "Partitioning of Dispersed Nanoparticles in a Realistic Nasal Passage for Targeted Drug Delivery." *International Journal of Pharmaceutics* 543 (1–2): 83–95. <https://doi.org/10.1016/j.ijpharm.2018.03.046>.
- Eldufani, Jabril, and Gilbert Blaise. 2019. "The Role of Acetylcholinesterase Inhibitors Such as Neostigmine and Rivastigmine on Chronic Pain and Cognitive Function in Aging: A Review of Recent Clinical Applications." *Alzheimer's & Dementia: Translational Research & Clinical Interventions* 5: 175–83. <https://doi.org/https://doi.org/10.1016/j.trci.2019.03.004>.
- Emborg, Marina E., and Jeffrey H. Kordower. 2000. "Delivery of Therapeutic Molecules into the CNS." *Progress in Brain Research* 128: 323–32. [https://doi.org/10.1016/S0079-6123\(00\)28029-1](https://doi.org/10.1016/S0079-6123(00)28029-1).
- Erdő, Franciska, Luca Anna Bors, Dániel Farkas, Ágnes Bajza, and Sveinbjörn Gizurarson. 2018. "Evaluation of Intranasal Delivery Route of Drug Administration for Brain Targeting." *Brain Research Bulletin* 143 (October): 155–70. <https://doi.org/10.1016/j.brainresbull.2018.10.009>.
- Eskander, Mariam F, Nicholas G Nagykerly, Elaine Y Leung, Bahiyyih Khelghati, and Changiz Geula. 2005. "Rivastigmine Is a Potent Inhibitor of Acetyl- and Butyrylcholinesterase in Alzheimer's Plaques and

Tangles.” *Brain Research* 1060 (1): 144–52.

<https://doi.org/https://doi.org/10.1016/j.brainres.2005.08.039>.

Fachel, Silveira, Luana Roberta, Juliana Hofst, Valquíria Linck Bassani, Amelia Teresinha Henriques, and Letícia Scherer. 2020. “Chitosan-Coated Rosmarinic Acid Nanoemulsion Nasal Administration Protects against LPS-Induced Memory Deficit , Neuroinflammation , and Oxidative Stress in Wistar Rats” 141 (October). <https://doi.org/10.1016/j.neuint.2020.104875>.

Fan, Lihong, Huibin Zhu, Hua Zheng, Yongmei Xu, and Chaocan Zhang. 2007. “Structure and Properties of Blend Fibers Prepared from Alginate and Konjac Glucomannan.” <https://doi.org/10.1002/app>.

Fang, Fei, Dan Zou, Wei Wang, Ying Yin, Tieying Yin, Shilei Hao, Bochu Wang, Guixue Wang, and Yazhou Wang. 2017. “Non-Invasive Approaches for Drug Delivery to the Brain Based on the Receptor Mediated Transport.” *Materials Science and Engineering C* 76: 1316–27. <https://doi.org/10.1016/j.msec.2017.02.056>.

Fantasia, Heidi Collins. 2020. “Esketamine Nasal Spray for Treatment-Resistant Depression.” *Nursing for Women’s Health*, no. May: 3–7. <https://doi.org/10.1016/j.nwh.2020.03.004>.

Fine, Jared M., Benjamin M. Stroebel, Katherine A. Faltesek, Kaoru Terai, Lucas Haase, Kristin E. Knutzen, Jacob Kosyakovsky, et al. 2020.

- “Intranasal Delivery of Low-Dose Insulin Ameliorates Motor Dysfunction and Dopaminergic Cell Death in a 6-OHDA Rat Model of Parkinson’s Disease.” *Neuroscience Letters* 714: 134567. <https://doi.org/10.1016/j.neulet.2019.134567>.
- Fuh, Jong-Ling, T F Chen, T H Lan, Y W Yang, C F Tsai, L J Chuo, Pei Ning Wang, Ming-Jang Chiu, and S J Wang. 2017. “A 52-Week Open-Label Study to Investigate Tolerability of Rivastigmine Switching from Oral Capsule to Transdermal Patch in Mild to Moderate Alzheimer’s Disease Patients in Taiwan.” *Journal of the Neurological Sciences* 381 (October): 1030–31. <https://doi.org/10.1016/j.jns.2017.08.2909>.
- Gänger, Stella, and Katharina Schindowski. 2018. “Tailoring Formulations for Intranasal Nose-to-Brain Delivery: A Review on Architecture, Physico-Chemical Characteristics and Mucociliary Clearance of the Nasal Olfactory Mucosa.” *Pharmaceutics* 10 (3). <https://doi.org/10.3390/pharmaceutics10030116>.
- Gonçalves, Joana, Joana Bicker, Filipa Gouveia, Joana Liberal, Rui Caetano Oliveira, Gilberto Alves, Amílcar Falcão, and Ana Fortuna. 2019. “Nose-to-Brain Delivery of Levetiracetam after Intranasal Administration to Mice.” *International Journal of Pharmaceutics* 564: 329–39. <https://doi.org/10.1016/j.ijpharm.2019.04.047>.
- Gouda, Radhakant, Himankar Baishya, and Zhao Qing. 2017. “Application

- of Mathematical Models in Drug Release Kinetics of Carbidopa and Levodopa ER Tablets” 6 (2): 1–8. <https://doi.org/10.4172/2329-6631.1000171>.
- Graff, Candace L., and Gary M. Pollack. 2005. “Nasal Drug Administration: Potential for Targeted Central Nervous System Delivery.” *Journal of Pharmaceutical Sciences* 94 (6): 1187–95. <https://doi.org/10.1002/jps.20318>.
- Hussein, Nozad Rashid, Huner Kamal Omer, Abdelbary M A Elhissi, and Waqar Ahmed. 2020. “Chapter 15 - Advances in Nasal Drug Delivery Systems.” In , edited by Waqar Ahmed, David A Phoenix, Mark J Jackson, and Charalambos P B T - Advances in Medical and Surgical Engineering Charalambous, 279–311. Academic Press. <https://doi.org/https://doi.org/10.1016/B978-0-12-819712-7.00015-2>.
- ICH guidelines Q1F. 2021. “Stability Testing of Active Pharmaceutical Ingredients ICH,” no. February 2003: 309–52.
- ICH guidelines Q2(R1). 2005. “Q2(R1)-Validatio of Analytical Procedures: Texts and Methodology.” In .
- Illum, Lisbeth. 1996. “Nasal Delivery. The Use of Animal Models to Predict Performance in Man.” *Journal of Drug Targeting* 3 (6): 427–42. <https://doi.org/10.3109/10611869609015963>.
- Inoue, Daisuke, Akiko Tanaka, Shunsuke Kimura, Akiko Kiriyaama,

- Hidemasa Katsumi, Akira Yamamoto, Ken-ichi Ogawara, et al. 2018. “The Relationship between in Vivo Nasal Drug Clearance and in Vitro Nasal Mucociliary Clearance: Application to the Prediction of Nasal Drug Absorption.” *European Journal of Pharmaceutical Sciences* 117: 21–26. <https://doi.org/https://doi.org/10.1016/j.ejps.2018.01.032>.
- J.K. ARONSON MA, DPhil, MBChB, FRCP, FBPharmacolS, FFPM (Hon). 2010. *Side Effects of Drugs Annual* 32.
- Karasulu, Ercument, Altug Yavasoglu, Z. Evren, sanal, Yigit Uyanıkgil, and H. Ye, sim Karasulu. 2008. “Permeation Studies and Histological Examination of Sheep Nasal Mucosa Following Administration of Different Nasal Formulations with or without Absorption Enhancers Erc Ument,” 219–25. <https://doi.org/10.1080/10717540802006377>.
- Karasulu, H. Yeşim, Z. Evren Şanal, Sumru Sözer, Tamer Güneri, and Gökhan Ertan. 2008. “Permeation Studies of Indomethacin from Different Emulsions for Nasal Delivery and Their Possible Anti-Inflammatory Effects.” *AAPS PharmSciTech* 9 (2): 342–48. <https://doi.org/10.1208/s12249-008-9053-9>.
- Kavoi, Boniface, Andrew Makanya, Jameela Hassanali, Hans-erik Carlsson, and Stephen Kiama. 2010. “Annals of Anatomy Comparative Functional Structure of the Olfactory Mucosa in the Domestic Dog and Sheep.” *Annals of Anatomy* 192 (5): 329–37.

<https://doi.org/10.1016/j.aanat.2010.07.004>.

Khan, Abdur Rauf, Mengrui Liu, Muhammad Wasim Khan, and Guangxi Zhai. 2017. "Progress in Brain Targeting Drug Delivery System by Nasal Route." *Journal of Controlled Release* 268 (September): 364–89. <https://doi.org/10.1016/j.jconrel.2017.09.001>.

Ko, Kuang-ta, T E Needham, and H Zia. 1998. "Emulsion Formulations of Testosterone for Nasal Administration" 15 (2): 197–205.

Kozlovskaya, Luba, Mohammed Abou-Kaoud, and David Stepensky. 2014. "Quantitative Analysis of Drug Delivery to the Brain via Nasal Route." *Journal of Controlled Release* 189: 133–40. <https://doi.org/10.1016/j.jconrel.2014.06.053>.

Laffleur, Flavia. 2018. "Nasal Adhesive Patches - Approach for Topical Application for Dry Nasal Syndrome." *International Journal of Biological Macromolecules* 111: 493–97. <https://doi.org/10.1016/j.ijbiomac.2018.01.043>.

Laffleur, Flavia, Benedikt Strasdat, Arshad Mahmood, Tobias Reichenberger, Melanie Gräber, and Kesinee Netsomboon. 2018. "Nasal Patches Containing Naphazoline for Management of Nasal Impairments." *Journal of Drug Delivery Science and Technology* 45 (August 2017): 54–59. <https://doi.org/10.1016/j.jddst.2018.02.012>.

Leal, Jasmim, Hugh D C Smyth, and Debadyuti Ghosh. 2017.

- “Physicochemical Properties of Mucus and Their Impact on Transmucosal Drug Delivery.” *International Journal of Pharmaceutics* 532 (1): 555–72.
<https://doi.org/https://doi.org/10.1016/j.ijpharm.2017.09.018>.
- Li, Yan-hua, Ling Feng, Guang-Xian Zhang, and Cun-gen Ma. 2015. “Intranasal Delivery of Stem Cells as Therapy for Central Nervous System Disease.” *Experimental and Molecular Pathology* 98 (2): 145–51. <https://doi.org/https://doi.org/10.1016/j.yexmp.2015.01.016>.
- Li, Yang, Xiyong Wu, Quanguang Zhu, Zhongjian Chen, Yi Lu, Jianping Qi, and Wei Wu. 2019. “Improving the Hypoglycemic Effect of Insulin via the Nasal Administration of Deep Eutectic Solvents.” *International Journal of Pharmaceutics* 569 (April).
<https://doi.org/10.1016/j.ijpharm.2019.118584>.
- Liu, Xingxun, Zhili Ji, Weiwei Peng, Min Chen, Long Yu, and Fan Zhu. 2020. “Chemical Mapping Analysis of Compatibility in Gelatin and Hydroxypropyl Methylcellulose Blend Films.” *Food Hydrocolloids* 104 (September 2019): 105734.
<https://doi.org/10.1016/j.foodhyd.2020.105734>.
- Loboa, E G. 2016. 23 - *Nanofibrous Smart Bandages for Wound Care. Wound Healing Biomaterials - Volume 2*. Vol. 2. Elsevier Ltd.
<https://doi.org/10.1016/B978-1-78242-456-7.00023-4>.

- Malaiya, Mayank Kumar, Ashish Jain, Hurkat Pooja, Anki Jain, and Dharmendra Jain. 2018. "Controlled Delivery of Rivastigmine Using Transdermal Patch for Effective Management of Alzheimer's Disease." *Journal of Drug Delivery Science and Technology* 45: 408–14. <https://doi.org/https://doi.org/10.1016/j.jddst.2018.03.030>.
- Meng, Ying, Christopher B. Pople, Harriet Lea-Banks, Agessandro Abrahao, Benjamin Davidson, Suganth Suppiah, Laura M. Vecchio, et al. 2019. "Safety and Efficacy of Focused Ultrasound Induced Blood-Brain Barrier Opening, an Integrative Review of Animal and Human Studies." *Journal of Controlled Release* 309: 25–36. <https://doi.org/10.1016/j.jconrel.2019.07.023>.
- Menzel, Claudia, Max Jelkmann, Flavia Laffleur, and Andreas Bernkop-Schnürch. 2017. "Nasal Drug Delivery: Design of a Novel Mucoadhesive and in Situ Gelling Polymer." *International Journal of Pharmaceutics* 517 (1–2): 196–202. <https://doi.org/10.1016/j.ijpharm.2016.11.055>.
- Mercadante, Sebastiano, Federica Aielli, Claudio Adile, Andrea Costanzi, and Alessandra Casuccio. 2016. "Fentanyl Pectin Nasal Spray Versus Oral Morphine in Doses Proportional to the Basal Opioid Regimen for the Management of Breakthrough Cancer Pain : A Comparative Study." *Journal of Pain and Symptom Management* 52 (1): 27–34. <https://doi.org/10.1016/j.jpainsymman.2016.01.010>.

- Mittal, Deepti, Asgar Ali, Sanjula Baboota, and Jasjeet K Sahni. 2014. "Insights into Direct Nose to Brain Delivery : Current Status and Future Perspective" 7544. <https://doi.org/10.3109/10717544.2013.838713>.
- Morgan, Timothy M., and Bob Soh. 2017. "Absolute Bioavailability and Safety of a Novel Rivastigmine Nasal Spray in Healthy Elderly Individuals." *British Journal of Clinical Pharmacology* 83 (3): 510–16. <https://doi.org/10.1111/bcp.13133>.
- Morsy, Reda, Marwa Hosny, Fikry Reicha, and Tarek Elnimr. 2017. "Developing and Physicochemical Evaluation of Cross-Linked Electrospun Gelatin e Glycerol Nano Fi Brous Membranes for Medical Applications." *Journal of Molecular Structure* 1135: 222–27. <https://doi.org/10.1016/j.molstruc.2017.01.064>.
- Nasereddin, Jehad M., Nikolaus Wellner, Muqdad Alhijjaj, Peter Belton, and Sheng Qi. 2018. "Development of a Simple Mechanical Screening Method for Predicting the Feedability of a Pharmaceutical FDM 3D Printing Filament." *Pharmaceutical Research* 35 (8): 151. <https://doi.org/10.1007/s11095-018-2432-3>.
- Nižić, Laura, Joanna Potaś, Katarzyna Winnicka, Marta Szekalska, Iva Erak, Matija Gretić, Mario Jug, and Anita Hafner. 2020. "Development, Characterisation and Nasal Deposition of Melatonin-Loaded Pectin/Hypromellose Microspheres." *European Journal of*

Pharmaceutical Sciences 141.

<https://doi.org/10.1016/j.ejps.2019.105115>.

Onur, E. 2004. "Nasal Route and Drug Delivery Systems •," 137–42.

Pandey, Preeti, Peter J. Cabot, Benjamin Wallwork, Benedict J. Panizza, and

Harendra S. Parekh. 2017. "Formulation, Functional Evaluation and Ex

Vivo Performance of Thermoresponsive Soluble Gels - A Platform for

Therapeutic Delivery to Mucosal Sinus Tissue." *European Journal of*

Pharmaceutical Sciences 96: 499–507.

<https://doi.org/10.1016/j.ejps.2016.10.017>.

Pandey, Vikas, Anuradha Gadeval, Saket Asati, Priyanka Jain, Navneet Jain,

Ram Kumar Roy, Muktika Tekade, Vandana Soni, and Rakesh K.

Tekade. 2019. *Formulation Strategies for Nose-to-Brain Delivery of*

Therapeutic Molecules. Drug Delivery Systems. Elsevier Inc.

<https://doi.org/10.1016/B978-0-12-814487-9.00007-7>.

Patel, Ashwini, Nazneen Surti, and Ashok Mahajan. 2019. "Intranasal Drug

Delivery: Novel Delivery Route for Effective Management of

Neurological Disorders." *Journal of Drug Delivery Science and*

Technology 52 (November 2018): 130–37.

<https://doi.org/10.1016/j.jddst.2019.04.017>.

Pathan, Shadab A, Zeenat Iqbal, Syed M A Zaidi, Sushma Talegaonkar,

Divya Vohra, K Jain, Adnan Azeem, et al. 2009. "CNS Drug Delivery

Systems : Novel Approaches,” 71–89.

Patrick J. Sinko, Yashveer Singh. 2011. *MARTIN'S PHYSICAL PHARMACY AND PHARMACEUTICAL SCIENCES*. 50th ed.

Penovich, Patricia, James W Wheless, R Edward Hogan, Cynthia Guerra, David F Cook, Enrique Carrazana, and Adrian L Rabinowicz. 2021. “Examining the Patient and Caregiver Experience with Diazepam Nasal Spray for Seizure Clusters : Results from an Exit Survey of a Phase 3 , Open-Label , Repeat-Dose Safety Study.” *Epilepsy & Behavior* 121: 108013. <https://doi.org/10.1016/j.yebeh.2021.108013>.

Petroudy, S R Djafari. 2017. *3 - Physical and Mechanical Properties of Natural Fibers. Advanced High Strength Natural Fibre Composites in Construction*. Elsevier Ltd. <https://doi.org/10.1016/B978-0-08-100411-1.00003-0>.

Prajapati Twinkle Kantibhai*, Kaushika S. Patel and Dr. Shreeraj Shah. 2015. “Test Methods of Bioadhesive System.” *World Journal of Pharmaceutical Research* 7 (2): 267–78. <https://doi.org/10.20959/wjpr20182-10636>.

Pund, Swati, Ganesh Rasve, and Ganesh Borade. 2013. “Ex Vivo Permeation Characteristics of Venlafaxine through Sheep Nasal Mucosa.” *European Journal of Pharmaceutical Sciences* 48 (1–2): 195–201. <https://doi.org/10.1016/j.ejps.2012.10.029>.

Rathod, Mansi, Disha Suthar, Hetal Patel, Pragna Shelat, and Punit Parejiya.

2019. "Microemulsion Based Nasal Spray: A Systemic Approach for Non-CNS Drug, Its Optimization, Characterization and Statistical Modelling Using QbD Principles." *Journal of Drug Delivery Science and Technology* 49: 286–300.
<https://doi.org/10.1016/j.jddst.2018.11.017>.

Ren, M, Steve S Chung, Barry Gidal, Aliceson King, Jerry Tomasovic, James W Wheless, and Peter J Van Ess. 2021. "Clinical Pharmacokinetic and Pharmacodynamic Profile of Midazolam Nasal Spray" 171. <https://doi.org/10.1016/j.eplepsyres.2021.106567>.

Rowe, Raymond C, Paul J Sheskey, and Marian E Quinn. 2009. *Handbook of Pharmaceutical Excipients 6t*.

Saeedi, Majid, Masoumeh Eslamifar, Khadijeh Khezri, and Solmaz Maleki Dizaj. 2019. "Applications of Nanotechnology in Drug Delivery to the Central Nervous System." *Biomedicine and Pharmacotherapy* 111 (December 2018): 666–75.
<https://doi.org/10.1016/j.biopha.2018.12.133>.

Salade, Laurent, Nathalie Wauthoz, Jonathan Goole, and Karim Amighi. 2019. "How to Characterize a Nasal Product. The State of the Art of in Vitro and Ex Vivo Specific Methods." *International Journal of Pharmaceutics* 561: 47–65.

<https://doi.org/10.1016/j.ijpharm.2019.02.026>.

Salazar, Ignacio, Pablo Sanchez-Quinteiro, Arthur W. Barrios, Manuel López Amado, and José A. Vega. 2019. "Anatomy of the Olfactory Mucosa." *Handbook of Clinical Neurology* 164: 47–65. <https://doi.org/10.1016/B978-0-444-63855-7.00004-6>.

Scienti, Annual Fall. 2018a. "CLINICAL IMPROVEMENTS IN ERECTILE FUNCTION AND MOOD IN HYPOGONADAL MEN TREATED WITH 4.5% NASAL TESTOSTERONE GEL (NATESTO)," 80–81. <https://doi.org/10.1016/j.jsxm.2017.11.193>.

———. 2018b. "Preservation of Normal Concentration of Pituitary Gonadotropins Despite Achievement of Normal Serum Testosterone Levels in Hypogonadal Men Treated with 4.5% Nasal Testosterone Gel (Natesto)," 42–43. <https://doi.org/10.1016/j.jsxm.2017.11.065>.

Sekerdag, Emine. 2017. "Chapter 5 - Nasal Physiology and Drug Transport." In , edited by Yasemin Gürsoy-Özdemir, Sibel Bozdağ-Pehlivan, and Emine B T - Nanotechnology Methods for Neurological Diseases and Brain Tumors Sekerdag, 93–102. Academic Press. <https://doi.org/https://doi.org/10.1016/B978-0-12-803796-6.00005-8>.

Shah, Brijesh, Dignesh Khunt, Himanshu Bhatt, Manju Misra, and Harish Padh. 2015. "Application of Quality by Design Approach for Intranasal Delivery of Rivastigmine Loaded Solid Lipid Nanoparticles: Effect on

- Formulation and Characterization Parameters.” *European Journal of Pharmaceutical Sciences* 78: 54–66.
<https://doi.org/https://doi.org/10.1016/j.ejps.2015.07.002>.
- Shaw, Chi Kee Leslie, Robert B. Dymock, Allison Cowin, and Peter John Wormald. 2000. “Effect of Packing on Nasal Mucosa of Sheep.” *Journal of Laryngology and Otology* 114 (7): 506–9.
<https://doi.org/10.1258/0022215001906246>.
- Silver, Robert D, Martin C Carey, and J Dueovi. 1987. “Effects of Sodium Taurodihydrofusldate on Nasal Absorption of Insulin in Sheep” 76 (5): 351–55.
- Simon, Alice, Maria Inês Amaro, Lucio Mendes Cabral, Anne Marie Healy, and Valeria Pereira De Sousa. 2016. “Development of a Novel Dry Powder Inhalation Formulation for the Delivery of Rivastigmine Hydrogen Tartrate.” *International Journal of Pharmaceutics* 501 (1–2): 124–38. <https://doi.org/10.1016/j.ijpharm.2016.01.066>.
- Škrovánková, Soňa, Ladislava Mišurcová, and Ludmila Machů. 2012. “Chapter Three - Antioxidant Activity and Protecting Health Effects of Common Medicinal Plants.” In , edited by Jeyakumar B T - Advances in Food and Nutrition Research Henry, 67:75–139. Academic Press.
<https://doi.org/https://doi.org/10.1016/B978-0-12-394598-3.00003-4>.
- Tahara, Koichiro, Ken Yamamoto, and Toshiaki Nishihata. 1996.

“International Application of Model-Independent and Model Analysis for the Investigation of Effect of Drug Solubility on Its Release Rate from Hydroxypropyl Methylcellulose Sustained Release Tablets” 133: 17–27.

Takeuchi, Yoshiko, Nozomi Ikeda, Kohei Tahara, and Hirofumi Takeuchi. 2020. “Mechanical Characteristics of Orally Disintegrating Films : Comparison of Folding Endurance and Tensile Properties.” *International Journal of Pharmaceutics* 589 (September): 119876. <https://doi.org/10.1016/j.ijpharm.2020.119876>.

Tamasree Majumder, Gopa Roy Biswas, and Sutapa Biswas Majee. 2016. “Hydroxy Propyl Methyl Cellulose: Different Aspects in Drug Delivery.” *Journal of Pharmacy and Pharmacology* 4 (8). <https://doi.org/10.17265/2328-2150/2016.08.003>.

Tangri, Pranshu, and N V Satheesh Madhav. 2016. “ORAL MUCOADHESIVE DRUG DELIVERY SYSTEMS : A REVIEW,” no. April 2009. <https://doi.org/10.1007/s11094-009-0271-6>.

Tedesco, Marcela P, Carla A Monaco-lourenço, and Rosemary A Carvalho. 2016. “Gelatin / Hydroxypropyl Methylcellulose Matrices — Polymer Interactions Approach for Oral Disintegrating Fi Lms.” *Materials Science & Engineering C* 69: 668–74. <https://doi.org/10.1016/j.msec.2016.07.023>.

- Tekade, Muktika, Neha Maheshwari, Susanne R Youngren-ortiz, Vikas Pandey, Yashu Chourasiya, Vandana Soni, Pran Kishore Deb, and Mukesh Chandra Sharma. 2019. *Thiolated-Chitosan: A Novel Mucoadhesive Polymer for Better-Targeted Drug Delivery. Biomaterials and Bionanotechnology*. Elsevier Inc. <https://doi.org/10.1016/B978-0-12-814427-5.00013-5>.
- The United States Pharmacopeial Convention. 2021. "United States Pharmacopoeia 43-National Formulary 38." In .
- Tiozzo Fasiolo, Laura, Michele Dario Manniello, Elena Tratta, Francesca Buttini, Alessandra Rossi, Fabio Sonvico, Fabrizio Bortolotti, Paola Russo, and Gaia Colombo. 2018. "Opportunity and Challenges of Nasal Powders: Drug Formulation and Delivery." *European Journal of Pharmaceutical Sciences* 113 (September 2017): 2–17. <https://doi.org/10.1016/j.ejps.2017.09.027>.
- Trotta, Valentina, Barbara Pavan, Luca Ferraro, Sarah Beggiato, Daniela Traini, Larissa Gomes Des Reis, Santo Scalia, and Alessandro Dalpiaz. 2018. "Brain Targeting of Resveratrol by Nasal Administration of Chitosan-Coated Lipid Microparticles." *European Journal of Pharmaceutics and Biopharmaceutics* 127: 250–59. <https://doi.org/10.1016/j.ejpb.2018.02.010>.
- Vasvári, Gábor, Bence Csontos, Tamás Sovány, Géza Regdon, Attila

- Bényei, Judit Váradi, Ildikó Bácskay, et al. 2018. “Development and Characterisation of Modified Release Hard Gelatin Capsules, Based on In Situ Lipid Matrix Formation.” *AAPS PharmSciTech* 19 (7): 3165–76. <https://doi.org/10.1208/s12249-018-1146-5>.
- Wang, Danyang, and Lin Ping Wu. 2017. “Nanomaterials for Delivery of Nucleic Acid to the Central Nervous System (CNS).” *Materials Science and Engineering C* 70: 1039–46. <https://doi.org/10.1016/j.msec.2016.04.011>.
- Wang, Qianwen, Zhong Zuo, Cheuk Kit Chucky Cheung, and Sharon Shui Yee Leung. 2019. “Updates on Thermosensitive Hydrogel for Nasal, Ocular and Cutaneous Delivery.” *International Journal of Pharmaceutics* 559: 86–101. <https://doi.org/10.1016/j.ijpharm.2019.01.030>.
- Wavikar, Preeti, Rohan Pai, and Pradeep Vavia. 2017. “Nose to Brain Delivery of Rivastigmine by In Situ Gelling Cationic Nanostructured Lipid Carriers: Enhanced Brain Distribution and Pharmacodynamics.” *Journal of Pharmaceutical Sciences* 106 (12): 3613–22. <https://doi.org/10.1016/j.xphs.2017.08.024>.
- Wingrove, Jed, Magda Swedrowska, Regina Scherließ, Mark Parry, Mervin Ramjeeawon, David Taylor, Gregoire Gauthier, et al. 2019. “Characterisation of Nasal Devices for Delivery of Insulin to the Brain

- and Evaluation in Humans Using Functional Magnetic Resonance Imaging.” *Journal of Controlled Release* 302 (Circ. Res. 118 11 2016): 140–47. <https://doi.org/10.1016/j.jconrel.2019.03.032>.
- Xie, Jinbing, Zheyu Shen, Yasutaka Anraku, Kazunori Kataoka, and Xiaoyuan Chen. 2019. “Nanomaterial-Based Blood-Brain-Barrier (BBB) Crossing Strategies.” *Biomaterials* 224: 119491. <https://doi.org/https://doi.org/10.1016/j.biomaterials.2019.119491>.
- Yang, Zhen Zhen, Yan Qing Zhang, Zhan Zhang Wang, Kai Wu, Jin Ning Lou, and Xian Rong Qi. 2013. “Enhanced Brain Distribution and Pharmacodynamics of Rivastigmine by Liposomes Following Intranasal Administration.” *International Journal of Pharmaceutics* 452 (1–2): 344–54. <https://doi.org/10.1016/j.ijpharm.2013.05.009>.
- Yarragudi, Sasi B., Robert Richter, Helen Lee, Greg F. Walker, Andrew N. Clarkson, Haribalan Kumar, and Shakila B. Rizwan. 2017. “Formulation of Olfactory-Targeted Microparticles with Tamarind Seed Polysaccharide to Improve Nose-to-Brain Transport of Drugs.” *Carbohydrate Polymers* 163: 216–26. <https://doi.org/10.1016/j.carbpol.2017.01.044>.
- Yavari, Leila, Marjan Ghorbani, Mahnaz Tabibiazar, Maryam Mohammadi, and Akram Pezeshki. 2021. “Advanced Properties of Gelatin Fi Lm by Incorporating Modi Fi Ed Kappa-Carrageenan and Zein Nanoparticles

for Active Food Packaging” 183: 753–59.

<https://doi.org/10.1016/j.ijbiomac.2021.04.163>.

Yu, Xi Chong, Jing Jing Yang, Bing Hui Jin, He Lin Xu, Hong Yu Zhang, Jian Xiao, Cui Tao Lu, Ying Zheng Zhao, and Wei Yang. 2017. “A Strategy for Bypassing the Blood-Brain Barrier: Facial Intradermal Brain-Targeted Delivery via the Trigeminal Nerve.” *Journal of Controlled Release* 258 (April): 22–33.
<https://doi.org/10.1016/j.jconrel.2017.05.001>.

Zhou, Bei, Yousef Heider, Songyun Ma, and Bernd Markert. 2018. “Phase-Field-Based Modelling of the Gelation Process of Biopolymer Droplets in 3D Bioprinting.” *Computational Mechanics*.
<https://doi.org/10.1007/s00466-018-1644-z>.

صياغة وتقييم لرقعة انف لإيصال الدواء من الانف إلى الدماغ لمادة الريفاستيجمين

إعداد

لينا شغليل

المشرف

الدكتور أنس أديب الشيشاني

المستخلص

توصيل الأدوية من الأنف إلى الدماغ يؤدي إلى تجاوز الحاجز الدموي الدماغي من خلال منطقة حاسة الشم باستخدام أجهزة وأشكال صيدلانية مختلفة. نهدف في هذا العمل إلى تصنيع وتحليل شكل صيدلاني جديد (لصقة أنفية) يحتوي على ريفاستيجمين. تم تطوير طريقة التحليل الريفاستيجمين والتحقق من صحتها. تم تصنيع أربع رقع أنفية باستخدام الجيلاتين / هيدروكسي ميثيل سيليلوز بنسب ودرجات مختلفة. تم فحص البقع الأنف المصنعة من حيث المظهر الخارجي، درجة الحموضة السطحية، القطر والطول، الخصائص الميكانيكية، وسلوك الالتصاق مع السائل المخاطي. تم أيضاً فحص توحيد المحتوى ونمط الإطلاق والعبور للريفاستيجمين تترارات. تم مطابقة أنماط الإطلاق لجميع بقع الأنف على نماذج الخواص الحركية. أخيراً، تم أيضاً فحص الثبات المادي للشكل الصيدلاني وللريفاستيجمين تترارات. بدت الصيغة F2 كأنها تركيبة واعدة، حيث إنها تمتلك أفضل نمط إطلاق مستدام مع أفضل سلوك التصاق ومرونة ومظهر مقبول.

الكلمات المفتاحية: توصيل الأدوية الأنفية، الأنف إلى الدماغ، ريفاستيجمين، لصقة الأنف،

الجيلاتين، هيدروكسي ميثيل.